Jarring Dynamics of Drillstrings

by

Manoj B. Keshavan

B.Tech., Indian Institute of Technology, Madras, India (1990)

Submitted to the Department of Ocean Engineering
in partial fulfillment of the requirements for the degree of

Master of Science in Ocean Engineering

at the

MASSACHUSETTS INSTITUTE OF TECHNOLOGY

September 1993

Author .....
Department of Ocean Engineering
June 4, 1993

Certified by .....
J. Kim Vandiver
Professor of Ocean Engineering
Thesis Supervisor

Accepted by .....
A. Douglas Carmichael
Chairman, Departmental Graduate Committee

Jarring Dynamics of Drillstrings

by

Manoj B. Keshavan

Submitted to the Department of Ocean Engineering
on June 4, 1993, in partial fulfillment of the
requirements for the degree of
Master of Science in Ocean Engineering

Abstract

A study of axial wave propagation in axisymmetric rods is undertaken in order to understand the jarring[2] dynamics of drillstrings

A transfer matrix solution to the equations of motion is used in determining the transfer functions between a response location at the surface and input locations at the jar and at the surface. The inputs and outputs considered are forces; however, they could also be modeled as displacements, velocities or accelerations. The transfer matrix formulation is capable of modeling changes in geometric/physical properties of the pipe sections. A realistic value of distributed damping is included to account for frictional and internal losses in the drillstring. Two models for the stuck length of the drillstring are analyzed – a) distributed stiffness model and b) distributed damping model. The transfer functions are calculated using a modified version of a program (DSVIB1) developed by H.Y.Lee (Ph.D '91 MIT). The effect on the transfer functions, of localized regions with different levels of distributed stiffness and distributed damping, is studied.

The behaviour of the system in the time domain is analyzed by calculating the impulse response from the transfer functions for the distributed stiffness and distributed damping models of the stuck region. The jarring event is modeled as a force impulse at the jar location. A non–linear signal processing technique, cepstral analysis, is used to identify the location of the stuck region, to compare and contrast the signatures obtained in the two different models of the stuck region, and to establish criteria for effective jarring.

Thesis Supervisor: J. Kim Vandiver
Title: Professor of Ocean Engineering

[2] A jar is an impact tool installed in the drillstring to free stuck pipe and the process of attempting to break free is referred to as jarring.

Acknowledgements

I thank my advisor, Prof. J. Kim Vandiver for his support during my stay at MIT. I thank Prof. Richard Lyon and Prof. Robert Fricke for their valuable comments and ideas during the course of my research.

I express my deepest gratitude to Rama Rao for his willingness to help me at all times and with whom I have had many useful discussions. I also thank all the members of my research group Li Li, C. Fei, Seth and Steve for all their help.

I am extremely grateful to Charles, Djamil and Mohamed who have seen me through the most trying times. For this, I shall be forever indebted to them. I am especially thankful to Beth, Scott, Karen and Liana for all the wonderful moments I have shared with them and who have always endeavoured to keep my spirits high. I thank Randy and Greg for the many entertaining discussions I have had with them. I also wish to thank Frank and Michele for making my life meaningful and enjoyable on the social front.

I am indeed fortunate to have had the most wonderful parents and I am at a loss for words to express my gratitude to them.

This work was sponsored by an industry consortium known as DEA 29 whose members included Agip, Amoco, Baker Hughes INTEQ, British Petroleum, Elf Aquitaine, Shell Development Co., Statoil and Total Compagnie Francaise des Petroles. My thanks to them all for their support.

To My Dad,

from whom I draw inspiration

Contents

List of Figures

Chapter 1

Introduction

Oilfield professionals have long recognized that preventing stuck pipe is always less expensive than unsticking pipe. Stuck pipe[1] affects as many as 25% of the wells at an estimated annual cost of $ 200 to $ 500 million. Cutting this cost lies mainly in preventing stuck pipe and promoting alert and rapid response to keep incipient sticking from ballooning into severe sticking. Successful prevention lies in understanding the mechanisms of pipe sticking. Since no prevention program is guaranteed so far, research has continued into jars and jarring physics.

The main focus of research, in the area of jarring dynamics to date, has been on the problem of optimizing jar location within the drillstring. In this thesis, we address a different issue, namely that of using surface measurements to identify the location of the stuck region, to infer the nature of downhole sticking and to develop criteria for evaluation of jarring effectiveness. These are of primary importance in a stuck pipe situation, where a decision has to be taken on the subsequent course of action, in a short period of time. In the absence of any method of inference on the nature of the sticking mechanism or evaluation of the efficacy of jarring, one could end up jarring for days without any results.

The success of a jarring operation depends on the correct interpretation of surface measurements. The acoustic signals reaching the surface as a result of tripping the

[1] Oilfield Review, *October '91*

jar are modified by a number of factors such as the presence of a stuck region, change in formation properties, geometry of the drillstring, boundary conditions, distortion effects arising due to differing speeds of propagation of different modes and so forth. Thus, the signal arriving at the surface contains information about the structure through which it propagates and the structure with which it interacts. In this thesis, we exploit this aspect to infer the type of sticking mechanism and to develop criteria for evaluating the progress made during jarring. A one dimensional wave propagation model is considered for drillstring axial vibration. The drillstring is modeled as a piecewise uniform bar and the jarring action, as a force impulse delivered to the drillstring in the axial direction, at the jar location.

The stuckpipe problem is described in the second chapter, which serves as the motivation for undertaking this research. A brief review of the various causes of sticking, types of jars commonly employed in the drilling industry and the criteria used for jar placement is discussed. This chapter culminates with a recap of the work done in the area of jarring and jarring dynamics.

The third chapter covers the background theory on axial vibration of drillstrings. The solution technique used is the transfer matrix method, which relates the kinematic and dynamic variables at one boundary of a system to those at the other. With a knowledge of the transfer matrices for a mass–spring–damper system and a uniform bar, the transfer matrix for a complex drillstring is built up. The transfer matrix, along with the appropriate boundary conditions[2] is then used in obtaining the forced response of the system. This leads us to the transfer function, which is the response at any station due to a unit harmonic excitation at another or the same location.

The fourth chapter focuses on the modeling details relevant to the jarring problem. The jarring event is modeled as a force impulse delivered to the drillstring. The impulse response is obtained from the transfer function by taking its inverse fourier transform and is subsequently windowed to smooth it. The response to a realistic jarring signal can be obtained by convolving it with the impulse response. The

[2]Inputs are included as boundary conditions in the transfer matrix formulation, in solving for the system response.

damping is considered to be uniformly distributed in the drillstring. Two different models for the stuck region are considered – a) The distributed stiffness model and b) The distributed damping model. The dispersion relations for these two models, and the effect of varying levels of distributed stiffness and distributed damping on group and phase velocities are studied. The top side boundary condition is modeled by a mass–spring –damper subsystem. The boundary conditon at the bit is taken to be free, since in most cases, the drillstring gets stuck while tripping out and under these circumstances, the bit is off–bottom.

The fifth chapter uses the models and tools developed in the earlier chapters to analyze realistic cases. Three examples are studied in detail. The first example considers two semi–infinite regions separated by a barrier of finite length. The stiffness and damping values are varied in the barrier and its effect on the reflected and transmitted waveforms (when a unit area impulse is incident on the stuck region), is studied. Example 2 analyzes a typical stuck pipe condition. This is studied for distributed damping as well as distributed stiffness models of the stuck region. Transfer functions (obtained from surface force measurements) are then compared for different levels of stiffness and damping, as a means of establishing an indicator for jarring effectiveness. Example 3 considers a case, where an impulse is delivered to the drillpipe at the surface. The motivation behind studying this case is that, jars typically used in the drilling industry are uphit jars, and hence the signature of the free drillstring usually, cannot be obtained. A homomorphic deconvolution technique known as *cepstral analysis* is introduced, and used to identify the exact location of the stuck region, to compare and contrast the signatures obtained in the two different models used to represent the stuck region, and to establish criteria for effective jarring.

Finally, the sixth chapter concludes the study and suggestions for future work are summarized.

Chapter 2

Background

This chapter provides the background needed to better understand the stuckpipe problem and serves as a motivation for undertaking this study. It starts out with the description of a typical drillstring followed by a discussion on the causes of sticking, types of jars and criteria for jar placement. Finally, a review of the work done so far in jarring and jarring dynamics is presented.

2.1 Schematic of a typical rig

A schematic diagram of a typical land based rig is shown in figure 2-1 on page 17. A brief glossary of the commonly used terminology is included below.

Drilling rig It performs three essential functions: raising or lowering the drill pipe; rotating the drill bit; circulating drilling mud for lubrication, counterbalancing formation pressure and carrying cuttings to the surface.

Formation It is the extended rock mass into which the hole has been drilled.

Drill pipe It is the medium through which torque is transmitted from the top drive or the rotary table to the bottom hole assembly. Drill pipe is added continually as the drilling progresses. Drill pipes range from 3-5" in diameter.

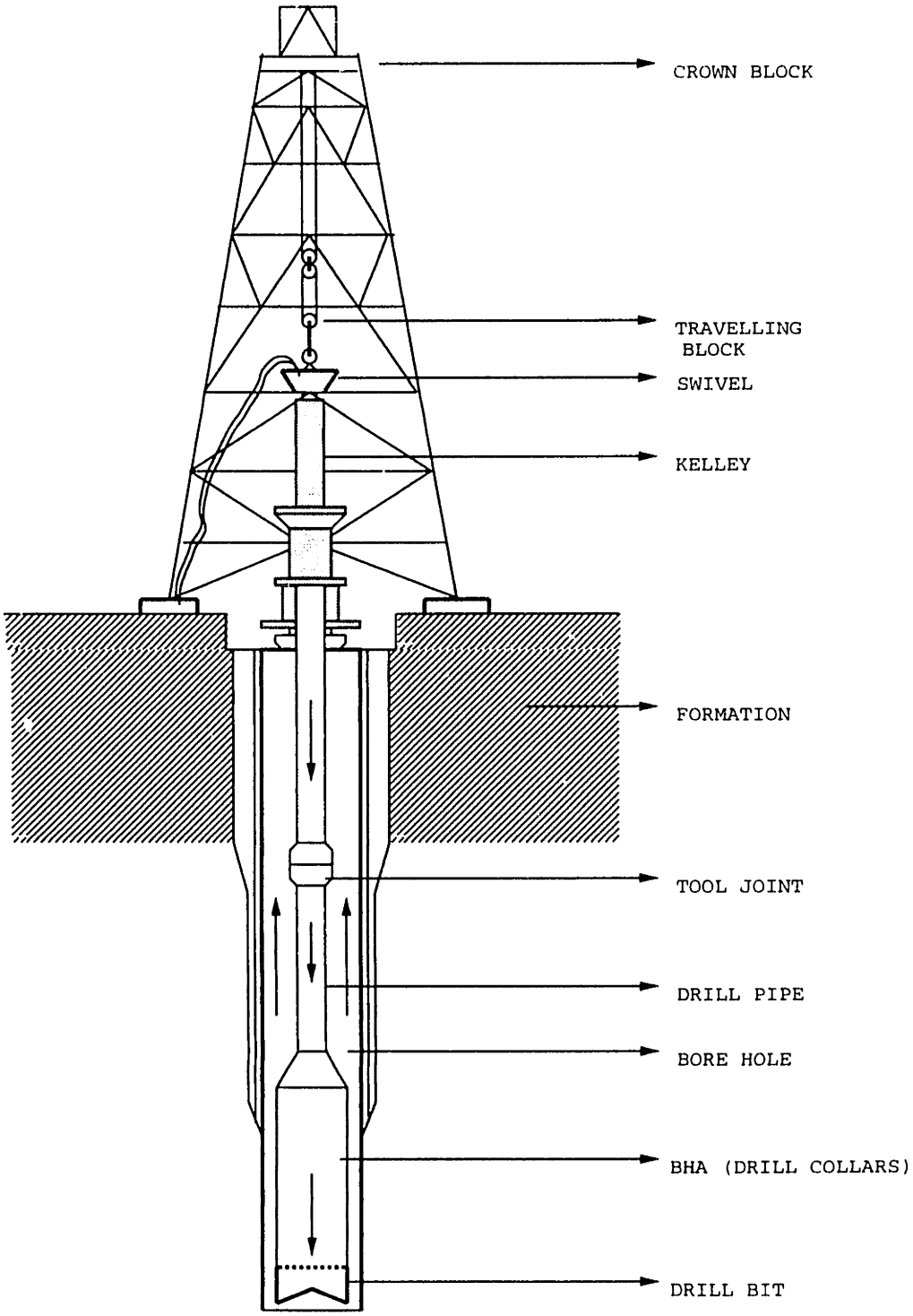

Figure 2-1: Schematic of a typical drilling rig

Drill collars They are larger in diameter than drill pipes and constitute the bottom hole assembly. Drill collars provide a substantial weight on bit necessary for drilling operation. Drill collars range between 6–11" in diameter.

Bottom Hole Assembly (BHA) It extends from the drill pipe to the bit and is mostly comprised of drill collars. The BHA also includes the jars and any other downhole sensors that may be present in the drillstring.

drillstring The entire array of drill pipes and the BHA is collectively referred to as the drillstring.

2.2 Causes of stuckpipe

Formation related : Unconsolidated formations such as loosely compacted sands and gravel can collapse into the wellbore forming a bridge around the drillstring. Mobile formations like salt and plastic shales flow into the wellbore when restraining stresses are removed thereby jamming the drillstring.

Mechanical : Poor hole cleaning leads to the overloading of the annulus between the drillstring and the borehole wall with cuttings, causing the drillstring to get stuck. Keyseats, or grooves cut in the borehole wall by the rotating drill pipe stick the larger diameter drill collars when tripping out. Occasionally, the casing may collapse as a result of excessive formation pressure causing sticking of the drillstring.

Differential sticking : Differential sticking occurs when the drillstring gets embedded in a mudcake and is pinned to the borehole wall by the differential pressure between the mud and formation. This type of sticking gets progressively worse with time.

2.3 Techniques for freeing the drillstring

There are a number of techniques employed by the drilling industry to free stuckpipe. They range from the use of gentler measures like using spotting fluids, hole conditioning and changes in hydrostatic pressure to more brute force methods like jarring. Spotting fluids essentially change the downhole conditions so as to weaken the bond between the mudcake and the pipe. Hole conditioning involves increasing the mud flow rate or changing mud physical properties. Reduction in hydrostatic pressure is used mainly to free differentially stuck pipe. When the gentler methods of persuasion fail to produce the desired results, jarring is resorted to.

Jars are impact tools run in the drillstring to free stuck pipe and the process of attempting to free stuck pipe is called jarring. A jar is similar in appearance to a drill collar and it consists of a sliding mandrel inside a sleeve which accelerates upwards/downwards, once the tripping load is reached causing the drillstring above/below it to accelerate as well. Once the mandrel has traversed the stroke length of the jar, it collides with a shouldered sleeve also known as the anvil. This impact creates a shock wave that traverses up and down the drillstring and to the stuck region. The intention is to break the drillstring loose from the stuck region.

2.4 Types of jars

1. Mechanical jars
2. Hydraulic jars

Mechanical jars : Mechanical jars consist of a series of springs and lock & release mechanisms. The jar trips when the axial force reaches a preset value. The tripping load can be set either at the surface or downhole depending on the jar design. A schematic of a typical mechanical jar is shown in figure 2-2 on page 20

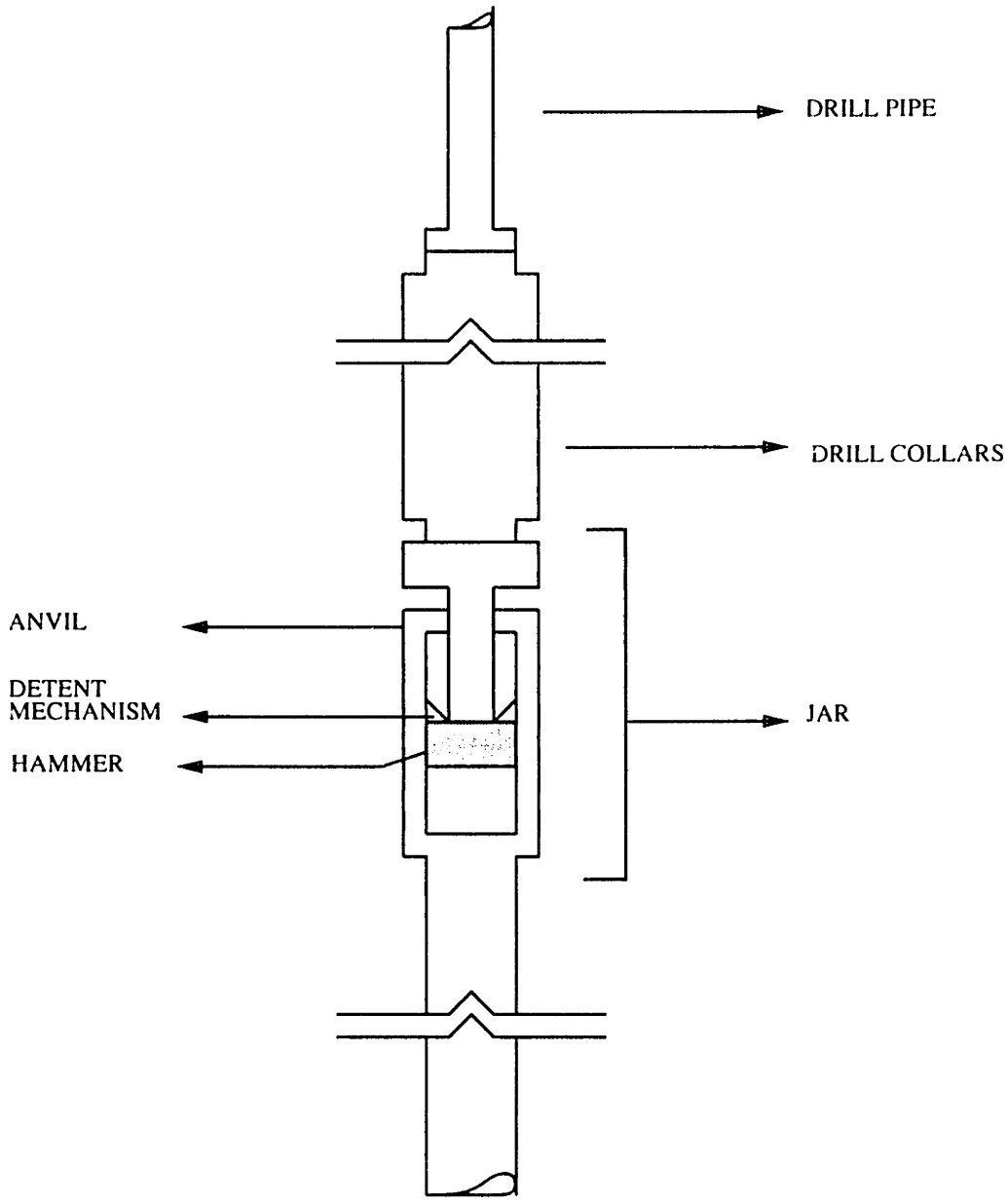

Figure 2-2: Schematic of a Mechanical jar

Hydraulic jars : Hydraulic jars do not trip at a preselected threshold. The jarring force delivered is determined by the magnitude of the overpull. The higher the tensile or compressive load, the sooner the jar trips and greater is the impact. Thus the hydraulic jar has the advantage of having a continuously variable jarring force. Also the hydraulic jar has a larger inner diameter than a comparable mechanical jar allowing for the smooth passage of a wireline cable. However, a significant drawback of the hydraulic jar is that repeated jarring can overheat the hydraulic fluid thereby lowering its viscosity. This may cause the jar to trip sooner than the desired tension/compression can be reached.

2.5 Criteria for jar placement

Criteria for jar placement normally vary from one operator to the other and also frequently depend on the particular geographic area of the drilling operation. However, the general guidelines followed by the drilling industry are given below.

- It is recommended that all drilling jars be run under tension irrespective of the jar type. The primary concern with running jars under compression is accidental downjarring while drilling leading to undesirable effects including damaging the bit. This implies that jars must be placed above the zero-stress point in the drillstring. Consequently, BHA design, mud weight and weight on bit are the parameters to be taken into consideration to ensure that jars operate in tension.
- Jars should be placed sufficiently high up in the drillstring so as to minimize the possibility of getting stuck above the jar. The trip setting of the jar is dependent on the maximum allowable overpull at the surface and the jar position in the BHA.
- The jar position in the BHA should be optimized so that the available impulse to free the drillstring is maximized at the same time maintaining a high peak jarring force.

2.6 Review of earlier work

Although[1] many of the drilling operators rely on empirical evidence and experience for jar placement, the use of computer programs nontheless has expanded in recent years. These programs analyse wave propagation along the drillstring during jarring to model the jarring force for various jar positions, BHA configurations and well trajectories. The aim is to determine the jar position that is an optimum compromise between the magnitude of the peak jarring force and the duration of this force at the stuck ppoint. To achieve this, placement programs optimize two variables:

- Velocity of the BHA above the jar
- Length of the BHA above the jar

Peak force is proportional to the velocity of the BHA above the jar, since a higher terminal velocity of the hammer implies a greater peak force albeit of extremely short duration. On the other hand, the longer the BHA above the jar, the longer it takes to come to rest after impact and greater is the duration of the peak force. Note however, that the magnitude of the peak force in this case is proportionately reduced. Most of the jarring programs are aimed at determinining the position in the BHA where a jar can be placed to achieve the optimum combination of the peak force and its duration.

The first significant work involving jarring dynamics addressing the above problem was by *Skeem et al* [14]. Their analysis was based on one-dimensional stress wave propagation theory in an elastic rod. A systematic wave tracking approach was employed to derive the timing, duration and qualitative value of peak jarring force at a preknown stuck point. It was concluded that the optimum jar position depends on the magnitude of the stuck force. Furthermore, since sticking in most of the cases may not occur at a point but occurs along a length, the

[1] Oilfield Review *October '91*

peak jarring force must not only exceed the sticking force, but also be maintained long enough to displace the stuck portion of the drillstring. They also assumed that the stuck point is known which often is not. Other shortcomings in Skeem's model included the stuck point being modeled as a rigid boundary and total neglect of the effects of damping.

The need for a better model prompted *Kalsi, Wang & Chandra* [6] to come up with a model based on the finite element method. A non-linear transient dynamic analysis was performed using a general purpose FEM code to track the stress and displacement waves through the drillstring. The damping in the drill collars and mud and the magnitude of the sticking force were assumed. Time histories of displacent, velocity, acceleration and impact force were obtained at different locations along the length of the drillstring. However, this FEM analysis requires extensive computational facilities & long solution times and a high level of engineering expertise to perform the analysis and to interpret the results.

Practical analysis in the field required that jarring programs be as versatile as possible and easy to interpret without any significant amount of post-processing. This led to the development of two jarring analysis programs, one by *Askew* [2] of Anadrill and another by *Wang et al* [17]. *Askew's* Computerized Analysis & Placement (CAP) program models the BHA and predicts forces at the stuck point for a given jar location and trip setting. The program also suggests optimal trip setting and BHA design for effective jarring. The jar placement program by *Wang & colleagues* improved upon Skeem's work by including the effects of drill collar movements below the jar and the use of Heavy Weight Drill Pipe (HWDP) in the BHA's.

Despite the recent advancements made in developing increasingly better programs for jar placement, the nature of the sticking mechanism is not well enough understood to be modeled accurately and the peak force required to free the drillstring is apriori unknown; hence optimization of jar location is an issue yet

to be resolved completely.

Chapter 3

Axial Vibration of Drillstrings

The drillstring is essentially a very long shaft used to transmit energy from the surface to the bit. Most of the drillstring except for a small portion above the surface is concealed and hence one cannot rely on visual senses to infer the dynamic behaviour of the drillstring. Consequently, the knowledge of the behaviour of drillstrings under different operating conditions is significant, since the dynamic stresses along the string dictate its life and that of the drill bit.

This is particularly so in the case of jarring where large dynamic stresses come into play when the hammer impacts the anvil. Many downhole tools are now mounted on the drillstring BHA close to the bit. For these tools to provide a reliable and an economic service, they must endure the high stresses caused by jarring. Furthermore, for any jarring operation to be effective, the highest stress should be at the stuck region and not at arbitrary locations in the BHA, which could result not only in ineffective jarring, but also damage special tools or take away from the life of the drillstring and the bit. Thus there is no exaggeration in stating that understanding the dynamics of drillstrings is of primary importance in improving the efficiency of the drilling process and in increasing the effectiveness of the jarring operations.

3.1 One dimensional wave propagation model of drillstring axial vibration

Typically, a drillstring or any shaft for that matter, can undergo vibration in three principal modes: axial, torsional and lateral. Among these, axial vibration is the most conspicuous at the surface and has been analyzed in great detail in the literature starting with Dareing [4].

The phenomenon of jarring lends itself particularly well to being modeled as an axial wave propagation problem since it involves an impact between two long extended elastic members leading to the propagation of transient stress and displacement waves in the drillstring. The drillstring can be considered as a one-dimensional elastic medium with piece-wise constant properties. The analytic formalism for axial wave propagation in drillstrings is well established and the reader may refer to Hyun Lee's thesis [8] for further details.

In the proposed model, the effects of lateral motions due to bending and whirling are neglected and axial and torsional vibrations are assumed to be uncoupled. Since the differential equations of motion and the boundary conditions for the longitudinal and torsional motions are similar, the same general solution can be used for both cases.

In the analytical model, the drillstring is modeled as a step-wise uniform bar and the surface/topside boundary conditions are modeled with appropriate masses, springs and damping elements.

The one–dimensional axial wave propagation in a uniform bar is governed by the following partial differential equation

$$\frac{1}{c^2}\frac{\partial^2 u}{\partial t^2} = \frac{\partial^2 u}{\partial x^2} - \frac{R}{EA}\frac{\partial u}{\partial t} - \frac{Ku}{EA} \tag{3.1}$$

where

$$c = \sqrt{\frac{E}{\rho}} \tag{3.2}$$

E :	Young's modulus of the bar (N/m^2)
A :	Cross-sectional area of the bar (m^2)
R :	Distributed damping constant per unit length $(N - s/m^2)$
K :	Distributed stiffness per unit length $(N/m/m)$
c :	Speed of longitudinal wave propagation (m/s)
u :	Longitudinal displacement at any given location x
ρ :	Volume density (Kg/m^3)

Note that all the assumptions mentioned earlier are implicit in the above equation. For the purpose of completeness, they are again listed below.

- The bar is homogeneous i.e. material properties are spatially invariant.
- Plane, parallel cross-sections remain plane and parallel.
- Stress distribution is uniform over the cross-section.
- Lateral inertia effects associated with contraction–expansions in the lateral direction have been ignored.

Also, an additional term involving the distributed stiffness has been introduced into the wave equation. Although the introduction of this term doesn't particularly change the form of the solution to the wave equation, it manifests itself in the "*dispersion relationship*" which will be discussed in a future section.

3.2 Solution Technique: The Green's function approach

The solution to the wave equation is obtained by calculating the displacement response at any position ($0 \leq x \leq l$) in the rod due to applied unit harmonic

axial forces at the top or bottom boundary. The mobilities of the uniform rod are calculated from these displacements which are then used to build the transfer matrix for the bar.

The following governing equation with boundary conditions is solved for the displacement response using the Green's function approach.

$$\rho A\frac{\partial^2 u}{\partial t^2} + R\frac{\partial u}{\partial t} + Ku = EA\frac{\partial^2 u}{\partial x^2} \tag{3.3}$$

$$\frac{\partial u}{\partial x}(x = 0) = 0 \tag{3.4}$$

$$EA\frac{\partial u}{\partial x}(x = l) = e^{i\omega t} \tag{3.5}$$

where

u	: longitudinal displacement
x, t	: axial coordinate, time coordinate
ρ, E	: density, elastic modulus
R	: damping constant per unit length
K	: stiffness per unit length
l	: length of the bar

The solution of equations (3.3) to (3.5) is:

$$u = -\frac{\cos kx}{EAk \sin kl} \tag{3.6}$$

where

$$k^2 = (\frac{\omega^2}{c^2} - \frac{K}{EA}) - i\frac{R\omega}{EA} \tag{3.7}$$

Figure 3-1 on page 32 shows the free body diagram of a uniform bar. The dis-

placements (u_R, u_L) due to the forces at both the ends (F_R, F_L) can be obtained by using the mobilities of the uniform bar as follows:

$$\begin{Bmatrix} u_R \\ u_L \end{Bmatrix} = \begin{bmatrix} M_{RR} & M_{RL} \\ M_{RL} & M_{LL} \end{bmatrix} \begin{Bmatrix} F_R \\ F_L \end{Bmatrix} \tag{3.8}$$

The mobilities M's are responses due to a unit harmonic force, and are defined as:

M_{RR} : displacement at the right end due to a unit force at the right end

M_{RL} : displacement at the right end due to a unit force at the left end

M_{LR} : displacement at the left end due to a unit force at the right end

M_{LL} : displacement at the left end due to a unit force at the left end

From the above solution, M_{RL} and M_{LL} can be obtained

$$M_{RL} = -\frac{1}{EAk \sin kl} \tag{3.9}$$

$$M_{LL} = -\frac{\cos kl}{EAk \sin kl} \tag{3.10}$$

Since we are considering a uniform bar, M_{RR} and M_{LL} have equal magnitudes but differ in signs, which is also true of M_{LR} and M_{RL}:

Thus,

$$\begin{Bmatrix} u_R \\ u_L \end{Bmatrix} = \begin{bmatrix} \frac{\cos kl}{EAk \sin kl} & -\frac{1}{EAk \sin kl} \\ \frac{1}{EAk \sin kl} & -\frac{\cos kl}{EAk \sin kl} \end{bmatrix} \begin{Bmatrix} F_R \\ F_L \end{Bmatrix} \tag{3.11}$$

3.3 The Transfer Matrix Method

The key modeling tool used throughout this thesis is the "Transfer Matrix". The transfer matrix is a linear transformation, which relates a state vector at one cross-section of an elastic system to the state vector at the succeeding cross-section namely,

$$z_j^R = [T] z_j^L \tag{3.12}$$

This is a difference equation, where the matrix $[T]$ can be thought of as a spatial state transition matrix evaluated between L and R. The state vector z_j^R at a point R of an elastic system is a column vector, the components of which are the displacements (or rotations) of the point R and the corresponding internal forces (or moments). Thus the transfer matrix relates the kinematic and dynamic variables at one boundary of a system (say, the left in the case of a pipe system) to those at the other (the right of the pipe system). The transfer matrix method is ideally suited to systems that have a chain-like topology i.e. cables, rods, beams etc. The transfer matrix for a system can be found by manipulation of the dynamic equations of motion of that system. Its formulation assumes a harmonic time dependence ($e^{i\omega t}$) in the equations of motion. The transfer matrix is usually of *even* dimension and so is the state vector. A more complete discussion on transfer matrices can be found in *Matrix Methods in Elastomechanics* [7].

3.3.1 Coordinate System and Sign Convention

Signs are often a source of confusion when dealing with transfer matrices and it is imperative to clearly define the sense of positive quantities. We make use of a right -handed coordinate system, the x axis coinciding with the centroidal axis of the elastic body. A cut across the body exposes the two faces, and the face

whose outward normal points in the positive direction of the x axis is known as the positive face, the other being the negative face. Displacements are positive if they coincide with the positive direction of the coordinate system, and forces are positive if, when acting on the positive (negative) face, their vectors are in the positive (negative) directions.

3.3.2 Transfer Matrix for a Uniform Bar

The transfer matrix of a uniform pipe system of finite length hence relates the state vector z_R (*right* boundary) to the state vector z_L (*left* boundary) as shown in figure 3-1 on page 32. In our case and in the remainder of the thesis, the pipe systems are modeled with 2x2 transfer matrices, which in turn means that each state vector is 2x1. The quantities of interest, here are, the longitudinal displacement of the pipe and the internal force in the pipe. The transfer matrix then obeys the following relation:

$$\begin{Bmatrix} u_R \\ F_R \end{Bmatrix} = \begin{bmatrix} T_{RR} & T_{RL} \\ T_{LR} & T_{LL} \end{bmatrix} \begin{Bmatrix} u_L \\ F_L \end{Bmatrix} \tag{3.13}$$

where

u_R : displacement at the right boundary

u_L : displacement at the left boundary

F_R : force at the right boundary

F_L : force at the left boundary

T_{RL} : displacement at the **R**ight boundary due to a unit harmonic force at the **L**eft boundary

R, L : subscripts indicating the right and left boundaries

Since the mobility matrix for a uniform bar has already been determined in

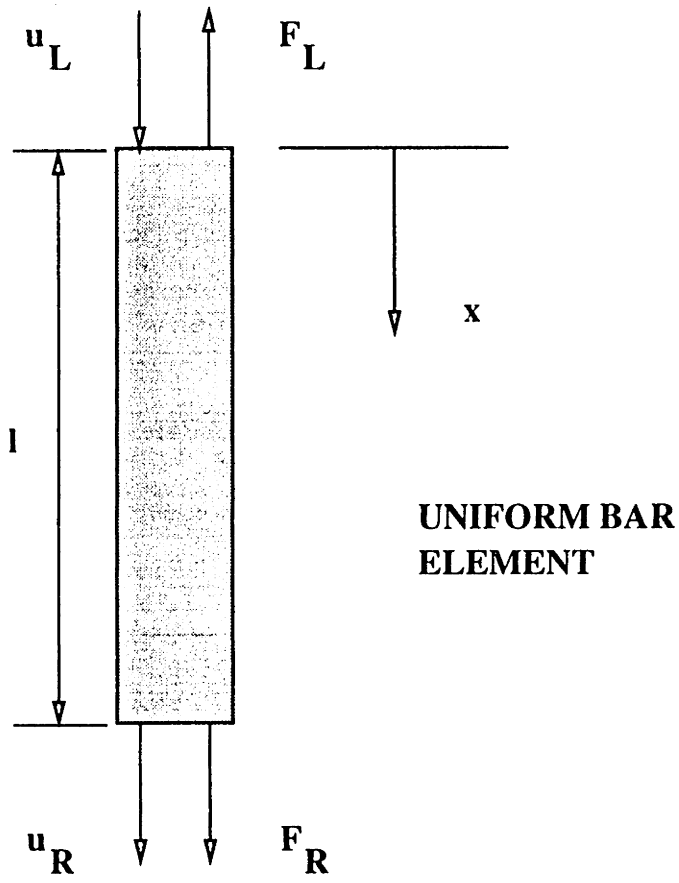

Figure 3-1: Free body diagram of a uniform bar element

equation 3.11, it is a matter of simple algebra before one gets the transfer matrix for a uniform rod.

Thus,

$$[T] \equiv \begin{bmatrix} T_{RR} & T_{RL} \\ T_{LR} & T_{LL} \end{bmatrix} = \begin{bmatrix} \cos kl & \frac{\sin kl}{EAk} \\ -EAk \sin kl & \cos kl \end{bmatrix} \tag{3.14}$$

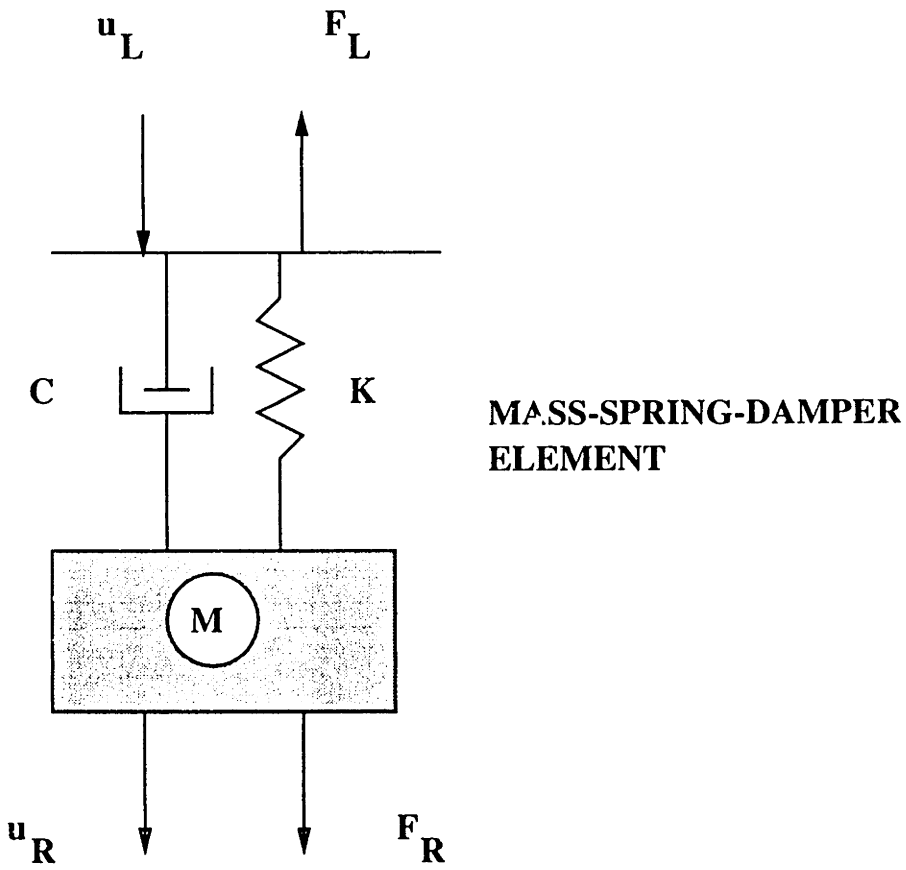

Figure 3-2: Free body diagram of a mass–spring–damper system

3.3.3 Transfer Matrix for a Mass–Spring–Damper System

The free body diagram of a mass–spring–damper system is shown in figure 3-2 on page 33. The transfer matrix relates the displacement and force at the lower end (u_R, F_R) to those at the upper end (u_L, F_L). The transfer matrix is a function of frequency 'ω'. They are so called because they '*transfer*' or map the state vector at one position L (z_j^L) to the state vector at position R (z_j^R).

For the case of a simple mass–spring–damper system, the Transfer matrix can readily be determined to be :

$$\begin{Bmatrix} u_R \\ F_R \end{Bmatrix} = \begin{bmatrix} T_{RR} & T_{RL} \\ T_{LR} & T_{LL} \end{bmatrix} \begin{Bmatrix} u_L \\ F_L \end{Bmatrix} \tag{3.15}$$

where

$$[T] \equiv \begin{bmatrix} T_{RR} & T_{RL} \\ T_{LR} & T_{LL} \end{bmatrix} = \begin{bmatrix} 1 & \frac{1}{K+i\omega C} \\ -\omega^2 M & 1 - \frac{\omega^2 M}{K+i\omega C} \end{bmatrix} \tag{3.16}$$

u_L, F_L	: displacement, force at the upper (left) end
u_R, F_R	: displacement, force at the lower (right) end
M	: mass
C	: damping constant (*Force/unit velocity*)
K	: spring constant (*Force/unit displacement*)

3.4 Modeling the Drillstring as a Complex Pipe System

In sections (3.3.2) and (3.3.3), we have seen the development of transfer matrices for a uniform bar and for a mass–spring–damper system. Now we proceed to do the same for a drillstring which can be modeled as a combination of uniform rods and mass–spring–damper elements. The advantage of using the transfer matrix formulation is that it is tailored for exploitation by digital computers and hence is computationally far more efficient than Finite Element techniques. Thus, with the knowledge of transfer matrices for common elastic elements, it is possible to build up the transfer matrix for a complex linear one dimensional system by linking the constituent elements in a chain-like manner with appropriate

compatibility conditions imposed between adjacent elements. The various bar elements could vary in :

Geometric properties	: changes in cross-sectional area A and/or length l
Physical properties	: changes in distributed stiffness K or distributed damping R

It is in the utilization of the latter idea to investigate the problem of jarring, which is the principal contribution of this research.

Consider the non-uniform pipe system in figure 3-3 on page 36 which is representative of a typical drillstring. An analytical model can be easily constructed with just a knowledge of the transfer matrices for homogeneous finite pipe systems. The complex non-uniform pipe system can be reduced to represent a combination of a finite number of uniform pipe systems connected together. The relationship between state vectors at two adjacent stations for the j^{th} subsystem is given by :

$$z_j^R = [T_j] z_j^L \tag{3.17}$$

The compatibility conditions yield the relationship between adjacent subsystems as:

$$z_{j+1}^L = [C_j] \left[z_j^R + terms\ due\ to\ forcing\ function \right] \tag{3.18}$$

$[C_j]$ is known as the *Compatibility matrix* and it ensures that kinematic and dynamic boundary conditions are satisfied at the junction between two subsystems with respect to displacements and internal forces.

3.4.1 Free Vibration Response

The boundary conditions to be satisfied at the interface are:

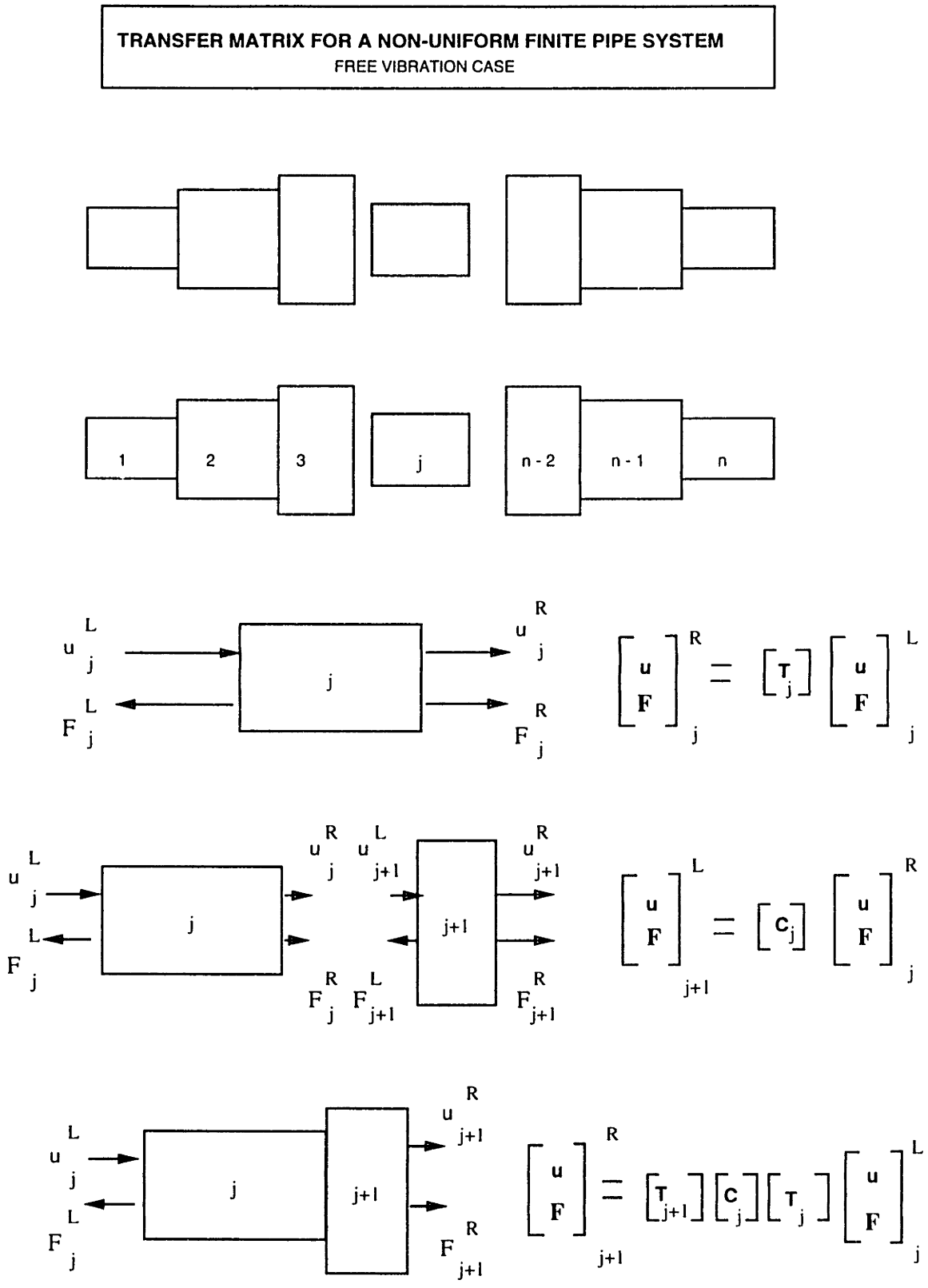

Figure 3-3: Transfer matrix assembly for a complex pipe system: *(Free vibration case)*

1. Continuity of displacements at the junction

$$u_{j+1}^{L} = u_{j}^{R} \tag{3.19}$$

2. Force balance at the boundary

$$F_{j+1}^{L} = F_{j}^{R} \tag{3.20}$$

The steps leading to the synthesis of a relationship between state vectors of a complex pipe system is shown in figure 3-3. It is evident that it is possible to progress through the structure by multiplying the transfer and compatibility matrices according to equations 3.17 and 3.18, so that the state vector at the far end, z_n^R, is related to the state vector at the starting end, z_1^L, by an equation of the form:

$$z_n^R = [T_n][\mathcal{C}_{n-1}][T_{n-1}]...[T_{j+1}][\mathcal{C}_j][T_j]...[T_2][\mathcal{C}_1][T_1]z_1^L \tag{3.21}$$

Since the compatibility matrix $[\mathcal{C}]$ is an identity matrix in our case, we get,

$$z_n^R = [T_n][T_{n-1}]...[T_{j+1}][T_j]...[T_2][T_1]z_1^L \tag{3.22}$$

The preceding matrix relationship contains 4 variables related by 2 equations. If any two variables are specified through boundary conditions, then the two unknowns can be solved for in terms of these specified quantities. One can hence obtain the natural frequencies and mode shapes as detailed in Rama Rao's thesis [12].

3.4.2 Forced Vibration Response

Consider the complex pipe system shown in figure 3-4 on page 39 with an external harmonic forcing function imposed at the junction between the j^{th} and

the $j+1^{th}$ subsystems. The external excitation could be either a displacement or a force excitation. Depending on the kind of excitation, the kinematic and the dynamic boundary conditions and hence the compatibility requirements at the junction get modified to account for the forcing term.

1. Continuity of displacements at the junction (displacement excitation)

$$u_{j+1}^{L} = u_{j}^{R} = u_{exc,j} \tag{3.23}$$

where

$u_{exc,j}$ is the forced displacement excitation between the j^{th} and the $j+1^{th}$ subsystems

2. Force balance at the boundary

$$F_{j}^{R} = F_{j+1}^{L} \pm \mathcal{F}_{exc,j} \tag{3.24}$$

where

$\mathcal{F}_{exc,j}$ denotes the external forced excitation at the interface between the j^{th} and the $j+1^{th}$ subsystems. The sign to be chosen depends on the manner in which the external excitation is defined. Note that the sign convention adopted must be consistent with that defined in section (3.3.1).

In the case of a force excitation as shown in figure 3-4 and recalling the sign convention defined in section(3.3.1), one can write :

$$z_{j+1}^{L} = [C_j]\,[T_j] z_j^{L} - [C_j]\,\left[\{0 \;\; \mathcal{F}_{exc,j}\}^{T}\right] \tag{3.25}$$

It can be seen that the compatibility requirement as defined by equation 3.18 can now be written as :

$$z_{j+1}^{L} = [C_j]\,\left[[T_j]...[T_2][C_1][T_1] z_1^{L} - \{0 \;\; \mathcal{F}_{exc,j}\}^{T}\right] \tag{3.26}$$

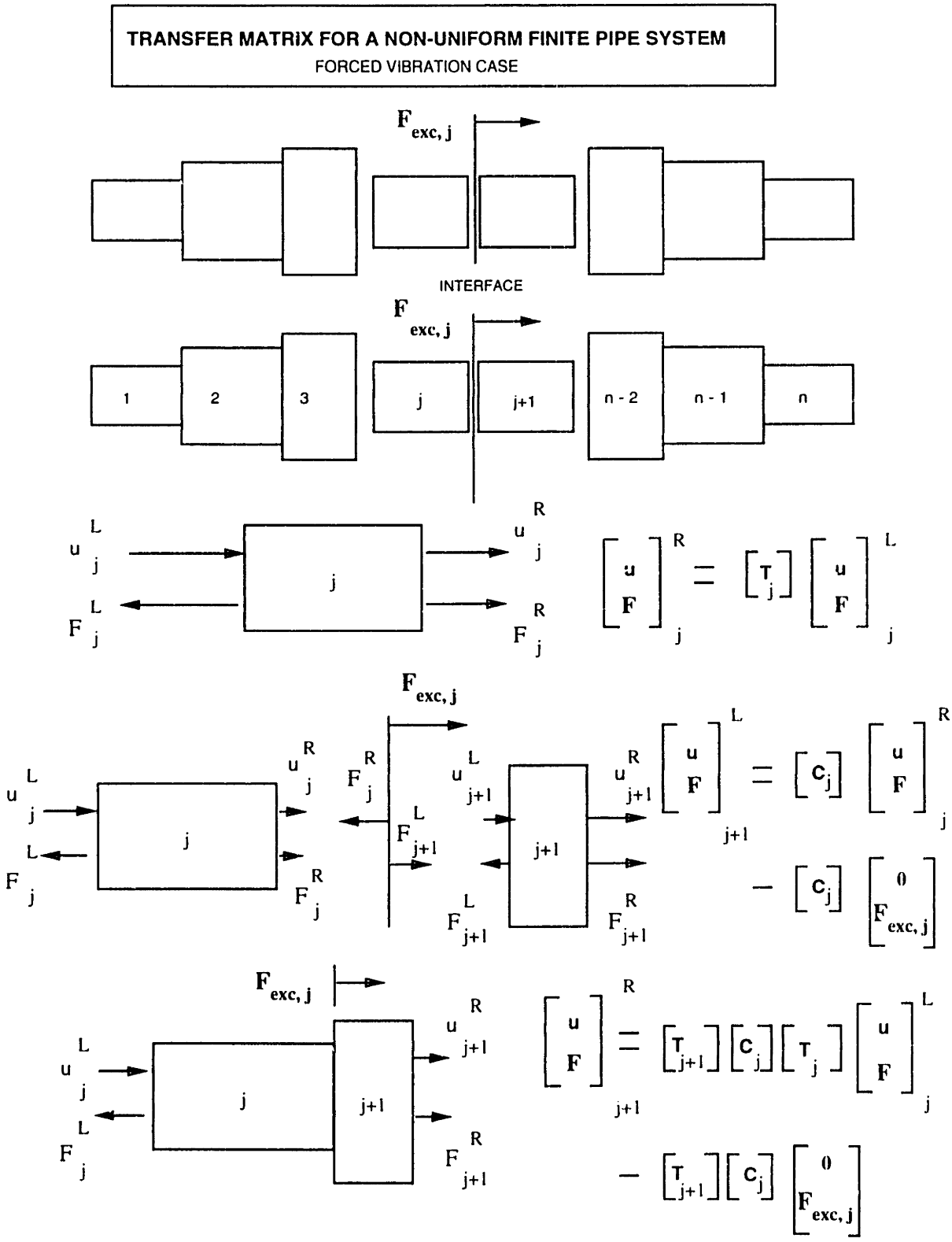

Figure 3-4: Transfer matrix assembly for a complex pipe system: *(Forced vibration case)*

Stepping through the structure by multiplying the transfer and compatibility matrices, as was done in the "Free Vibration Response" case,
one obtains,

$$z_n^R = [T_n][\mathcal{C}_{n-1}][T_{n-1}]...[\mathcal{C}_j]\ \left[[T_j]...[T_2][\mathcal{C}_1][T_1]z_1^L - \{0\ \ \mathcal{F}_{exc,j}\}^T\right] \tag{3.27}$$

$$= [T_n][\mathcal{C}_{n-1}][T_{n-1}]...[T_2][\mathcal{C}_1][T_1]z_1^L - [T_n][\mathcal{C}_{n-1}][T_{n-1}]...[\mathcal{C}_j]\left\{\begin{array}{c} 0 \\ \mathcal{F}_{exc,j} \end{array}\right\} \tag{3.28}$$

In all our analyses, the compatibility matrix $[\mathcal{C}]$ is an identity matrix, which can be seen trivially.
Hence, we obtain,

$$z_n^R = [T_n][T_{n-1}]...[T_2][T_1]z_1^L - [T_n][T_{n-1}]...[T_{j+1}]\left\{\begin{array}{c} 0 \\ \mathcal{F}_{exc,j} \end{array}\right\} \tag{3.29}$$

$$= [\Pi]z_1^L - [\Gamma]\left\{\begin{array}{c} 0 \\ \mathcal{F}_{exc,j} \end{array}\right\} \tag{3.30}$$

Expanding, we get,

$$\left\{\begin{array}{c} u_n^R \\ F_n^R \end{array}\right\} = \left[\begin{array}{cc} \Pi_{11} & \Pi_{12} \\ \Pi_{21} & \Pi_{22} \end{array}\right]\left\{\begin{array}{c} u_1^L \\ F_1^L \end{array}\right\} - \left[\begin{array}{cc} \Gamma_{11} & \Gamma_{12} \\ \Gamma_{21} & \Gamma_{22} \end{array}\right]\left\{\begin{array}{c} 0 \\ \mathcal{F}_{exc,j} \end{array}\right\} \tag{3.31}$$

The power of the transfer matrix approach lies in the fact that the unknown quantity say, the force at the left end of element 1 need not be carried through each station as in the algebraic set of equations. This makes it amenable for manipulation by a computer.

Once again, we have 4 variables and 2 equations. If any 2 variables are specified, then all the components of the state vectors z_n^R and z_1^L would be known. The *"Drillstring VIBration"* program (DSVIB) written by H.Y.Lee (Ph.D'91) [8] models the drillstring as a complex pipe system consisting of uniform bar and mass–spring–damper elements where the top[1] (Left) boundary is fixed. Hence, only one additional condition, either displacement/force at the bottom (Right) boundary is required to solve for the remaining 2 unknowns namely, the force at the top fixed boundary and the force/displacement at the bottom boundary in terms of the excitation force.

Thus, equations 3.31 with $u_1^L = 0$ reduce to

$$u_n^R = \Pi_{12}\, F_1^L - \Gamma_{12}\, \mathcal{F}_{exc,j} \tag{3.32}$$

$$F_n^R = \Pi_{22}\, F_1^L - \Gamma_{22}\, \mathcal{F}_{exc,j} \tag{3.33}$$

which can be solved for F_1^L.

Once the force at the top fixed end is known, the state vector at any junction within the complex pipe system can be determined by multiplying the transfer matrices of individual subsystems between the junction and the top boundary. If for example, the state vector at the bottom of subsystem n, z_n^R (refer figure 3-4) is to be determined, we would have,

for $n \leq j$

$$z_n^R = [T_n][T_{n-1}]...[T_2][T_1] \begin{Bmatrix} 0 \\ F_1^L \end{Bmatrix} \tag{3.34}$$

for $n > j$

[1] *"upper"* is used synonymously with *"Left"* & *"lower"* is used synonymously with *"Right"*

$$z_n^R = [T_n][T_{n-1}]...[T_2][T_1]\begin{Bmatrix} 0 \\ F_1^L \end{Bmatrix} - [T_n][T_{n-1}]...[T_{j+1}]\begin{Bmatrix} 0 \\ \mathcal{F}_{exc,j} \end{Bmatrix} \quad (3.35)$$

Thus the response of the structure at any arbitrary point to a harmonic force excitation can be determined by subdividing the structure so that the excitation and response locations lie on boundaries between subsystems. A similar approach is utilized to find the response to a displacement excitation. The *displacement response* to an imposed harmonic *force excitation* is calculated at the *input location*. This can be treated as a *displacement excitation* at the *input location* and the state vector at any other desired station can be thought of as the response to *this displacement input*.

3.5 The Transfer Function

The ratio of the fourier transform of a response to the fourier transform of a source is called the system function $H(\omega)$. System functions could be either driving point functions or transfer functions depending on whether they relate the response to the source at the same or different stations. The ratio of the output to the input yields the transfer function between the state variable of interest and the harmonic excitation. Since the transfer matrix is a function of frequency, it follows that the transfer function is also frequency dependent. In the preceding section, we saw how the response at any station due to a harmonic excitation at a specified location could be obtained using the transfer matrix formulation. Specifically, we considered cases where the input was either a force or a displacement and the response was a state vector of displacement and force at the desired location. It is a simple extension to calculate the transfer function for velocity/acceleration input and/or velocity/acceleration response, once the transfer function with a displacement input and/or a displacement output has

been evaluated.

To illustrate, if the transfer function between a velocity response and an acceleration input is desired, we would first evaluate:

$$H_{XX}(\omega) = \frac{X(\omega)_{output}}{X(\omega)_{input}} \tag{3.36}$$

where

$H_{XX}(\omega)$: Transfer function between a displacement output and a displacement input

$X(\omega)_{output}$: Fourier transform of the displacement, at the response location

$X(\omega)_{input}$: Fourier transform of the displacement, at the input location

Now, extending this further,

$$\begin{aligned} H_{VA}(\omega) &= \frac{V(\omega)}{A(\omega)} \\ &= \frac{i\omega X(\omega)_{output}}{-\omega^2 X(\omega)_{input}} \\ &= \frac{-iH_{XX}(\omega)}{\omega} \end{aligned} \tag{3.37}$$

where

$H_{VA}(\omega)$: Transfer function between a velocity output and an acceleration input

$V(\omega)_{output}$: Fourier transform of the velocity, at the response location

$A(\omega)_{input}$: Fourier transform of the acceleration, at the input location

The essential feature of the transfer function is that a stimulus of harmonic form at a given frequency produces a response that is of the *same* form and the *same* frequency regardless of the choice of frequency. Thus, we can speak of a harmonic response to an harmonic input. This basic property is a consequence of *Linearity* and *Time invariance* and we shall exploit this property of *Linear systems* to understand the jarring dynamics of drillstrings.

Chapter 4

Jarring Dynamics of Drill Strings

Most of the research work in *jarring dynamics* to date has laid focus on trying to optimize jar placement in the drill string so that an optimum combination of peak force and duration of this peak force is delivered to the "stuck region", when the jar is tripped. However, neither the magnitude of the sticking force nor the location of the stuck point/region are known in advance which make the task of jar optimization extremely difficult. The jar placement programs currently in use by the drilling industry observe the following guidelines in their approaches to seeking out the best possible location to run the jar in the drill string :

- The magnitude of the sticking force has to be greater than the trip threshold set for the jar, as otherwise the drill string would break free under the overpull force applied at the surface and the need for jarring does not arise.
- The stuck region is assumed to be in the BHA and usually near the bit, as it is the larger diameter drill collars which normally get stuck while pulling out.

Though these guidelines serve as a useful tool in developing better BHA designs and improved jar placement programs, they are nevertheless limited in their scope just because of the assumptions they are based on. To illustrate, the

sticking force could either be 10 times greater than the peak jarring force or of the same order of magnitude as the peak force; in each case however, one would obtain different results for the optimum jar location. Hence, one is led to believe that unless the nature or type of sticking most likely to be encountered is known apriori and its mechanism well understood in order to be able to predict the magnitude of the jarring force needed to overcome it, the jar placement programs will have to live with their limitations.

This thesis, therefore deviates from the commonly addressed problem of jar placement optimization and focuses instead on real issues of relevance to the drilling engineer on encountering stuck pipe. The aim is to extract useful information from *surface force and acceleration measurements* when the jar is tripped. In the jar placement optimization problem, it was unnecessary to track signals transmitted into the drill pipe and up to the surface because the drill pipe is much longer compared to the BHA and consequently, by the time the signal returns from the surface the primary jarring event[1] would be over. The emphasis of this research however, is to interpret surface responses when the jar is released to infer the nature of down-hole sticking.

Specifically, the following questions are raised:

- Is the location of the stuck region determinable from surface measurements?
- Can anything be inferred about the nature of the stuck region by inspection of surface responses ?... Does the stuck region behave as a conservative medium or is it absorptive in nature ?
- Is the jarring proving to be effective ?... Are we making progress towards freeing the drill string ?

All of the above mentioned points are of great importance to an on-site field engineer who when faced with a stuck pipe situation has to decide on the future

[1] Drill string Dynamics During Jar Operation: *Skeem et al* JPT Nov'79

course of action under time constraints. One could easily end up jarring for days without any significant improvement causing both loss of time and money if no method of evaluation of jarring effectiveness is available at hand. An attempt has been made in this thesis to shed light on the questions raised above and thus pave the way for a whole new perspective in looking at the jarring problem.

4.1 Modeling the Jarring event

The essential features of a drilling jar are the hammer, the anvil and the detent mechanism as was explained in chapter 2. In the event of stuck pipe, the hook load at the surface is increased (for up–hitting jars) sufficiently to cause the jar to trip. The amount of overpull[2] exerted must be below the allowable tensile load that the drill string can withstand safely. Once triggered, the hammer, all of a sudden goes from a pre–stressed state to a stress–free state and this sets up a stress release wave which propagates towards the surface. However, due to the cross-sectional discontinuity at the drill collar/drill pipe interface, this compressive relief signal is predominantly reflected as a tensile signal back towards the jar. As a result the hammer speed increases in a step-wise manner as each stress wave reflection arrives from the drill collar/drill pipe interface. Impact occurs when the distance between the released ends reaches the jar stroke length. The impact force magnitude, which can be several times the tripping threshold for the jar, depends on the velocities of the hammer and anvil at the time of impact. After impact stress waves propagate from the jar both upwards and downwards as the hammer and anvil are now in contact with each other. These stress waves travel to the stuck region and attempt to dislodge the drill string.

As a first step in the analysis of the jarring phenomenon, a suitable means to model the jarring event needs to be formulated. The hammer and the anvil

[2]Overpull = Hook load - String weight

can be modeled as uniform bars of identical material and cross-sectional areas, but dissimilar lengths. The jarring action can be considered as a longitudinal collinear impact between the hammer which has a finite uniform velocity at the time of impact and the anvil which is assumed to be *"stationary"*. Truly speaking, the anvil end starts to move downward immediately after the release of the jar for an interval of time during which the compressive wave travels down and is reflected from the stuck region back to the anvil. A relief wave then starts at the anvil since the anvil end is now a free boundary, and propagates towards the stuck region. This cycle repeats itself with the anvil end oscillating up and down until impact occurs. The effects of the motion of the anvil and the lower drill collars was first accounted for, by Kalsi et al [6] in their FEM approach to jarring analysis. They included the stuck location as one of the parameters in the determination of jarring force time histories in the BHA.

Our objective is to determine the location and the nature of the stuck region. Hence, it is not possible to take into account the anvil velocity *at the time of impact*, since it is a function of the length of the drill collar section between the stuck region & the anvil end, and also of the reflected stress wave from the stuck region. The magnitude of the reflection coefficient strongly depends on the type of sticking mechanism in play and therefore any assumption about the boundary condition at the stuck region would be erroneous. It is due to these constraints that the lower drill collars are assumed to be stationary at the time of impact. After impact, upward and downward propagating stress waves are created in the hammer, and the wave action occurring for $t > 0$ is governed by the interaction of these propagating waves with various boundaries and discontinuities including the junction between the hammer and the anvil. Since we have assumed that they are identical in cross-section, there is in effect no discontinuity and the stress wave propagates across the interface to the anvil and through the lower drill collars to the stuck location.

We therefore end up with two rectangular force pulses of equal magnitude and duration propagating away from the site of impact. These force pulses are

modeled as *dirac-delta* functions in the time domain. We shall see in a later section how the finite duration of the pulse is accounted for in our analysis.

By definition, the dirac-delta function satisfies the relationship

$$\delta(t) = 0, \quad t > 0 \tag{4.1}$$

and

$$\int_0^\infty \delta(t)dt = 1 \tag{4.2}$$

However, the impulse symbol $\delta(t)$ does not represent a function in the sense in which the word is used in analysis and the above integral is not a meaningful quantity until some convention for its interpretation is declared. Here, it is used to mean

$$\lim_{\tau \to 0} \int_0^\infty \tau^{-1} \prod \left\{ \frac{t - \frac{\tau}{2}}{\tau} \right\} dt$$

where $\tau^{-1} \prod \left\{ \frac{t-\frac{\tau}{2}}{\tau} \right\}$ is a rectangle function of height τ^{-1} and base τ and has unit area; as τ tends to zero, the magnitude of the pulse generated tends to ∞. The value of the integral, in the limit goes to unity. Also note that the lower limit of integration is 0 and not $-\infty$. This is because we do not have an input for $t < 0$.

In the use of digital signal processing techniques, we work in a discrete domain and hence one cannot achieve a true unit impulse. However, one can approach the ideal case by making the duration of the impulse sufficiently small.

The advantage of modeling the jarring event as a *unit force impulse* lies in the fact that, as the applied pulses are made shorter and shorter, the response settles down to a definite form. The *form of the response* is then *independent* of the *input pulse shape*, be it rectangular or triangular. This is because the high

frequency components, which distinguish the different applied pulses, produce negligible response.

4.1.1 Calculation of the Impulse Response

In chapter 3, we saw how a Transfer function between an output quantity of interest and an input *harmonic* excitation could be calculated using the Transfer matrix approach. The Transfer function $H(\omega)$ gives the *steady state* response of a system to a harmonic input. By calculating $H(\omega)$, we completely define the dynamic characteristics of the system over the frequency range of interest. In this subsection and the next, we seek to determine the response of the system to a unit *"Impulsive input"* of the form described in section (4.1). The response to a unit impulse at $t = 0$ is represented by the *Impulse response function* $h(t)$. For any physically realizable system, the effects never precede their causes and hence the response to an impulse at $t = 0$, must be zero for negative values of t:

$$h(t) = 0 \qquad t < 0 \tag{4.3}$$

Since complete information about either $H(\omega)$ or $h(t)$ fully defines the system characteristics, one must be able to derive one from the other. The two are related as follows:

$$H(\omega) = \int_0^\infty h(t)e^{-j\omega t}dt \tag{4.4}$$

$$h(t) = \frac{1}{2\pi}\int_{-\infty}^{\infty} H(\omega)e^{j\omega t}d\omega \tag{4.5}$$

Equations 4.4 and 4.5 represent the **Fourier Transform pair**

4.1.2 Numerical Implementation : The Discrete Fourier Transform

Since the experimental measurements at the rig and our numerical simulations are carried out using algorithms from digital signal processing, it is necessary to understand how they are actually implemented.

A typical function to be measured $x(t)$ (time history of force or acceleration at the surface, say) is fed through an A/D converter which samples the function at a series of regularly spaced times as shown in figure 4-1. If the sampling interval is Δt, then the discrete value of $x(t)$ at time $t = i\Delta$ is written as x_i and one obtains a *discrete time series* $\{x_i\}$.

In practice, we only have a finite record length of the sample function to work with. Hence, $x(t)$ is assumed to be a periodic function with period T.

We then have,

$$x(t) = \frac{a_0}{T} + \frac{2}{T}\sum_{n=1}^{\infty}\left[a_n \cos(n\omega_0 t) + b_n \sin(n\omega_0 t)\right] \tag{4.6}$$

where

$$\omega_0 = \frac{2\pi}{T} \tag{4.7}$$

$$a_n = \int_0^T x(t)\cos(n\omega_0 t)dt \tag{4.8}$$

$$b_n = \int_0^T x(t)\sin(n\omega_0 t)dt \tag{4.9}$$

If we define

$$C_n = a_n - jb_n \tag{4.10}$$

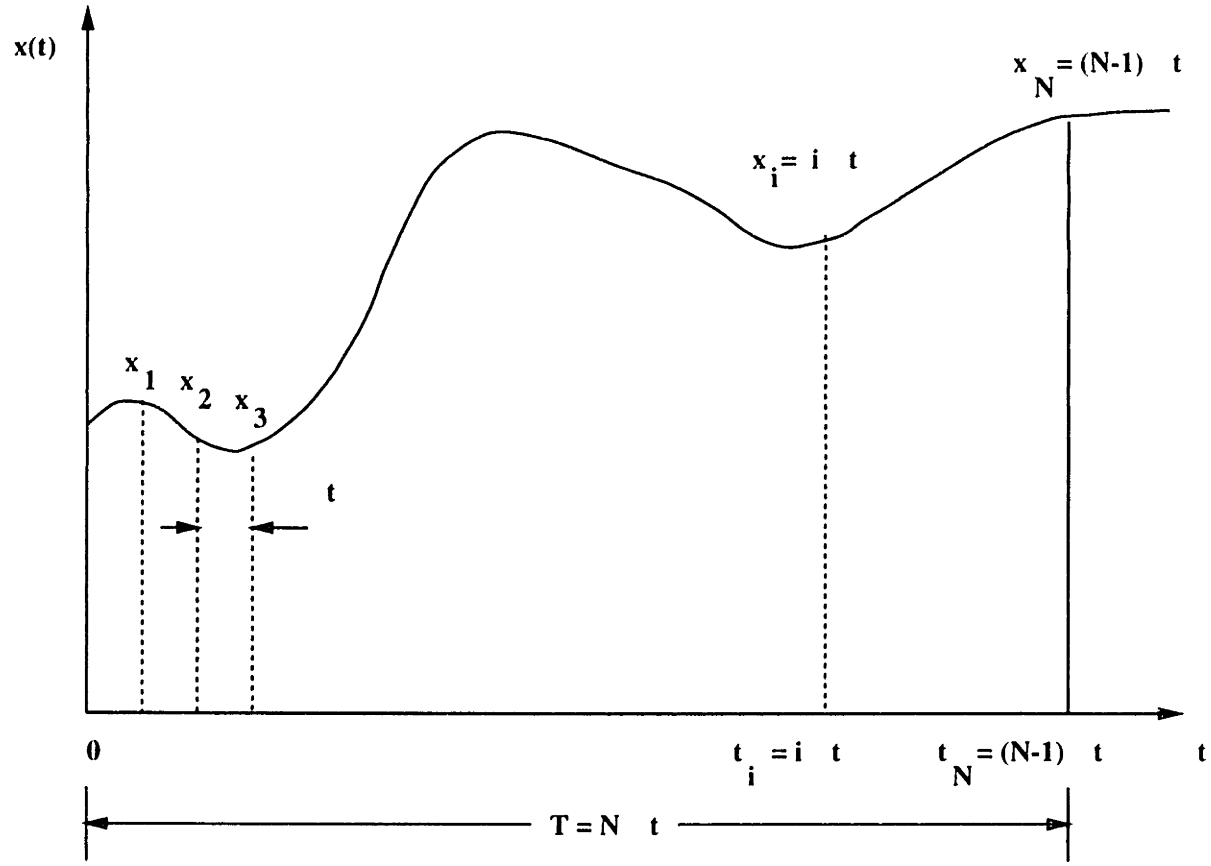

Figure 4-1: Discrete sampling of a continuous time function

we get using equations 4.6, 4.8 and 4.9,

$$C_n = \int_0^T x(t)e^{-jn\omega_0 t}dt \tag{4.11}$$

$$x(t) = \sum_{n=-\infty}^{n=\infty} \frac{C_n}{T} e^{jn\omega_0 t} \tag{4.12}$$

For a discrete time series, the integral in equation 4.11 is replaced by a summation and we obtain,

$$C_n = \sum_{i=0}^{N-1} x_i e^{-jn\frac{2\pi}{N\Delta t}i\Delta t}\Delta t \tag{4.13}$$

$$= \sum_{i=0}^{N-1} x_i e^{-jn\frac{2\pi}{N}i}\Delta t \tag{4.14}$$

Denoting,

$$X_n = \frac{C_n}{\Delta t} \tag{4.15}$$

$$W = e^{-j\frac{2\pi}{N}} \tag{4.16}$$

we get,

$$\boxed{\begin{aligned} X_n &= \sum_{i=0}^{N-1} x_i W^{in} \qquad n = 0...(N-1) \\ x_i &= \sum_{n=0}^{N-1} \frac{X_n}{N} W^{-in} \qquad i = 0...(N-1) \end{aligned}} \tag{4.17}$$

Equations 4.17 represent the **Discrete Fourier Transform pair** and form the bases of all calculations involving switching between time and frequency domains. One must however be careful to avoid **aliasing** while using discrete fourier transforms. Aliasing could occur in time/frequency domains depending on whether one proceeds from frequency domain to time domain or vice–versa. Aliasing can be avoided if,

- The sampling frequency (f_s) is greater than twice the highest frequency

component (f_h) in the signal, i.e.

$$f_s = \frac{1}{\Delta t} > 2f_h \tag{4.18}$$

- The time series is low pass filtered before digitizing to remove all frequency components greater than half the sampling frequency before beginning the analysis. The frequency $\frac{1}{2\Delta t}$ hz is also referred to as the *Nyquist frequency* or the *folding frequency.*

The discrete fourier transforms are implemented using the **F**ast **F**ourier **T**ransform algorithm (FFT). A complete discussion on the FFT can be found in *"Discrete Time Signal Processing"* by Oppenheim and Schafer [13].

4.1.3 Smoothing the Impulse Response

The Impulse response function is calculated by taking the **I**nverse **F**ourier **T**ransform of the Transfer function as was explained in subsection (4.1.1). Since we are computing the response to a Dirac-Delta function by taking the transform of a Frequency response function[3] which has information only up to a certain limiting frequency, there is an overshoot associated with any sharp change or discontinuity in the calculated impulse response. This is commonly referred to as the *Gibb's phenomenon.* The overshoot, amounting to 9 percent of the amount of discontinuity, remains at 9 percent as higher frequency components are included in the Transfer function, but the maximum is reached nearer to the discontinuity. The same applies to the minimum that occurs on the negative side.

To overcome this problem, several smoothing functions (*Window functions*) have been proposed, but which is the optimum ? The answer to this largely lies in the purpose of analysis and what we are trying to see in the calculated

[3] *Transfer function* and *Frequency response function* are used interchangeably

response. Although windowing the response is helpful for interpretation, there are a number of accompanying effects that may be introduced which distort the true picture. Some of these effects are listed below.

1. If there is a narrow feature of interest, then smoothing would give an erroneous value for the magnitude and a large value for the width and may also introduce a side–lobe structure. Thus, if the absolute strength measurement of the signal (say, the peak jarring force as measured at the surface) is of interest, then one must be cautious before proceeding to smooth the response.
2. If there are closely spaced features in the measured response, then smoothing would smear the features at the cost of resolution.

Thus, the decision to use a window and the type of window function to be used to smooth a response is an engineering judgement, based on experience and goes beyond the realms of mathematical analysis.

In our analysis, the principal use of a window is to reduce the high frequency oscillations (low pass filtering) in the impulse response caused as a result of the Gibb's phenomenon. A **Blackman window** was used to smooth the impulse response function. It is defined by the following equation :

$$\begin{aligned} w_n(t) &= 0.42 - 0.5\cos\left(\tfrac{2\pi n}{M}\right) + 0.08\cos\left(\tfrac{4\pi n}{M}\right); \qquad 0 \le n \le M \\ &= 0 \qquad\qquad\qquad\qquad\qquad\qquad\qquad\qquad\qquad\qquad\qquad\qquad\quad otherwise \end{aligned} \tag{4.19}$$

Of all the commonly used windows, the Blackman window has the lowest peak side–lobe amplitude with a reduction of -57 dB relative to the main lobe. The price paid for this enormous reduction achieved in the side–lobe levels is an increase in the width of the main lobe.

4.2 Response to a Realistic Jarring Signal

In practice, imperfections in the physical system and inadequacies of the governing theory cause deviations of the generated pulse from the ideal rectangular shape. In a realistic case, one would observe either of the following.

1. The corners of the pulse are rather rounded and the rise and fall of the pulse is nearly not as sharp. This is generally a result of the contact surfaces of the hammer and the anvil not being perfectly flat. It could also be due to the finite response time of the measuring system.
2. There are high frequency oscillations on the rise and fall of the pulse. This is a consequence of lateral inertia and other higher order effects neglected in the original development of the theory.

A complete review of the various theories on "Axial impact of rods" can be found in *Wave Motion in Elastic Solids* by Karl F. Graff [5].

In subsection (4.1.1), we saw how the response of a system to a unit impulse could be calculated. The impulse response function $h(t)$ gives the response at time t to a unit impulse applied at time $t = 0$. Any arbitrary input function $x(t)$ can be considered to be a continuous series of small impulses. For a linear system, using the *principle of superposition*, one can obtain the total response $y(t)$ by adding together the separate responses to all the "impulses" which constitute $x(t)$.

Thus one obtains,

$$y(t) = \int_0^\infty x(\tau)h(t-\tau)d\tau \tag{4.20}$$

Equation 4.20 is also known as the *convolution integral* or the *Duhamel's superposition integral* and is a very important input–output relationship for a linear system.

4.2.1 Modeling a Realistic Jarring Signal

It was pointed out in section 4.2 that higher order stress effects and lateral inertia effects cause a deviation of the pulse shape from that predicted by elementary theory. Aarrestad and Kyllingstad [1] have modeled the jarring cycle as consisting of five phases, namely,

Loading phase : An overpull is applied at the surface so that the axial force at the jar reaches the tripping threshold. This phase lasts a few seconds for mechanical jars.

Acceleration phase : This is also known as the pre-impact phase and is the time duration between the tripping of the jar and the time of impact of the hammer with the anvil. The duration of this phase ranges from 50 ms to 200 ms.

Impact phase : The jar hammer collides with the anvil during this phase lasting 50 ms to 100 ms.

Post–impact phase : It essentially consists of the ringing effects as a result of the impact delivered to the BHA. This phase lasts until the drill string has come to a complete rest again.

Resetting phase : The drill string is slacked off a little bit to have the jar reset and ready for a new jarring cycle.

In this thesis, we consider only the impact phase for modeling the realistic jarring signal as it is during this phase that the BHA is exposed to high stresses and the principal jarring event occurs. The impact phase is modeled by a discrete cosine function of the following form :

$$\begin{aligned} x_n(t) &= 0.5 - 0.5\cos\left[\tfrac{2\pi n}{M}\right] \quad 0 \le n \le M \\ &= 0 \qquad\qquad\qquad\qquad\quad otherwise \end{aligned} \tag{4.21}$$

where

M is the number of points chosen to represent the function and is a measure of the width of the pulse.

For a given resolution in the time domain, (determined by the FFT length and the frequency domain resolution) a high value of M yields a broad pulse, whereas a low value of M describes a narrow pulse. Thus, a suitable value of M can be chosen, depending on the duration of the impact phase to approximately represent the true jarring signal. Note that in any event, the amplitude of the signal represented is always unity. This can be scaled up or down based on the amplitude of the actual jarring force.

4.3 Modeling Damping in the Drillstring

The response of a drillstring to excitation is sensitive to damping. Kim Vandiver and Hyun Lee [15] have noted that the damping in the drillstring can be attributed to the following potential sources:

1. Internal hysteretic losses in the drillstring material.
2. Radiation losses to the surrounding formation.
3. Viscous losses due to drillstring movement relative to the wall and to the mud.
4. Damping mechanisms in the bit and in the rock.
5. Damping at the surface due to the draw works and the power swivel.

In the case of a stuck drillstring, only the hysteretic and radiation losses need be considered since the damping at the surface is relatively small. However, below a kilohertz, even sound radiation losses are negligible. For the purposes of this study, the internal damping in the drillstring was modeled as a *constant uniformly distributed damping* except in the stuck region, the models for which

will be discussed in the next section. Strictly speaking, the internal damping constant is a function of frequency, but since the frequency dependence is not exactly known, and to keep the analysis simple, a frequency independent distributed damping constant was chosen. The value of the damping constant selected was such that, a unit force impulse originating at the jar location would sustain itself through about two roundtrips of a free drillstring before dying away.

The damping in the drillstring during normal drilling operations would include all of the factors enumerated earlier. The damping at the bit is intimately connected with rock fracture mechanisms and is a topic under current research. In this thesis, the damping constant while drilling was taken to be the same as that when the drillstring was stuck, mainly for the purposes of simplicity and easy comparison of results between stuck and free cases.

4.4 Modeling the Stuck Region

In chapter 2, the various causes of stuck pipe were reviewed briefly. These causes have been known for a long time now; it has been the inability to model the sticking mechanisms and incorporate them into the programs currently used for jar placement optimization that have predominantly kept them from achieving complete success. In this section, two models for the stuck region are analysed:

1. **The Distributed Damping Model**
2. **The Distributed Stiffness Model**

Both these models represent ideal cases. In the *distributed damping* model, the stuck region is thought of as a purely dissipative[4] region which serves to absorb the energy input as a result of jarring. Consequently, very little energy reaches the surface. The distributed stiffness model[5] on the other hand models

[4] *Differentially stuck pipes could be modeled as purely absorptive regions as a first approximation*
[5] *Keyhole seating could be modeled as a localized region of high stiffness*

the stuck region as a conservative medium. The energy may be either reflected or transmitted but is ultimately conserved. We shall see how modeling the stuck region as either of the extreme cases (distributed stiffness or distributed damping) effects the response at the surface. In reality, the stuck region behaves as some combination of distributed damping and distributed stiffness, but we shall confine ourseves to the ideal cases in this thesis.

4.4.1 The Distributed Stiffness Model

In the distributed stiffness model, the stuck region is assumed to be constrained by a set of springs uniformly distributed along its length. The spring constant together with the stuck length serves as a measure of the force required to cause a unit displacement of the BHA at the stuck region. Hence, one can consider the springs to be an *elastic foundation* of a certain elastic modulus. A schematic of the model is shown in figure 4-2 on page 61

4.4.2 The Distributed Damping Model

In the distributed damping model of the stuck region, the stuck region is assumed to be a dissipative region and is modeled by a set of dashpots uniformly distributed along the length of the stuck region. The damping constant and the length over which it is distributed serve as a measure of the force required to impart a unit velocity to the BHA at the stuck region. A schematic of the model is shown in figure 4-3 on page 62.

4.5 The Dispersion Relation

The dispersion relation for axial wave propagation in a rod with distributed stiffness and distributed damping as given by equation 3.7 on page 28 is

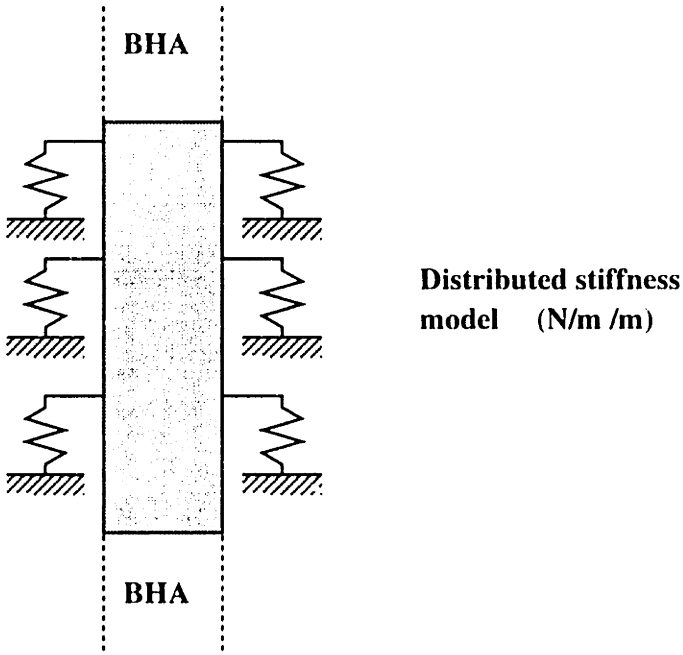

Figure 4-2: Distributed stiffness model of the stuck region

$$\begin{aligned} k^2 &= \left(\frac{\omega^2}{c^2} - \frac{K}{EA}\right) - i\left(\frac{R\omega}{EA}\right) \\ &= \frac{\omega^2}{c^{*2}} \end{aligned} \tag{4.22}$$

The most obvious result of adding distributed stiffness or distributed damping is that the major characteristic of the solution to the wave equation is some type of pulse distortion. The dispersion relation gives us an insight into the mechanism of pulse distortion. A harmonic wave of frequency ω can propagate only at a specific velocity c^*[6]. Thus, if we consider a sharp pulse at a given instant of time to be a Fourier superposition of harmonic waves; then as time advances, each Fourier component of the original pulse propagates with its own individual velocity. The various components become increasingly out of phase relative to one another so that the original pulse shape becomes increasingly

[6]Note that c^* is determined by equation 4.22, whereas c is defined by equation 3.2 on page 27

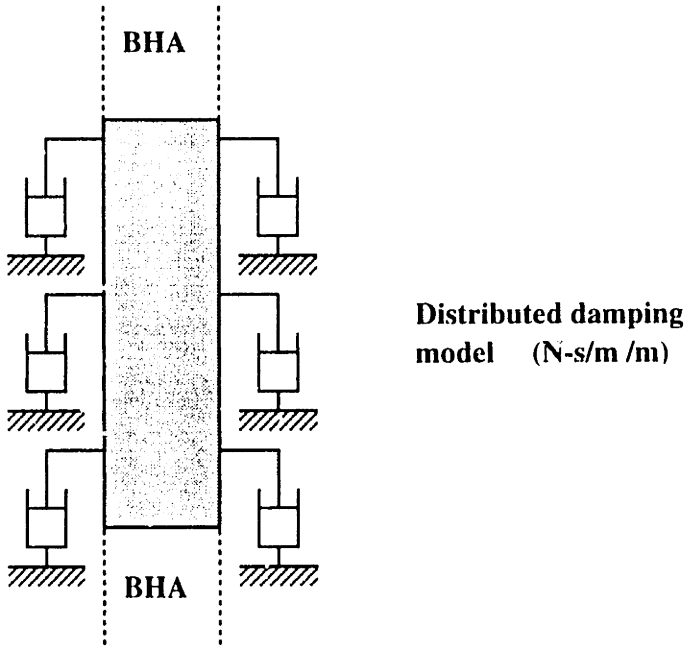

Figure 4-3: Distributed damping model of the stuck region

distorted.

The preceding interpretation also is the basis for the fact that no distortion occurs, if distributed stiffness and distributed damping are absent. While the direct prediction of this lack of distortion is given by the D'Alembert's solution to the wave equation, the indirect prediction arises due to the fact that the frequency, wave number and the wave velocity are related by $\omega = kc$, where c is a constant. Thus, each harmonic component propagates with the same velocity, so that the phase relationships of an original Fourier superposition are maintained for all time. This can be seen by setting $K, R = 0$ in equation 4.22.

In the following subsections we shall see the relevance of the dispersion relation to our models of the stuck region.

4.5.1 Dispersion Relation for the Stuck Region modeled as Distributed Stiffness

In the distributed stiffness model, the damping constant in the stuck region was chosen to be the same as in the rest of the drillstring. The order of magnitude of the damping constant is much smaller than the order of magnitude of the distributed stiffness. The value of the damping constant selected is consistent with the discussion in section 4.3 on damping in drillstrings. In this case, the dispersion relation can be approximated by

$$k^2 = \left(\frac{\omega^2}{c^2} - \frac{K}{EA}\right) \tag{4.23}$$

Thus,

$$k = \left(\frac{\omega^2}{c^2} - \frac{K}{EA}\right)^{\frac{1}{2}} \tag{4.24}$$

The above roots are real if the quantity in parentheses is positive. We know that the solution to the wave equation given by equation 3.1 is of the form $\sim\ e^{i(\omega t \pm kx)}$. Therefore, the two roots yield leftward or rightward propagating waves depending on the sign selected.

If $\left(\frac{\omega^2}{c^2} - \frac{K}{EA}\right) < 0$, then the wave number given by equation 4.24 is imaginary. Then the solution is of the form $\sim\ e^{\pm\bar{k}x}e^{i\omega t}$, where $\bar{k}^2 = -k^2$. This corresponds to a spatially varying but non-propagating disturbance.

The special case when $\left(\frac{\omega^2}{c^2} - \frac{K}{EA}\right) = 0$ ($c^* = 0$), represents a transition from propagation to non-propagation. In this case, $k = 0$ and $\omega_c = c\sqrt{\frac{K}{EA}}$. The solution to the wave equation is then of the form $\sim e^{i\omega_c t}$. The frequency ω_c is called the *cut-off frequency* of the propagating mode.

Frequency Spectrum for the Stuck Region modeled as Distributed Stiffness

A useful way to display the dispersion relation for easier interpretation is to plot the frequency versus the wave-number. Such a plot is also known as the *frequency spectrum* of the system. To plot the frequency spectrum, refer to equation 4.24. The frequency is assumed to be real and positive. It was shown earlier that k is imaginary for $\omega < \omega_c$ and real for $\omega > \omega_c$. Since the spectrum is symmetric with respect to the $Re(k) = 0$ and $Im(k) = 0$ planes, it suffices to present a two–dimensional plot containing the ω, $Re(k) > 0$ and $Im(k) > 0$ axes.

The results are shown in figures 4-4 and 4-5 on pages 66 and 67 for a 6.25″ drill collar and a 4.64″ drill pipe respectively. These represent the drill collar and drill pipe diameters for a typical drillstring. The stiffness values selected range from that of a very soft formation to that of a very hard formation. A small value of distributed damping was included to model the internal damping in the drillstring; but this does not affect the dispersion relation as can be seen in the figures. The data used for plotting the frequency spectrum is given below.

$$
\begin{aligned}
E &= 2.0417 \times 10^{11}\ N/m^2 && : \text{ Young's modulus for steel} \\
\rho &= 7.850 \times 10^{3}\ kg/m^3 && : \text{ Density of steel} \\
R &= 110\ N - s/m\ /m && : \text{ Internal damping in drillstring} \\
c &= \sqrt{\frac{E}{\rho}} && : \text{ Axial wave propagation speed in steel} \\
&= 5100\ m/s
\end{aligned}
$$

Distributed Stiffness K N/m $/m$	Remark	Symbol
1.0×10^4	$\ll$ Rock stiffness	-
1.0×10^7	$\sim$ Rock stiffness	-·
1.0×10^8	$>$ Rock stiffness	--
1.0×10^9	$\gg$ Rock stiffness	:

	Area	Remark
case 1	$A_1 = 0.01579\ m^2$	Cross-sectional area of BHA 6.25″ DC
case 2	$A_2 = 0.00349\ m^2$	Cross-sectional area of drill pipe 4.64″ DP

Discussion :

The frequency range selected was from 0.2 Hz to 819.2 Hz with a step size of 0.2 Hz. The curves or branches in the real plane are hyperbolas, while the imaginary branches are ellipses. The line $K = 0$ is the non-dispersive result for axial wave propagation in a rod. This wave number has a *non-zero* real part and a *zero* imaginary part over all frequencies. This implies that all frequencies propagate and there is no attenuation in the wave motion. However, as the distributed stiffness is increased, it can be noticed that only frequencies above a cut-off frequency propagate, while those below it undergo attenuation. Furthermore, for a given value of distributed stiffness, the cut-off frequencies are *inversely* proportional to the area of cross-section. The values of the cut-off frequencies for the two cases are given below.

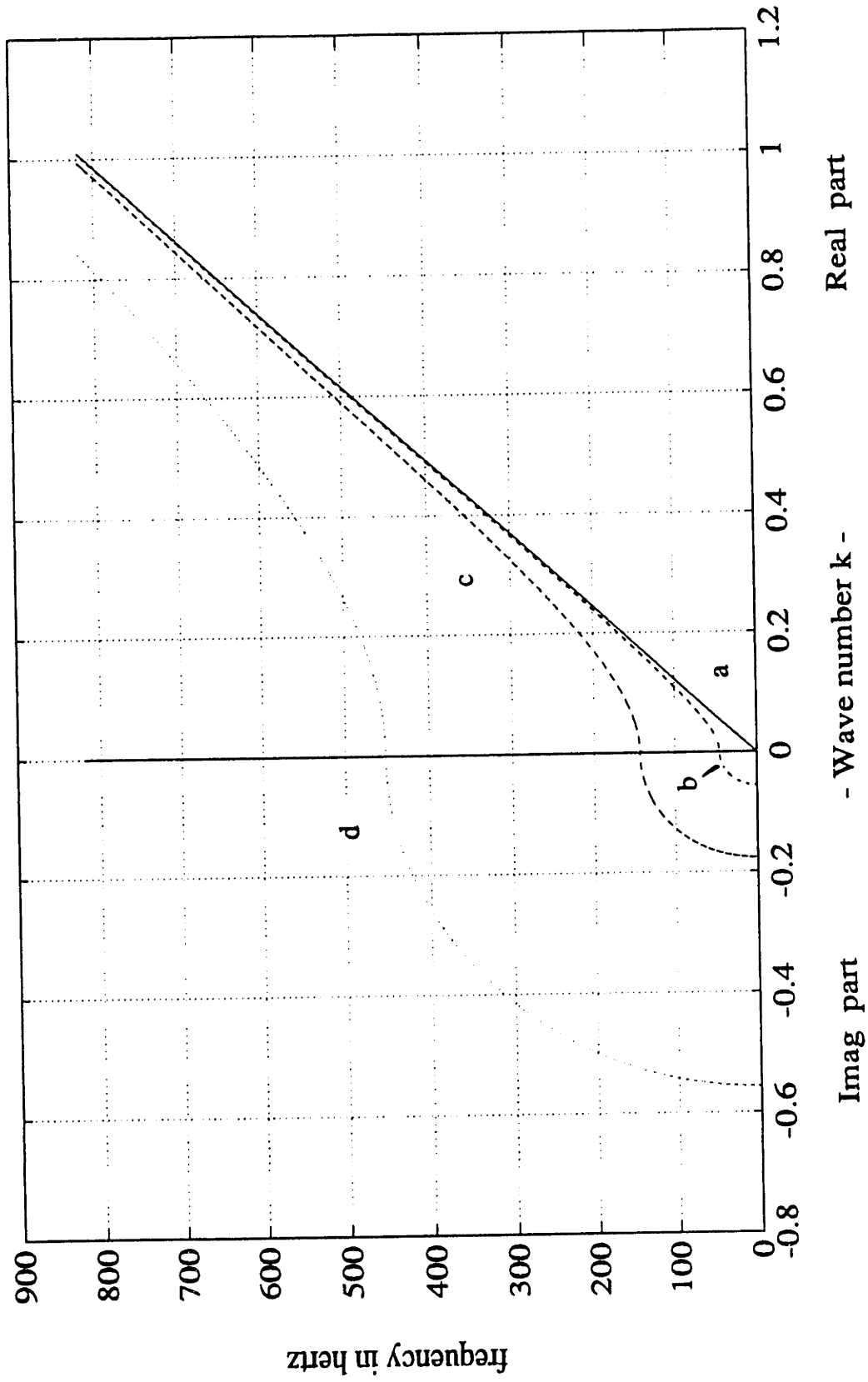

Figure 4-4: Wave number k versus frequency ω for various levels of distributed stiffness (6.25" DC)

a) – $K = 1.0 \times 10^4 N/m\ /m$ b) –· $K = 1.0 \times 10^7 N/m\ /m$

c) –– $K = 1.0 \times 10^8 N/m\ /m$ d) : $K = 1.0 \times 10^9 N/m\ /m$

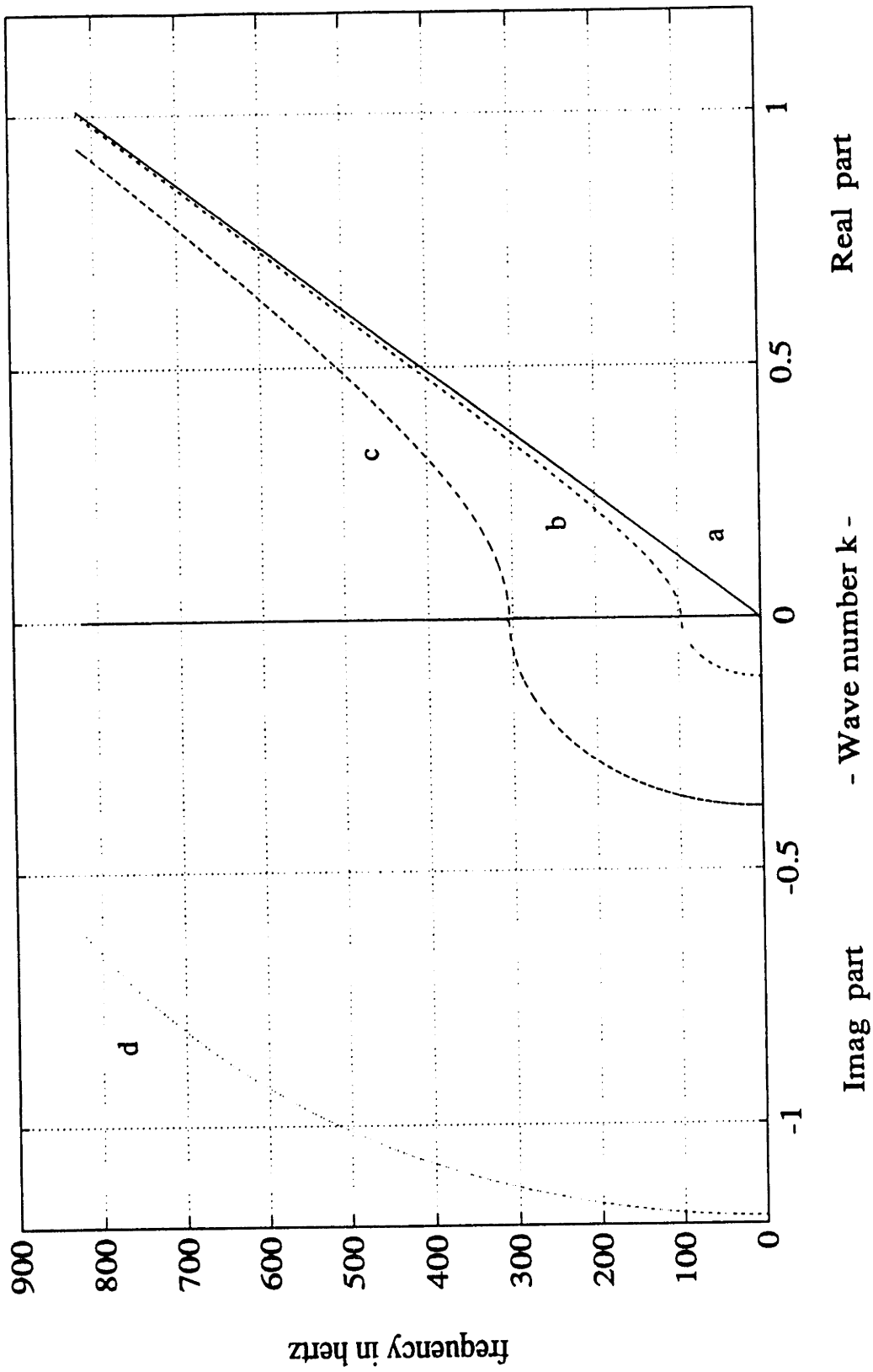

Figure 4-5: Wave number k versus frequency ω for various levels of distributed stiffness $(4.64''\ DP)$

a) - $K = 1.0 \times 10^4 N/m\ /m$ b) -· $K = 1.0 \times 10^7 N/m\ /m$

c) -- $K = 1.0 \times 10^8 N/m\ /m$ d) : $K = 1.0 \times 10^9 N/m\ /m$

	Stiffness N/m $/m$	Cut-off frequency f_c (Hz)
case 1	1.0×10^4	1.43
$A_1 = 0.01579\ m^2$	1.0×10^7	45.21
	1.0×10^8	142.96
	1.0×10^9	452.07
case 2	1.0×10^4	3.04
$A_2 = 0.00349\ m^2$	1.0×10^7	96.16
	1.0×10^8	304.07
	1.0×10^9	961.57

4.5.2 Dispersion Relation for the Stuck Region modeled as Distributed Damping

In the distributed damping model, the distributed stiffness in the stuck region is assumed to be zero, which is also the value assumed for the rest of the drillstring. Physically, this means that there are no external spring–like constraints (*Force* $\propto$ *displacement*) on the drillstring. The stuck region is modeled as a viscous damper (*Force* $\propto$ *velocity*) of varying distributed damping constants per unit length. Most of the energy input into the stuck region is dissipated as heat. In this case, the dispersion relation becomes

$$k^2 = \left(\frac{\omega^2}{c^2} - i\frac{R\omega}{EA}\right) \tag{4.25}$$

Thus,

$$k = \left(\frac{\omega^2}{c^2} - i\frac{R\omega}{EA}\right)^{\frac{1}{2}} \tag{4.26}$$

The above roots are in general complex. But, when the damping is very small, or more precisely, when $R\omega \ll EA$, the imaginary part in the parentheses can

be neglected and the dispersion relation reduces to the simple form

$$k = \pm\frac{\omega}{c} \tag{4.27}$$

Since the solution to the wave equation is of the form $e^{i(\omega t \pm kx)}$, the two roots yield leftward and rightward propagating waves depending on the sign selected.

Frequency Spectrum for the Stuck Region modeled as Distributed Damping

As in the stiffness case, the dispersion relation is plotted as shown in figures 4-6 and 4-7 for a 6.25″ drill collar and a 4.64″ drill pipe respectively. The damping values chosen ranged from the internal damping constant in the drillstring to very large damping values indicative of a highly dissipative region. The data used for plotting the frequency spectrum is given below.

$E = 2.0417 \times 10^{11}\ N/m^2$: Young's modulus for steel

$\rho = 7.850 \times 10^{3}\ kg/m^3$: Density of steel

$K = 0.0\ N/m\ /m$: Distributed stiffness in drillstring

$c = \sqrt{\frac{E}{\rho}}$: axial wave propagation speed in steel

$= 5100\ m/s$

Distributed Damping R $N-s/m\ /m$	Remark	Symbol
1.1×10^2	$\sim$ Internal damping	-
1.1×10^4	$>$ Internal damping	-·
1.1×10^5	$>$ Internal damping	--
1.1×10^6	$\gg$ Internal damping	:

	Area	Remark
case 1	$A_1 = 0.01579\ m^2$	Cross-sectional area of BHA 6.25″ DC
case 2	$A_2 = 0.00349\ m^2$	Cross-sectional area of drill pipe 4.64″ DP

Discussion :

The line $R = 1.1 \times 10^2\ N - s/m\ /m$ can be taken as the non-dispersive result since $R\omega \ll EA$ for the frequency range considered, which was fom 0.2 Hz to 819.2 Hz. The wave number corresponding to this damping constant can be seen to have a *non-zero* real part which is a linear function of frequency and a $\approx$ *zero* imaginary part over the entire frequency range. This means that all frequencies propagate and there is very little attenuation.

Case 1 :

When the damping is increased to $R = 1.1 \times 10^5\ N - s/m\ /m$, the real part of the wave number increases in the low frequency regime but approaches the non-dispersive result for higher frequencies. However, the imaginary part now has a finite non-zero value which assumes a constant value over higher frequencies. This implies that the attenuation is constant over a wide frequency range corresponding to the higher frequencies. As the damping constant is further increased to $1.1 \times 10^6\ N - s/m\ /m$, both the real and imaginary parts of the wave number increase significantly as can be seen from the figure. The imaginary part is a monotonic increasing function in the frequency range considered which shows that the high frequency waves attenuate much more than the low frequency waves. The significance of the real part of the wave number will be clear in the discussion on phase and group velocities in section (4.6).

Case 2 :

For a smaller cross–sectional area such as a drill pipe, the effects are similar to those in case 1, but vastly exaggerated.

Note that the main feature of the distributed stiffness model[7] (DSM) is the *presence of cut–off frequencies* which is absent in the distributed damping model[8] (DDM). Thus, if the excitation drops below the cut–off frequency, the wave number becomes imaginary and we obtain a spatially decaying, non–propagating *evanescent* mode. This mode doesn't represent a decay of energy which however was not the case with DDM where there was a dissipation of energy due to damping. The evanescent waves would always be confined to a region near the interface in a situation where we have an increase in distributed stiffness in going from one region to the other.

4.6 Phase velocity versus Group velocity

In section 4.5 and the succeeding subsections, the relationship between frequency and wave number for the DSM and the DDM of the stuck region was discussed. In this section, we endeavour to understand the significance of the frequency spectra for the two models.

4.6.1 Distributed Stiffness Model

It is possible to derive the phase velocity information from the frequency spectrum by the relation $\omega = kc^*$. Thus, for a given point on the real branch of the spectrum, the slope of the chord between the point and the origin is given by $\frac{\omega}{k} = c^*$, the phase velocity for that particular frequency. The phase velocity

[7] *Distributed Stiffness Model*: DSM
[8] *Distributed Damping Model*: DDM

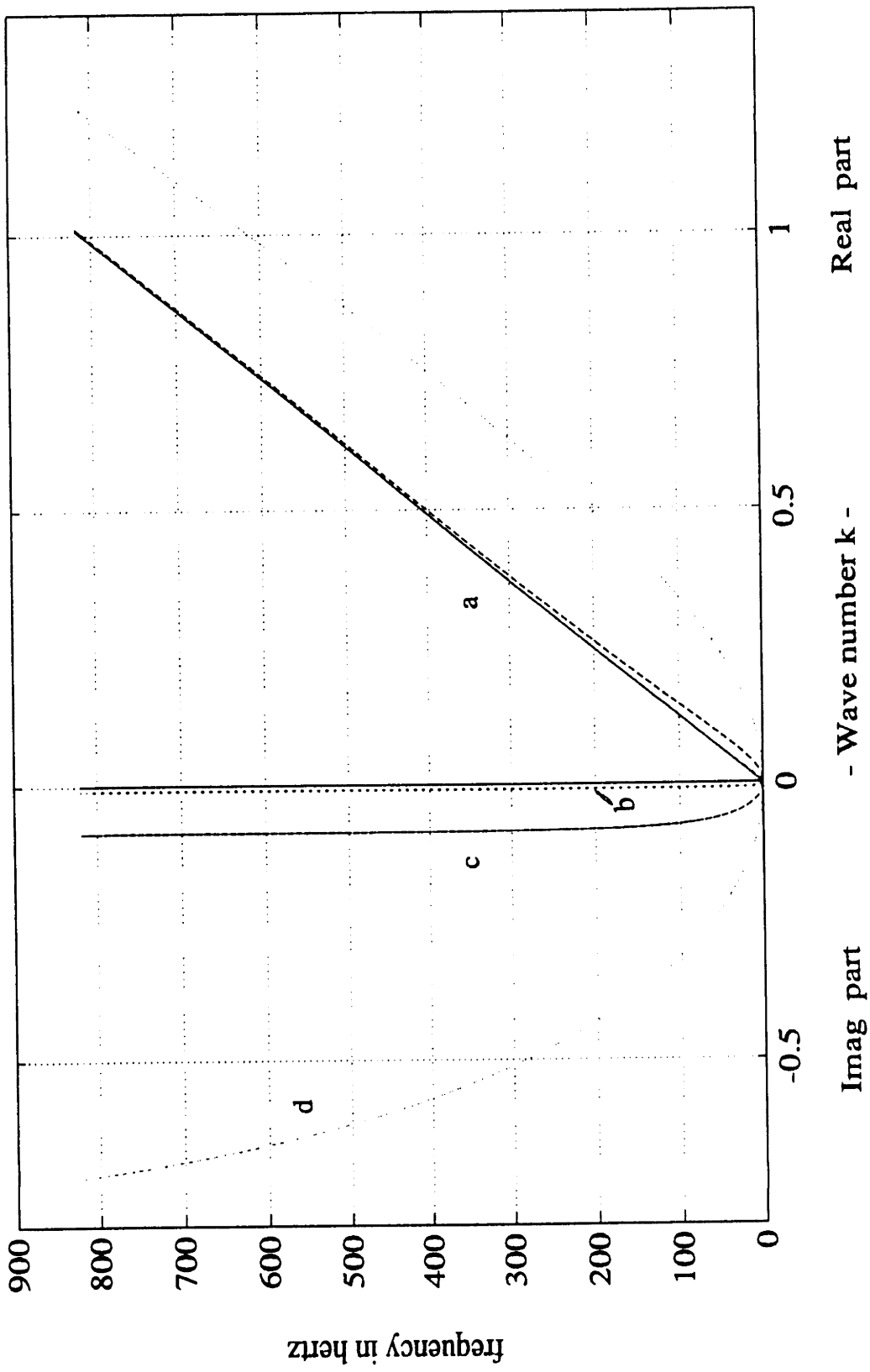

Figure 4-6: Wave number k versus frequency ω for various levels of distributed damping $(6.25''\ DC)$

a) - $R = 1.1 \times 10^2 N - s/m\ /m$ b) -· $R = 1.1 \times 10^4 N - s/m\ /m$

c) -- $R = 1.1 \times 10^5 N - s/m\ /m$ d) : $R = 1.1 \times 10^6 N - s/m\ /m$

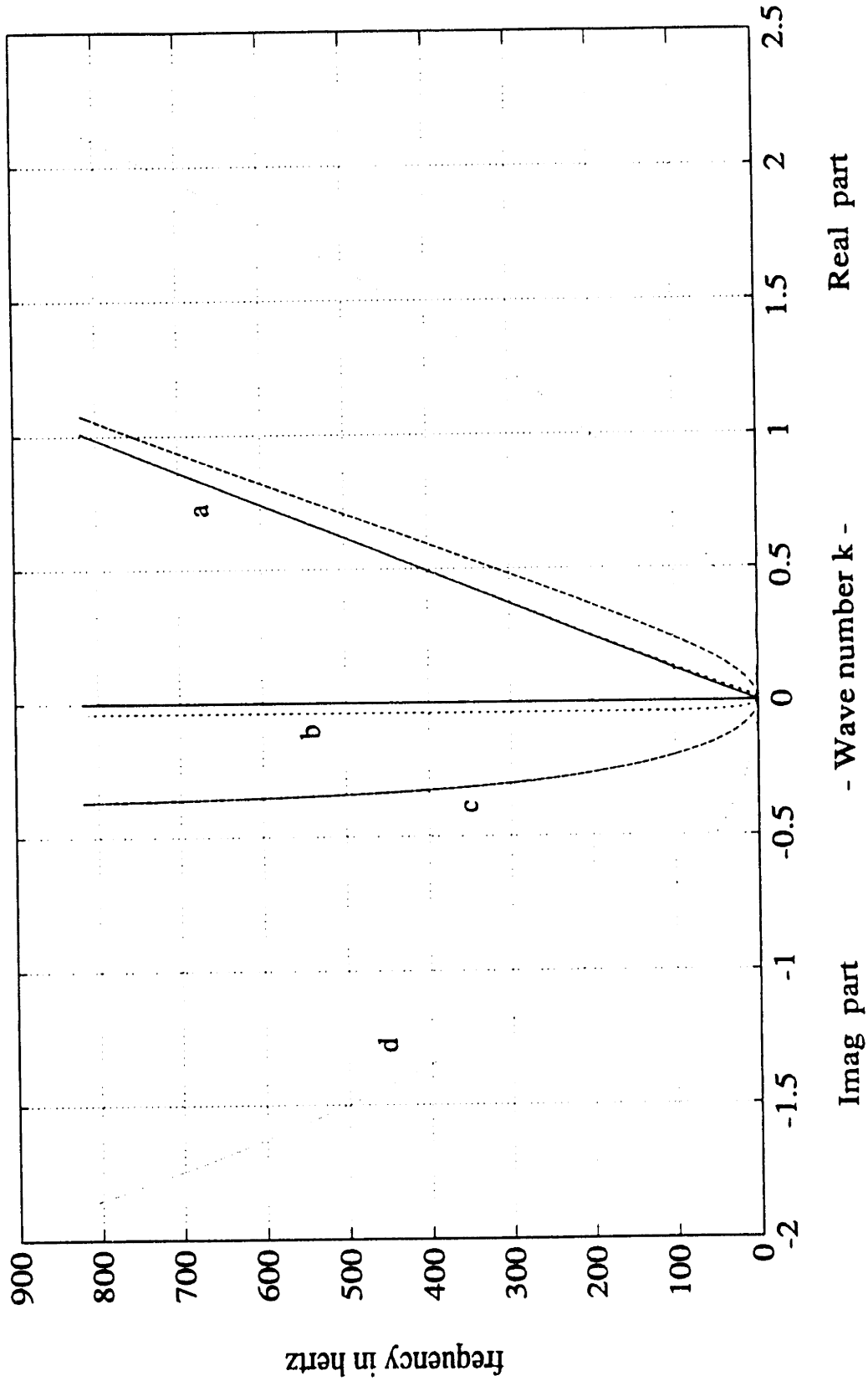

Figure 4-7: Wave number k versus frequency ω for various levels of distributed damping $(4.64''\ DP)$

a) – $R = 1.1 \times 10^2 N - s/m\ /m$ b) –· $R = 1.1 \times 10^4 N - s/m\ /m$

c) –– $R = 1.1 \times 10^5 N - s/m\ /m$ d) : $R = 1.1 \times 10^6 N - s/m\ /m$

versus frequency for different values of distributed stiffness have been plotted in figures 4-8 and 4-9 for a 6.25″ drill collar and a 4.64″ drill pipe respectively. It can be noticed that for a stiffness of 1.0×10^4 N/m $/m$, the curves are almost horizontal except at very low frequencies. These can therefore be considered to represent the non-dispersive rod where almost all frequencies propagate with the same velocity $c = 5100$ m/s. As the stiffness value is increased, the curves approach the classical result for higher frequencies corresponding to shorter wavelengths and large values of the wave number indicating that the stiffness effect is minimal. However, for small frequencies corresponding to small values of the wave number and hence long wavelengths, the phase velocity increases rapidly, approaching very large values as $\omega \rightarrow \omega_c$. Since there is a small amount of distributed damping present, the phase velocity does not go to ∞ in our case. Note that in the absence of damping, $k \rightarrow 0$, as $\omega \rightarrow \omega_c$, the cut-off frequency. The fact that $k = 0$ indicates uniform vibration as the wavelength is infinitely long. This uniform vibration may be interpreted as a disturbance traveling with infinite phase speed through the medium. It must be noted though that the group velocity is zero, which indicates that there is no energy propagation. The values of the cut-off frequency ω_c increase with increasing values of distributed stiffness for a given cross-sectional area.

The group velocity c_g is defined as the velocity of propagation of the modulation or the carrier impressed upon a train of waves having different frequency components. It can be shown that the group velocity is then given by the expression

$$c_g^* = \frac{\partial \omega}{\partial k} \tag{4.28}$$

A direct graphical interpretation of the group velocity can be made from the frequency spectrum. Since the frequency spectrum is a plot of ω versus k, the local slope of the tangent at any point of the spectrum yields the group velocity at that particular frequency. Plots of the group velocity versus frequency for

various levels of distributed stiffness are shown in figures 4-8 and 4-9 for two different cross–sectional areas. The group velocities are plotted only for frequencies above the cut–off frequency corresponding to a particular level of distributed stiffness because there is no *propagating wave* below the cut–off frequency.

It can be observed that for a very low level of distributed stiffness, ($K = 1.0 \times 10^4\ N/m\ /m$) the phase and group velocities are approximately the same since the dispersion relation is almost linear ($k = \omega c$). With increasing levels of distributed stiffness, the cut–off frequencies become larger, and the deviation from the linear relationship is conspicuous. However, the group velocities approach the phase velocities for large values of frequency, each tending asymptotically to the axial speed of propagation of sound in steel (5100 m/s).

4.6.2 Distributed Damping Model

The DDM of the stuck region is essentially a rod on a viscous foundation. The phase and group velocities as a function of frequency are plotted in figures 4-10 and 4-11 for typical BHA and drill pipe cross–sectional areas respectively. The phase velocities were determined by taking the slopes of the chords between points on the real branch of the spectrum and the origin. The group velocity as a function of frequency was found by taking the local slope of the tangent to the real part of the frequency spectrum. Thus, according to our definitions, we have the following relations

$$c_p = \frac{\omega}{Re(k)} \tag{4.29}$$

$$c_g = \frac{\partial \omega}{\partial Re(k)} \tag{4.30}$$

Note that c_p and c_g are real whereas c^* and c_g^* defined earlier are in general complex.

It has been assumed until now in our analyses that, the group velocity is actually

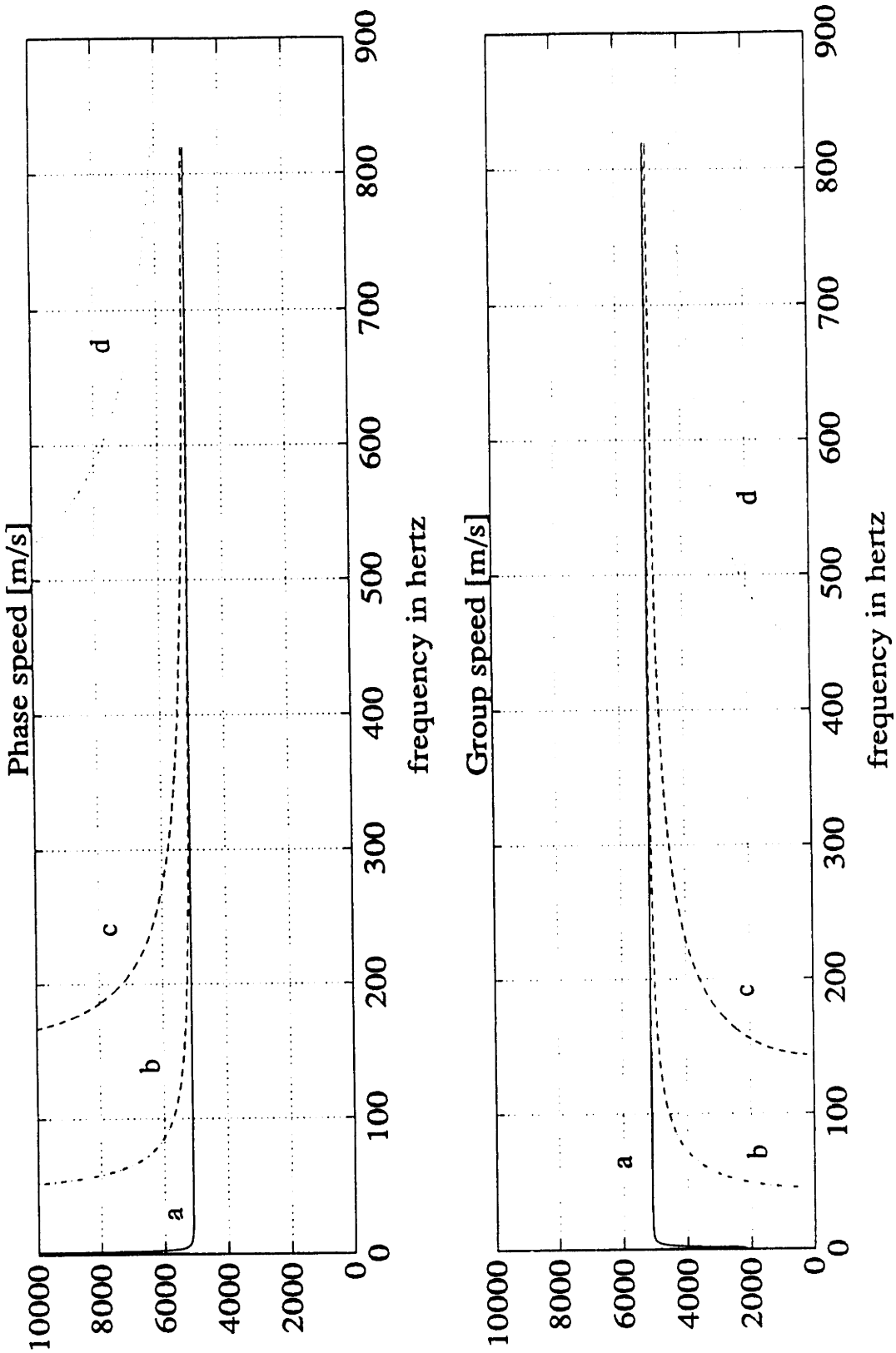

Figure 4-8: (6.25″ *DC*)

A. Phase speed c^* versus frequency ω for various levels of distributed stiffness

B. Group speed c_g^* versus frequency ω for various levels of distributed stiffness

a) – $K = 1.0 \times 10^4 N/m\ /m$ b) –· $K = 1.0 \times 10^7 N/m\ /m$

c) –– $K = 1.0 \times 10^8 N/m\ /m$ d) : $K = 1.0 \times 10^9 N/m\ /m$

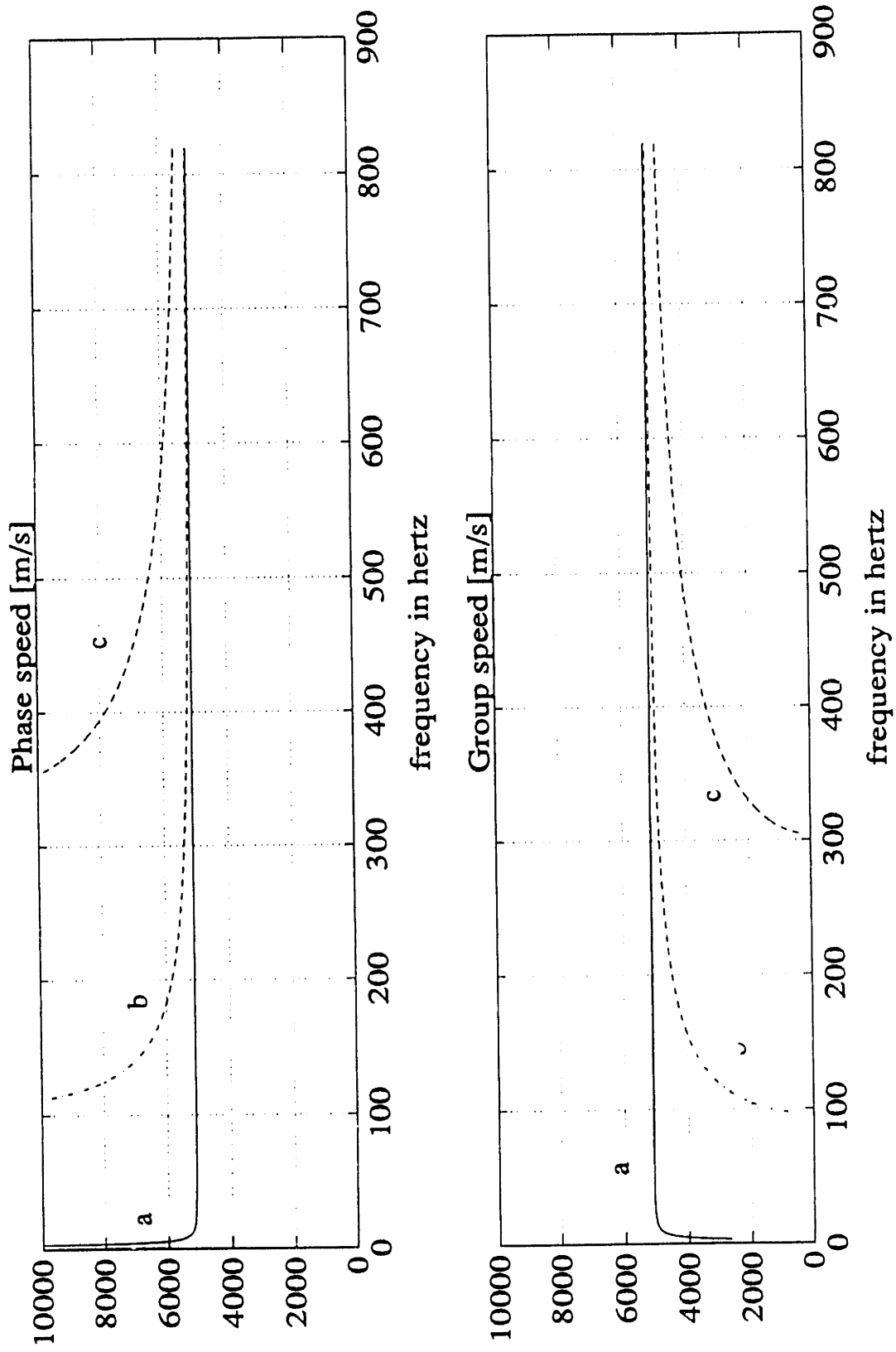

Figure 4-9: $(4.64''\ DP)$
A. Phase speed c^* versus frequency ω for various levels of distributed stiffness
B. Group speed c_g^* versus frequency ω for various levels of distributed stiffness
a) – $K = 1.0 \times 10^4 N/m\ /m$ b) –· $K = 1.0 \times 10^7 N/m\ /m$
c) –– $K = 1.0 \times 10^8 N/m\ /m$ d) : $K = 1.0 \times 10^9 N/m\ /m$

the velocity at which a finite signal propagates through a medium, but this is only an approximation. The signal is significantly distorted as it travels through the medium as can be noticed by the large imaginary parts in the wave number with increasing values of distributed damping. The signal velocity in this case becomes hard to define on account of the change in shape. This is especially true for an absorbing medium. Absorption is strongly frequency dependent and is associated with strong dispersion. For very low values of damping it can be seen that the phase and group velocities are each equal to the axial speed of propagation of sound in the material. In the case of a wide–band pulse, the problem of defining a group velocity is even more formidable. In such a case, an approximate method known as the *Saddle Point Method* is employed.

In the case of a wide–band excitation with dispersion but no absorption, another method called the *Stationary Phase Method* is used. This method is based on the principle that the Fourier representation of a pulse is comprised of waves of all frequencies and wave lengths. Initially, the different components superimpose to produce the pulse. At any subsequent time, the existing disturbance is obtained by summing the contributions of the propagating harmonic components. Thus, one can find positions and times at which a large number of components have the same phase and reinforce each other, while other elements are practically destroyed by interference. In the case of dispersion without absorption, the saddle point method and the method of stationary phase agree. For a detailed analysis, one can refer to [3] and [5].

4.7 Modeling the Boundaries

The boundary conditions are modeled based on information derived from Hyun Lee's thesis [8] and the paper by Clayer, Vandiver and Lee [15]. The bottom boundary condition is considered for two cases; normal drilling operation and when the drillstring is stuck at a point or along some length of the BHA. The

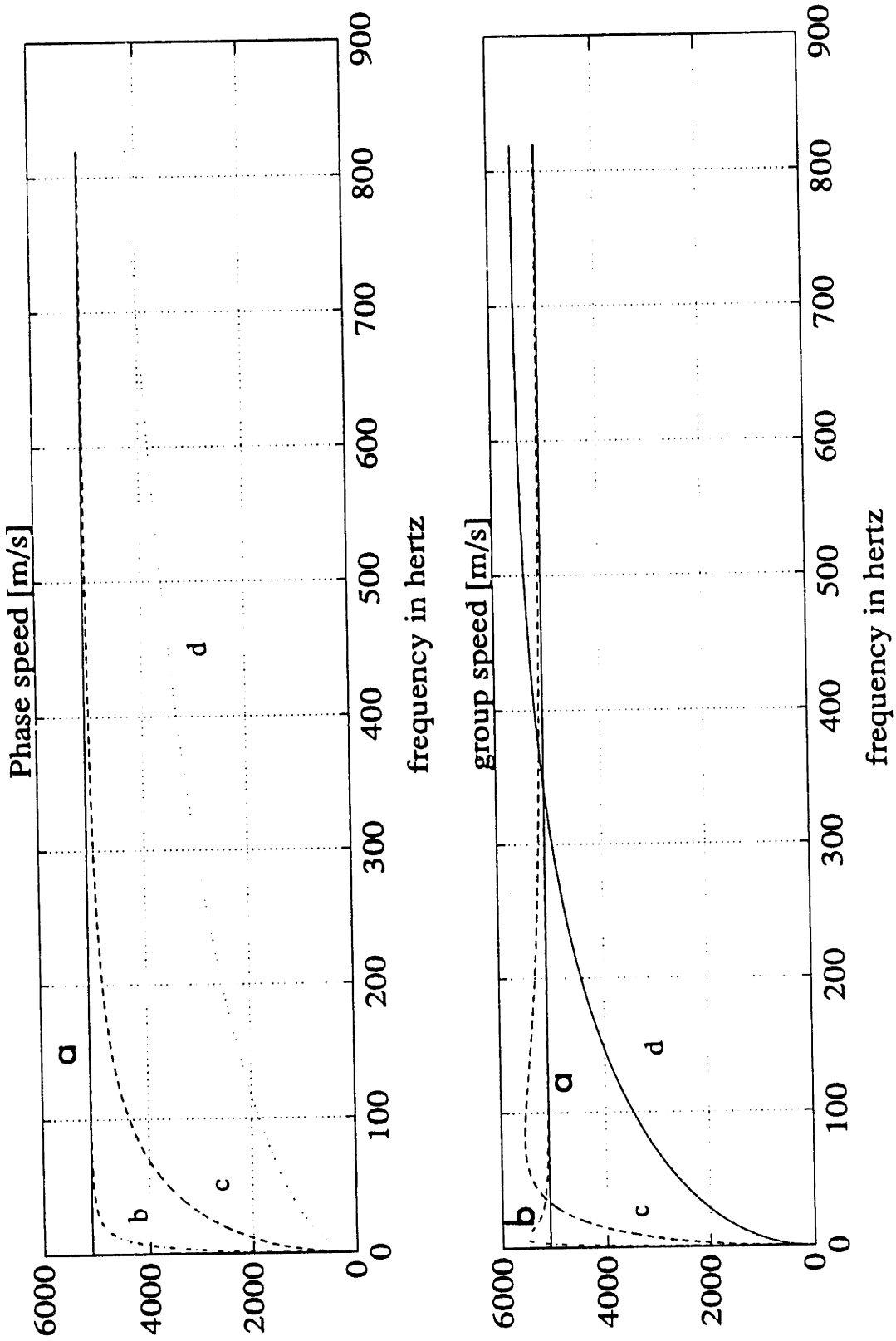

Figure 4-10: $(6.25''\ DC)$
A. Phase speed c_p versus frequency ω for various levels of distributed damping
B. Group speed c_g versus frequency ω for various levels of distributed damping
a) - $R = 1.1 \times 10^2 N - s/m\ /m$ b) $-\cdot$ $R = 1.1 \times 10^4 N - s/m\ /m$
c) $--$ $R = 1.1 \times 10^5 N - s/m\ /m$ d) : $R = 1.1 \times 10^6 N - s/m\ /m$

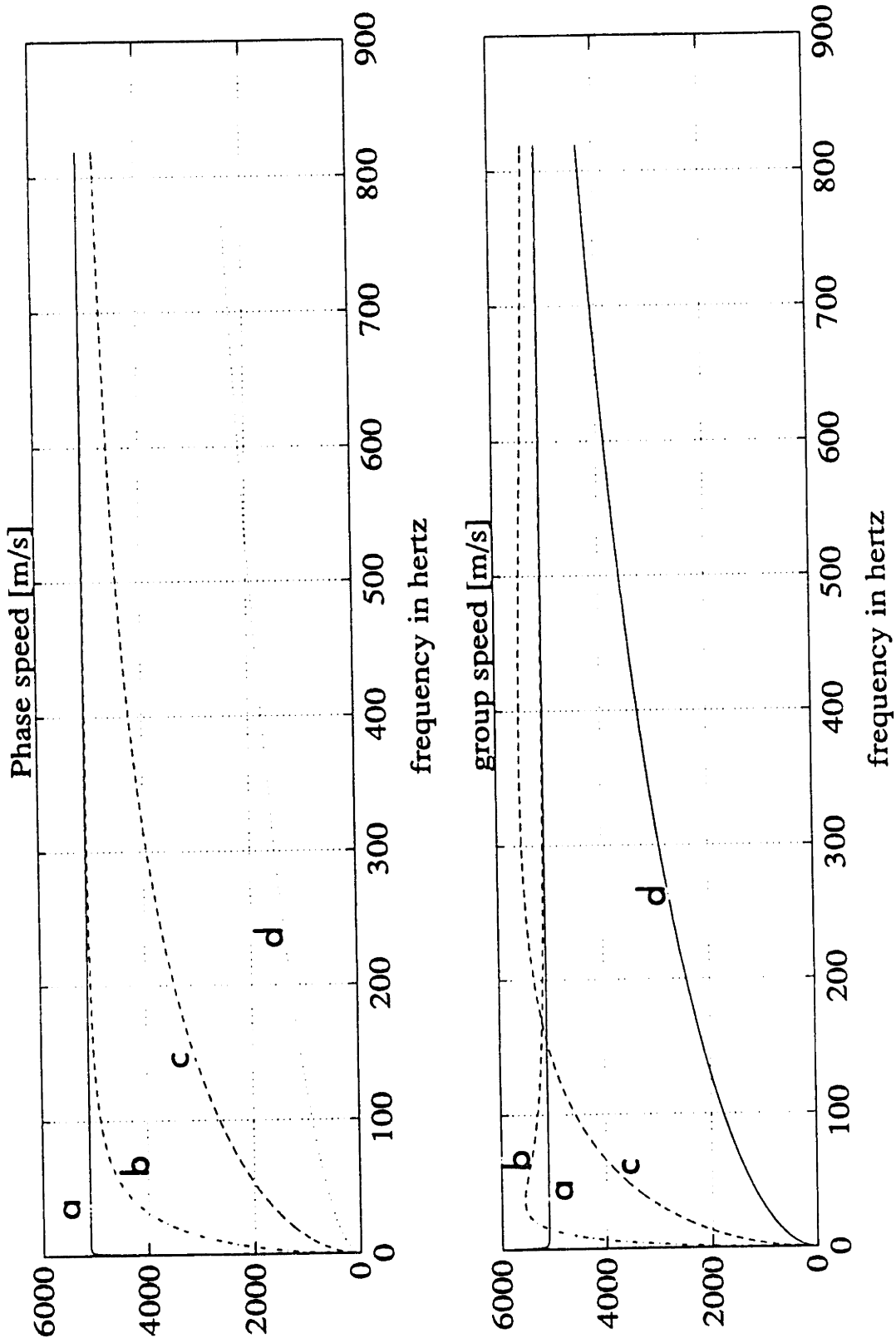

Figure 4-11: $(4.64''\ DP)$
A. Phase speed c_p versus frequency ω for various levels of distributed damping
B. Group speed c_g versus frequency ω for various levels of distributed damping
a) - $R = 1.1 \times 10^2 N - s/m\ /m$ b) $-\cdot$ $R = 1.1 \times 10^4 N - s/m\ /m$
c) $--$ $R = 1.1 \times 10^5 N - s/m\ /m$ d) : $R = 1.1 \times 10^6 N - s/m\ /m$

topside boundary condition takes into account the dynamic properties of the swivel, derrick and drawworks.

4.7.1 Modeling the Topside Boundary Condition

The surface boundary condition is modeled as a mass–spring–damper element as shown in figure 3-2. The values of the mass, spring and damper elements were chosen based on the measurement of the drive point function between the force and acceleration at the surface. The drive point function between force and acceleration is independent of the composition of the drillstring below the measurement point and depends on the dynamic properties of the system above the measurement point as long as the excitation comes from below the response location (the bit in this case).

4.7.2 Modeling the Bottom Boundary Condition

Normal Drilling Operation

The bottom boundary condition is modeled by an equivalent spring and damper placed in parallel between the bit and a fixed bottom reference point. The compliance of the rock is taken into account by the spring stiffness value; the damper represents the energy loss mechanisms related to rock fracture.

Stuck Condition

The drillstring could get stuck under any of the following conditions.

1. *Drillstring is stationary :* This usually happens in the case of differential sticking. In this case the drillstring can neither be rotated nor moved up or down. This type of sticking can be avoided if early warning signs are heeded and suitable action is taken.

2. *Tripping out :* Encountering stuck pipe while tripping out is the most common occurence in the drilling industry. The reasons could be numerous; from keyhole sticking to collapse of the surrounding formation.

In this thesis, we consider the case when sticking occurs while tripping out. The bit at the time of sticking is modeled as a *free boundary*, as the bit is off–bottom at such a time.

4.8 Modeling the source

"Modeling the source" refers to modeling the excitation at the bit at the time of normal drilling operation. As described by Hyun Lee [8] and Kim Vandiver [15], the action of the bit is modeled as a relative displacement source inserted between the bit and the flexible formation. As the formation impedance becomes small (soft rock) compared to the impedance of the drillstring, the surface response becomes small as most of the energy is utilized in crushing the rock. On the other hand, if the formation impedance is large (hard rock) relative to the impedance of the drillstring, most of the energy is input into the drillstring. If one were to use a force input at the bit, then the resonances of the drillstring would correspond to a free boundary condition at the bit. An absolute displacement excitation of the the bit would yield resonances of the drillstring corresponding to a fixed boundary condition at the bit. These represent the extremes of the possible boundary condition at the bit. Thus the relative displacement excitation represents an intermediate case between the two extremes.

Chapter 5

Implementation and Results

In chapter 4, the tools and models needed for the analysis of jarring dynamics of drillstrings were developed. In this chapter, we shall use these models to analyze a few specific cases.

5.1 Reflection and Transmission of a Force Impulse at a Barrier

In order to better understand the dynamics of drillstrings while jarring, and to identify the location and type of sticking mechanism by way of interpretation of signatures at a surface measurement location, it is necessary to analyze the nature of the reflected and transmitted *force* pulse through a stuck region of finite length. The stuck region is thought of as a barrier and the sticking mechanism within this barrier is modeled either as distributed stiffness or distributed damping as was detailed in chapter 4. The length of the barrier is an indication of the stuck length and can be varied depending upon the type of sticking mechanism considered. For example, keyhole sticking would be modeled as a very high stiffness concentrated at a point or over an exceedingly small length, whereas differential sticking would be modeled as distributed damping over a

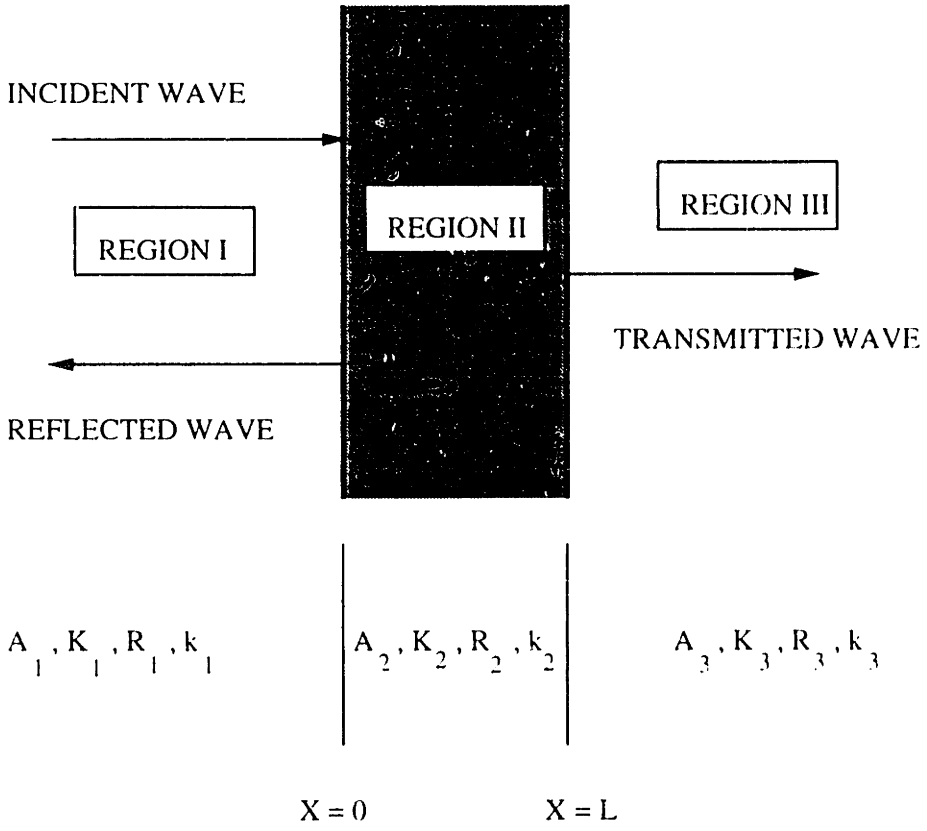

Figure 5-1: Reflection and Transmission of a Force Impulse at a barrier

finite length. It must be noted however, that these ideal models are just a first step towards understanding the different sticking mechanisms and in a realistic situation, the stuck region would behave as some combination of distributed stiffness and distributed damping.

We now consider a case wherein we have two semi-infinite regions (Region I and Region III) separated by a barrier (Region II) of length L as shown in figure 5-1. The plane $x = 0$ represents the boundary between region I and region II. Similarly, the plane $x = L$ represents the boundary between region II and region III. The parameters governing the the three regions are as follows :

A_1, A_2, A_3 : Areas of cross–section of regions I, II and III

K_1, K_2, K_3 : Distributed stiffness in regions I, II and III

R_1, R_2, R_3 : Distributed damping in regions I, II and III

k_1, k_2, k_3 : Wave number in regions I, II and III

When an incident signal in region I arrives at the boundary between regions I & II, some of the energy is reflected and some of it is transmitted into region II. The portion of the wave transmitted proceeds through region II to interact with the boundary between regions II & III where again, a portion of the energy is reflected and some transmitted into region III. The reflected wave then proceeds back to the interface between regions I & II and the whole process is repeated.

The incident **displacement** wave can be assumed to be of the form

$$u_i = \tilde{U}_i e^{j(\omega t - k_1 x)} \tag{5.1}$$

The various transmitted and reflected waves now combine so that in the steady state condition, the wave reflected into region I can be represented as

$$u_r = \tilde{U}_r e^{j(\omega t + k_1 x)} \tag{5.2}$$

The transmitted and and reflected waves in region II can be represented by

$$u_a = \tilde{U}_a e^{j(\omega t - k_2 x)} \tag{5.3}$$

$$u_b = \tilde{U}_b e^{j(\omega t + k_2 x)} \tag{5.4}$$

The wave transmitted into region III is given by

$$u_t = \tilde{U}_t e^{j(\omega t - k_3 x)} \tag{5.5}$$

Here

$\tilde{U}_i$: Complex displacement amplitude of the incident wave in region I

$\tilde{U}_r$: Complex displacement amplitude of the reflected wave in region I

$\tilde{U}_a$: Complex displacement amplitude of the transmitted wave in region II

$\tilde{U}_b$: Complex displacement amplitude of the reflected wave in region II

$\tilde{U}_t$: Complex displacement amplitude of the transmitted wave in region III

Associated with each of these *displacement* waves, one can define *force* waves as

$$\begin{aligned} f_i &= \tilde{F}_i e^{j(\omega t - k_1 x)} \equiv EA_1 \frac{\partial u_i}{\partial x} \\ f_r &= \tilde{F}_r e^{j(\omega t + k_1 x)} \equiv EA_1 \frac{\partial u_r}{\partial x} \\ f_a &= \tilde{F}_a e^{j(\omega t - k_2 x)} \equiv EA_2 \frac{\partial u_a}{\partial x} \\ f_b &= \tilde{F}_b e^{j(\omega t + k_2 x)} \equiv EA_2 \frac{\partial u_b}{\partial x} \\ f_t &= \tilde{F}_t e^{j(\omega t - k_3 x)} \equiv EA_3 \frac{\partial u_t}{\partial x} \end{aligned} \tag{5.6}$$

where

$\tilde{F}_i$: Complex force amplitude of the incident wave in region I

$\tilde{F}_r$: Complex force amplitude of the reflected wave in region I

$\tilde{F}_a$: Complex force amplitude of the transmitted wave in region II

$\tilde{F}_b$: Complex force amplitude of the reflected wave in region II

$\tilde{F}_t$: Complex force amplitude of the transmitted wave in region III

Continuity of displacement at $x = 0$ implies

$$u_i + u_r = u_a + u_b \tag{5.7}$$

which yields

$$\tilde{U}_i + \tilde{U}_r = \tilde{U}_a + \tilde{U}_b \tag{5.8}$$

Force balance at $x = 0$ implies

$$f_i + f_r = f_a + f_b \tag{5.9}$$

Using equations 5.1, 5.2, 5.3, 5.4 and 5.6, one obtains,

$$\tilde{U}_i - \tilde{U}_r = \left(\frac{A_2 k_2}{A_1 k_1}\right)(\tilde{U}_a - \tilde{U}_b) \tag{5.10}$$

Dividing equation 5.8 by 5.10, one obtains

$$\frac{\tilde{U}_i + \tilde{U}_r}{\tilde{U}_i - \tilde{U}_r} = \left(\frac{\tilde{U}_a + \tilde{U}_b}{\tilde{U}_a - \tilde{U}_b}\right)\left(\frac{A_1 k_1}{A_2 k_2}\right) \tag{5.11}$$

Similarly,

Continuity of displacement at $x = L$ implies

$$u_a + u_b = u_t \tag{5.12}$$

which gives

$$\tilde{U}_a e^{-jk_2 L} + \tilde{U}_b e^{jk_2 L} = \tilde{U}_t e^{-jk_3 L} \tag{5.13}$$

Force balance at $x = L$ implies

$$f_a + f_b = f_t \tag{5.14}$$

which gives

$$\tilde{U}_a e^{-jk_2 L} - \tilde{U}_b e^{jk_2 L} = \left(\frac{A_3 k_3}{A_2 k_2}\right) \tilde{U}_t e^{-jk_3 L} \tag{5.15}$$

Dividing equation 5.13 by 5.15, we get

$$\left(\frac{\tilde{U}_a e^{-jk_2 L} + \tilde{U}_b e^{jk_2 L}}{\tilde{U}_a e^{-jk_2 L} - \tilde{U}_b e^{jk_2 L}}\right) = \left(\frac{A_2 k_2}{A_3 k_3}\right) \tag{5.16}$$

We can define *Displacement Reflection* and *Transmission coefficients*

$$\tilde{R}_d = \frac{\tilde{U}_r}{\tilde{U}_i} \tag{5.17}$$

$$\tilde{T}_d = \frac{\tilde{U}_t}{\tilde{U}_i} \tag{5.18}$$

Define

$$\begin{aligned} r_1 &= A_1 k_1 \\ r_2 &= A_2 k_2 \\ r_3 &= A_3 k_3 \end{aligned}$$

Eliminating U_a and U_b from equations 5.11 and 5.16, and using the definition given by equation 5.17 for the displacement reflection coefficient $\tilde{R}_d$, we get

$$\boxed{\tilde{R}_d = \frac{\left(1-\frac{r_3}{r_1}\right)\cos k_2 L \; - \; j\left(\frac{r_2}{r_1}-\frac{r_3}{r_2}\right)\sin k_2 L}{\left(1+\frac{r_3}{r_1}\right)\cos k_2 L \; + \; j\left(\frac{r_2}{r_1}+\frac{r_3}{r_2}\right)\sin k_2 L}} \tag{5.19}$$

Using equations 5.13 & 5.15, and then eliminating $\tilde{U}_a$, $\tilde{U}_b$ using equations 5.8 & 5.10, the displacement transmission coefficient $\tilde{T}_d$ defined by equation 5.18 can be obtained as

$$\tilde{T}_d = \frac{(1-\tilde{R}_d)\cos k_2 L \;-\; j\frac{r_2}{r_1}(1+\tilde{R}_d)\sin k_2 L}{\frac{r_3}{r_1}(\cos k_3 L - j \sin k_3 L)} \tag{5.20}$$

Substituting for $\tilde{R}_d$ from equation 5.19, we get

$$\boxed{\tilde{T}_d \;=\; \frac{2\left(\frac{r_1}{r_3}\right)}{\left[2\cos k_2 L + j\left(\frac{r_1}{r_2}+\frac{r_2}{r_1}\right)\sin k_2 L\right](\cos k_3 L - j \sin k_3 L)}} \tag{5.21}$$

Equations 5.19 and 5.21 represent the most general relations for the displacement reflection and transmission coefficients. The values of the wave numbers in both these expressions are governed by the dispersion relations for those particular regions. If region I and region III are the same, as would be the case in a realistic situation when you are stuck along a certain length of the BHA, equations 5.19 and 5.21 would reduce to

$$\tilde{R}_d = \frac{j\left(\frac{r_1}{r_2}-\frac{r_2}{r_1}\right)\sin k_2 L}{2\cos k_2 L \;+\; j\left(\frac{r_1}{r_2}+\frac{r_2}{r_1}\right)\sin k_2 L} \tag{5.22}$$

$$\tilde{T}_d = \frac{2}{\left[2\cos k_2 L + j\left(\frac{r_1}{r_2}+\frac{r_2}{r_1}\right)\sin k_2 L\right](\cos k_1 L - j \sin k_1 L)} \tag{5.23}$$

One can now define *Force Reflection* and *Transmission* coefficients

$$\tilde{R}_f \;=\; \frac{\tilde{F}_r}{\tilde{F}_i} \tag{5.24}$$

$$\tilde{T}_f = \frac{\tilde{F}_t}{\tilde{F}_i} \tag{5.25}$$

Using equations 5.6, 5.17, 5.18, 5.24 and 5.25, we can obtain the Force Reflection and Transmission coefficients as

$$\boxed{\tilde{R}_f = -\tilde{R}_d} \tag{5.26}$$

$$\boxed{\tilde{T}_f = \frac{r_3}{r_1}\tilde{T}_d} \tag{5.27}$$

The *displacement* and *force* waves in regions I & III can now be defined in terms of the *displacement* Reflection and Transmission coefficients as

$$u_i = \tilde{U}_i e^{j(\omega t - k_1 x)} \tag{5.28}$$

$$u_r = \tilde{R}_d \, \tilde{U}_i e^{j(\omega t + k_1 x)} \tag{5.29}$$

$$u_t = \tilde{T}_d \, \tilde{U}_i e^{j(\omega t - k_3 x)} \tag{5.30}$$

$$\begin{aligned} f_i &= \tilde{F}_i e^{j(\omega t - k_1 x)} \\ f_r &= \tilde{R}_f \, \tilde{F}_i e^{j(\omega t + k_1 x)} = -\tilde{R}_d \, \tilde{F}_i e^{j(\omega t + k_1 x)} \\ f_t &= \tilde{T}_f \, \tilde{F}_i e^{j(\omega t - k_3 x)} = \left(\frac{r_3}{r_1}\right) \tilde{T}_d \, \tilde{F}_i e^{j(\omega t - k_3 x)} \end{aligned} \tag{5.31}$$

The Reflection and Transmission coefficients are essentially *frequency domain* representations of the reflected and transmitted waveforms infinitesimally close to the interfaces, in regions I & III respectively. Thus, in the time domain, the reflected and transmitted waveforms at $x = 0 - \epsilon$ and at $x = L + \epsilon$ for a unit impulse impinging on the boundary between regions I & II can be determined by taking the Inverse Fourier Transform of the expressions for the reflection and

transmission coefficients. The ways to compute Discrete Fourier Transforms was discussed in chapter 4.

A few examples to illustrate the theory developed will now be discussed.

5.1.1 Examples

The examples considered analyze the interaction of a *force impulse* with a stuck region modeled as a) Distributed Stiffness and b) Distributed Damping. The levels of distributed stiffness and distributed damping used in the models are indicative of the magnitudes of forces per unit length required to impart a unit displacement and a unit velocity respectively, to the stuck portion of the BHA. Examples 5.1 and 5.2 discuss the fate of a force impulse as it propagates through a stuck region (modeled as distributed stiffness and distributed damping respectively) separating two semi–infinite half spaces.

5.1.2 Example 5.1 – Distributed Stiffness Model of the Stuck Region

The following example represents a situation where the BHA is stuck along a finite section of its length (region II) as shown in figure 5-2 on page 93. The stuck region is modeled as a distributed stiffness, which is a parameter whose value can be varied over a wide range. Regions I & III extend to infinity on either side and are identical in all respects. Region II, which is of a finite length differs from regions I & III in that it has a distributed stiffness. Figures 5-3, 5-4 and 5-5, 5-6 show the magnitude and phase of the *Force* Reflection and Transmission coefficients as a function of frequency at $x = 0 - \epsilon$ and $x = L + \epsilon$ respectively, for a *unit amplitude force wave* incident on the boundary between regions I and II. One can think of the Force Reflection coefficient as a drive point function between the force output and a unit harmonic force input in region I, infinitesimally close to the interface separating the free and the stuck

regions. Similarly, the Force Transmission coefficient can be considered as a transfer function representing the force response in region III, infinitesimally close to the boundary dividing regions II and III, due to a unit harmonic force input in region I very close to the interface between regions I and II.

The following tables give the data used for the analysis.

$E = 2.0417 \times 10^{11}\ N/m^2$	Young's modulus for steel
$\rho = 7.850 \times 10^3\ kg/m^3$	Density of steel
$R = 110\ N - s/m\ /m$	Internal damping in drillstring
$c = 5100\ m/s$	Axial wave propagation speed in steel
$L = 30\ m$	Length of the stuck region
$A = 0.01579\ m^2$	Area of cross-section of BHA (6.25 " DC)

Distributed Stiffness $N/m\ /m$				
	Region I	Region II	Symbol	Region III
case (a)	0.0	1.0×10^4	-	0.0
case (b)	0.0	1.0×10^7	-·	0.0
case (c)	0.0	1.0×10^8	--	0.0
case (d)	0.0	1.0×10^9	▬	0.0

Discussion :

The frequency range considered was from 0.2 Hz to 819.2 Hz with a step size of 0.2 Hz. Figure 5-3 shows the magnitude of the force reflection coefficient[1] for various levels of distributed stiffness in the stuck region. It can be seen that the magnitude of the reflection coefficient is unity for all frequencies below the cut-off frequency (explained in section 4.5.1) for a given value of distributed

[1] *Force Reflection coefficient* and *Reflection coefficient* will be used interchangeably

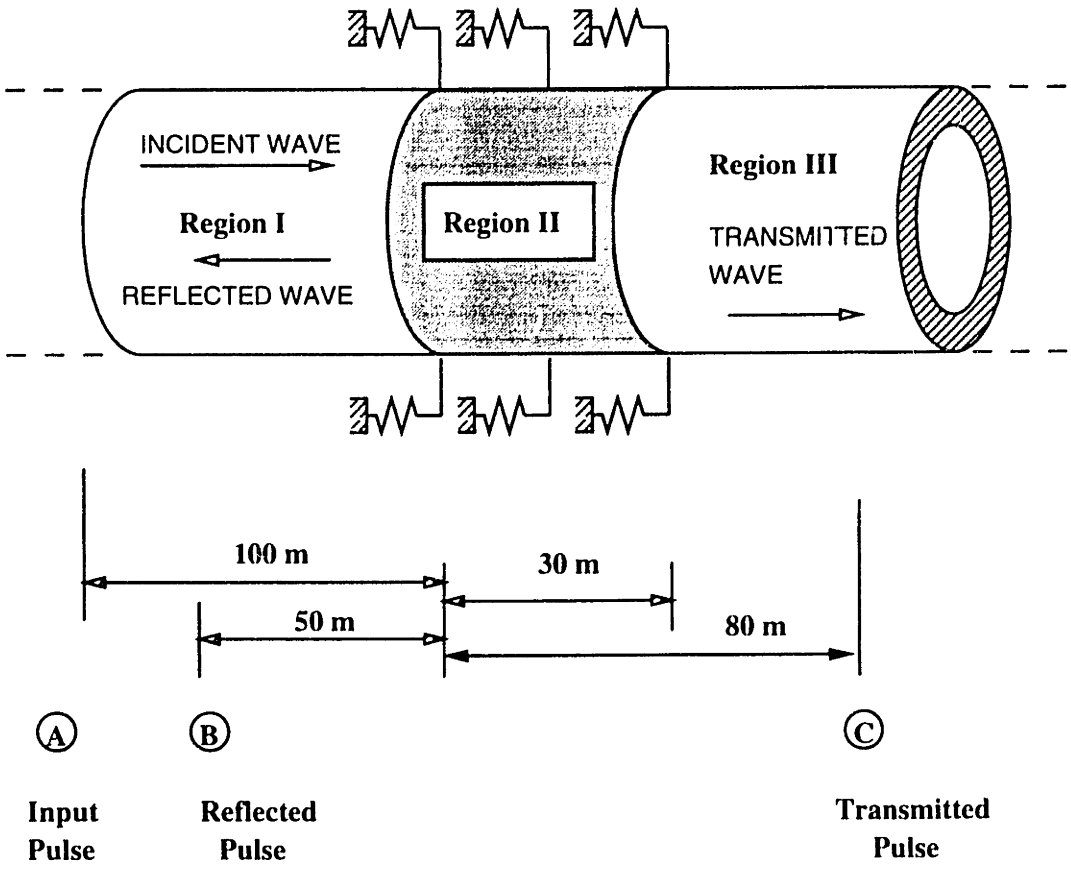

Figure 5-2: Reflection and Transmission of a Force Impulse at a barrier modeled as a distributed stiffness

stiffness. The reflected wave lags behind the incident wave in this frequency range as can be seen from figure 5-4. The values of the cut–off frequencies corresponding to different levels of distributed stiffness are given in section (4.5.1) for a 6.25 " drill collar. Below the cut–off frequency for a given level of distributed stiffness, there is no energy propagation into the stuck region; only an evanescent wave field exists in the stuck region whose magnitude decays exponentially with distance. For a given length of the stuck region, the effects of the evanescent wave field can be noticed in region III only for small values of distributed stiffness. This is apparent from the plot of the magnitude of the force transmission coefficient[2] versus frequency shown in figure 5-5 for different stiffness levels. It can be observed that the transmission coefficient drops off very steeply for frequencies below the cut–off frequency for large values of distributed stiffness (1.0×10^9 N/m $/m$). This can be attributed to the large imaginary part of the wave number (figure 4-4 on page 66) which is responsible for the rapid decay of the evanescent force field. The zero frequency case (wavelength $\rightarrow \infty$) presents an interesting result. The reflection coefficient is unity and the phase of the drive point function is zero. At the same time, the magnitude of the transmission coefficient is zero for all values of stiffness. Physically, this means that if the BHA above the stuck region were to be set into uniform motion, then the drill collars below the stuck region would be insensitive to this motion and would continue to remain stationary. The kinetic energy of the BHA above the stuck region in such a case would be converted to potential energy of the stiffness elements constituting the stuck region.

Above the cut–off frequency, waves start to propagate in the stuck region and beyond. It can be seen from figure 5-3 that for a given level of distributed stiffness, the magnitude of the reflection coefficient decreases with increasing frequency. This is because, the difference in wave number between the free and stuck regions is maximum at the cut–off frequency and progressively decreases

[2] *Force Transmission coefficient* and *Transmission coefficient* will be used interchangeably

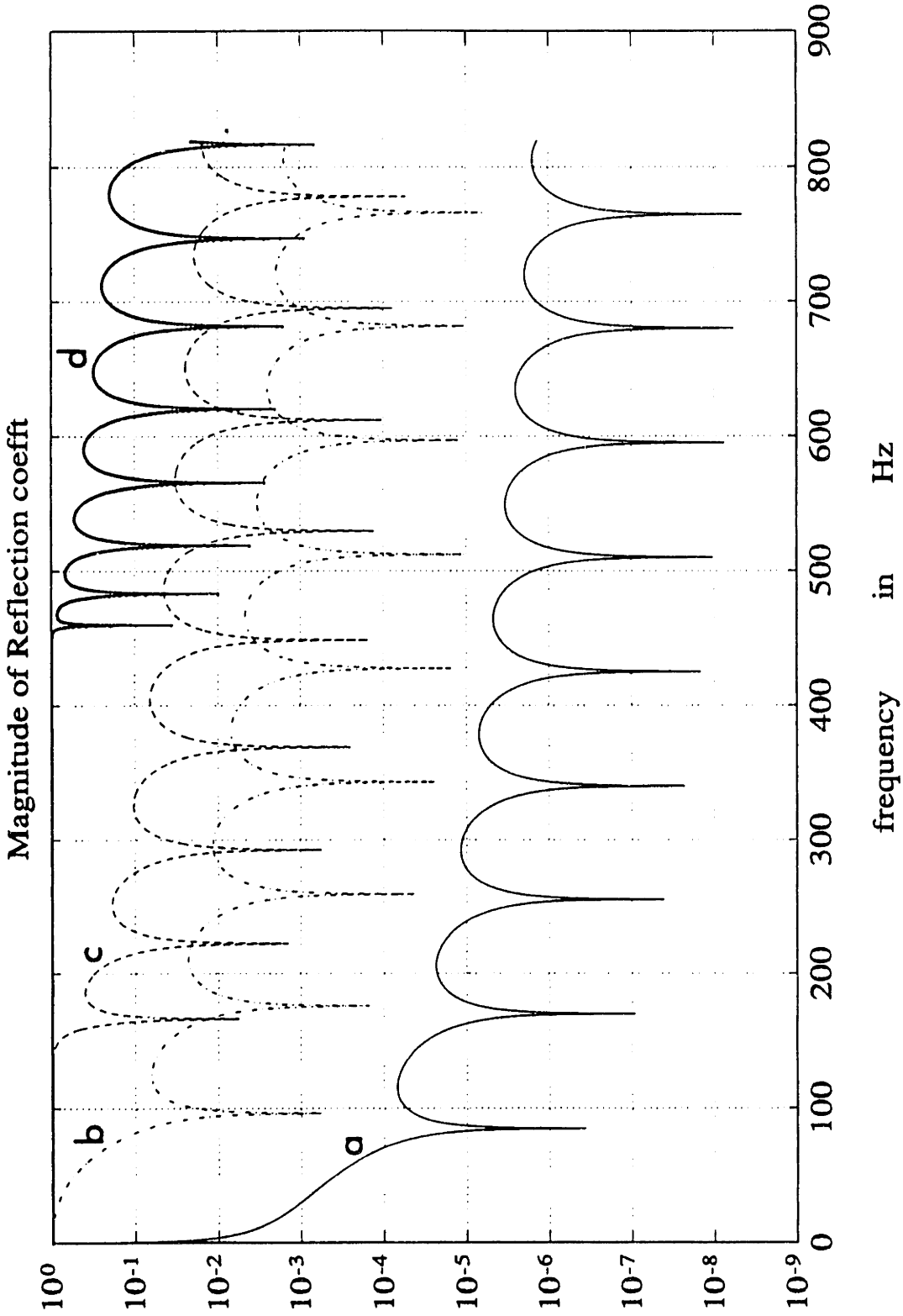

Figure 5-3: Magnitude of *Force Reflection coefficient* $\tilde{R}_f$ for a stuck region of length ($L = 30\ m$) for various levels of distributed stiffness $(6.25''\ DC)$

a) – $K = 1.0 \times 10^4 N/m\ /m$ b) –· $K = 1.0 \times 10^7 N/m\ /m$

c) –– $K = 1.0 \times 10^8 N/m\ /m$ d) ▬ $K = 1.0 \times 10^9 N/m\ /m$

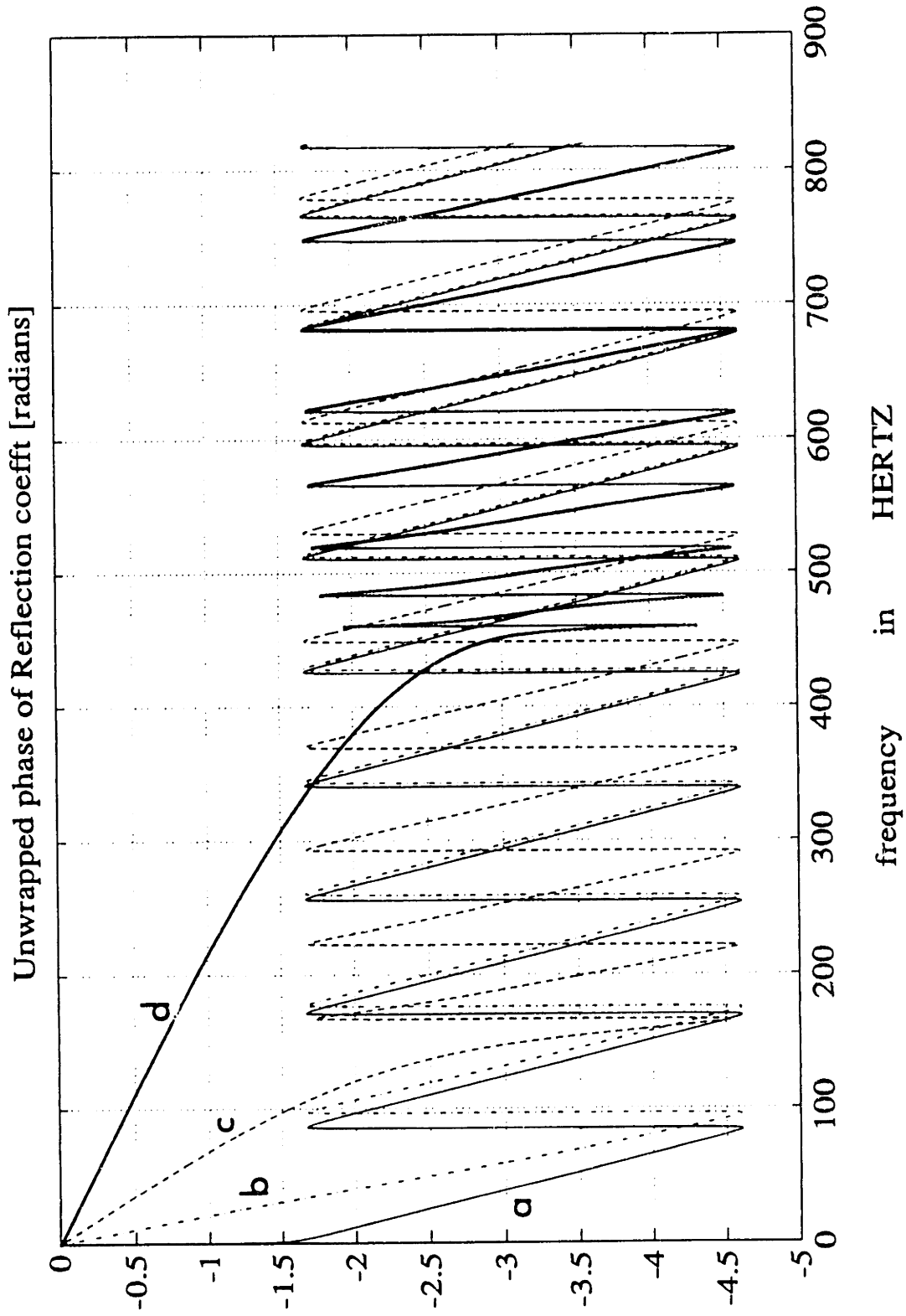

Figure 5-4: Unwrapped phase of *Force Reflection coefficient* $\tilde{R}_f$ for a stuck region of length ($L = 30\ m$) for various levels of distributed stiffness (6.25″ *DC*)

a) – $K = 1.0 \times 10^4 N/m\ /m$ b) –· $K = 1.0 \times 10^7 N/m\ /m$

c) – – $K = 1.0 \times 10^8 N/m\ /m$ d) ▬ $K = 1.0 \times 10^9 N/m\ /m$

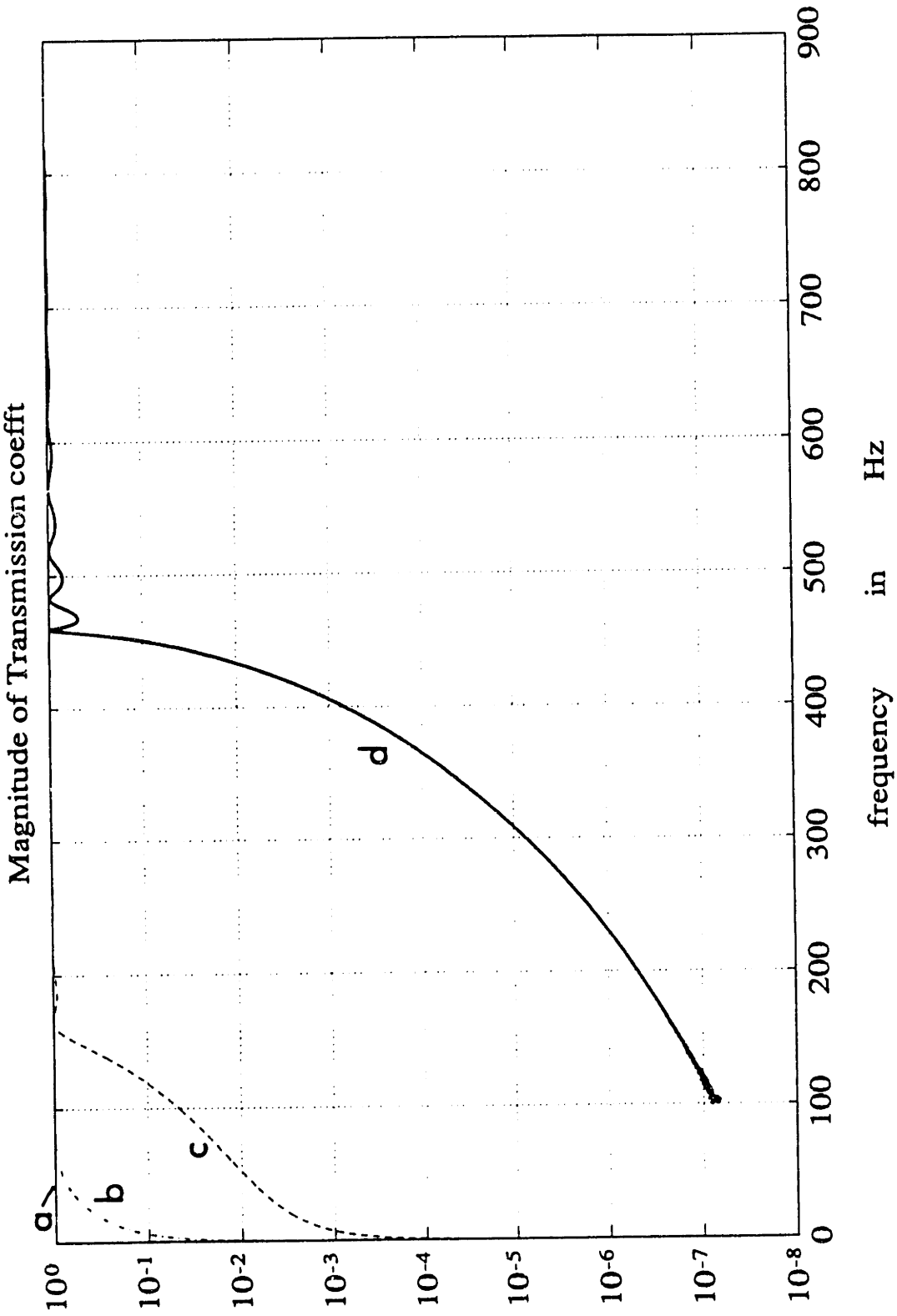

Figure 5-5: Magnitude of *Force Transmission coefficient* $\tilde{T}_f$ for a stuck region of length ($L = 30\ m$) for various levels of distributed stiffness (6.25″ *DC*)
a) – $K = 1.0 \times 10^4 N/m\ /m$ b) –· $K = 1.0 \times 10^7 N/m\ /m$
c) –– $K = 1.0 \times 10^8 N/m\ /m$ d) ▬ $K = 1.0 \times 10^9 N/m\ /m$

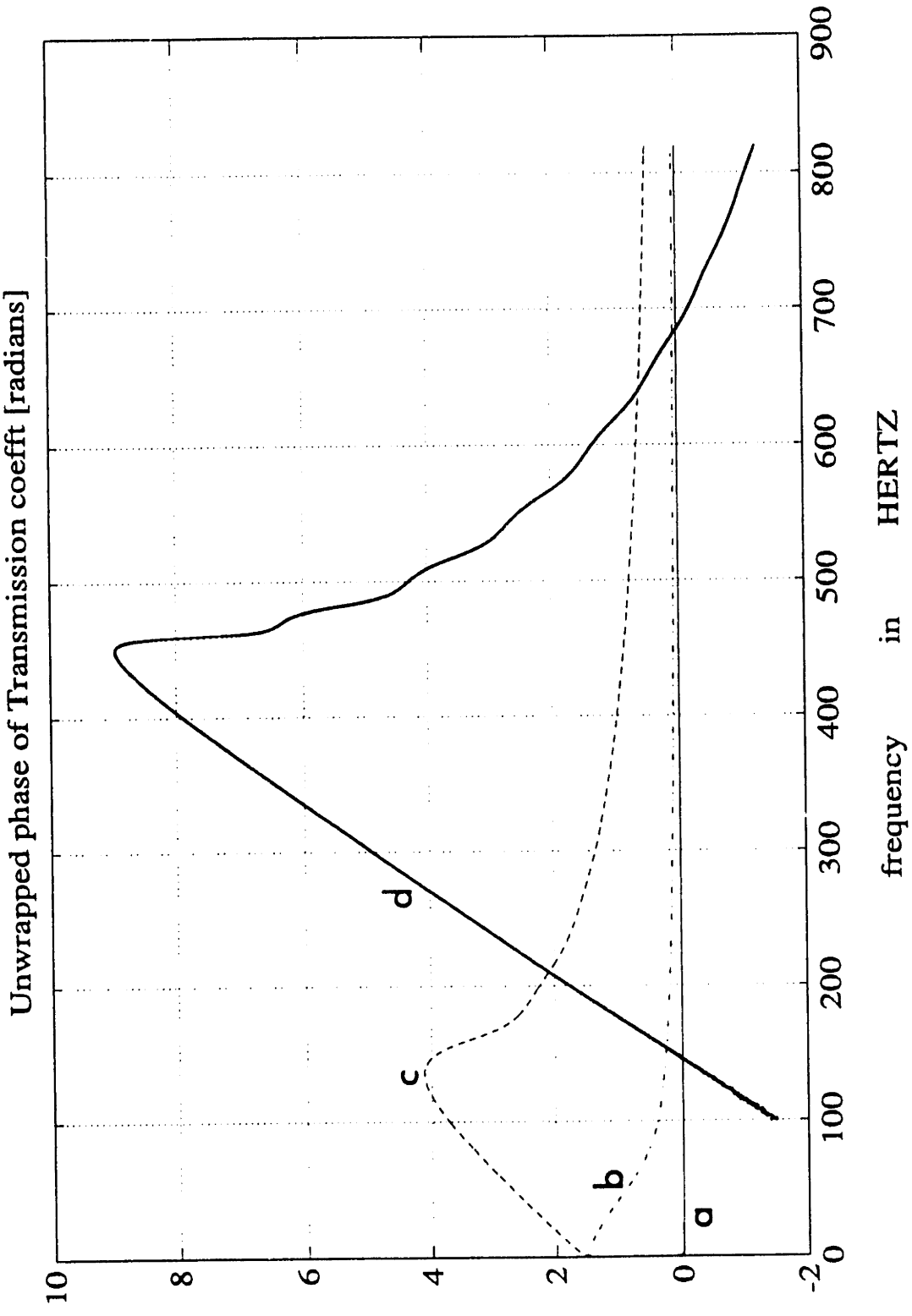

Figure 5-6: Unwrapped phase of *Force Transmission coefficient* $\tilde{T}_f$ for a stuck region of length ($L = 30\ m$) for various levels of distributed stiffness (6.25″ *DC*)
a) – $K = 1.0 \times 10^4 N/m\ /m$ b) –· $K = 1.0 \times 10^7 N/m\ /m$
c) –– $K = 1.0 \times 10^8 N/m\ /m$ d) ▬ $K = 1.0 \times 10^9 N/m\ /m$

with increasing frequency. As a result, the phase speed in the stuck region asymptotically approaches the phase speed in the free region of the BHA. Thus, as the frequency increases, the difference in impedance[3] between the free and the stuck regions becomes smaller resulting in a transmission of energy through the stuck region. This manifests itself as a decrease in the magnitude of the reflection coefficient with increasing frequency. It can also be noticed for the same reason that the magnitude of the reflection coefficient, above the cut-off frequencies decreases with decreasing values of distributed stiffness.

An interesting feature of figure 5-3 is the location of the zeros of the reflection coefficient. At the frequencies corresponding to the zeros, there is total transmission of energy into the stuck region. The expression for the reflection coefficient is given as

$$\tilde{R}_f = -\frac{j\left(\frac{r_1}{r_2}-\frac{r_2}{r_1}\right)\sin k_2 L}{2\cos k_2 L + j\left(\frac{r_1}{r_2}+\frac{r_2}{r_1}\right)\sin k_2 L} \tag{5.32}$$

The zeros occur for the values of the wave number k_2 satisfying the relation

$$\sin k_2 L = 0 \tag{5.33}$$

Note that k_2 is real for frequencies higher than the cut-off frequency. Since damping is negligible, the zeros occur at frequencies given by

$$f_n = \frac{c}{2\pi}\sqrt{\left(\frac{n\pi}{L}\right)^2 + \left(\frac{S}{EA}\right)} \qquad n = 1, 2, 3 \ldots \tag{5.34}$$

where

[3] *Characteristic impedance of a medium* is defined as ρc, where ρ is the density of the medium and c is the phase speed of the acoustic wave in that medium

L : Length of the stuck region

For very small values of distributed stiffness (1.0×10^4 N/m $/m$),

$$\left(\frac{S}{EA}\right) \ll \left(\frac{n\pi}{L}\right)^2 \tag{5.35}$$

and equation 5.34 reduces to

$$f_n = \frac{nc}{2L} \qquad n = 1, 2, 3 \ldots \tag{5.36}$$

Thus, the zeros of the magnitude of the reflection coefficient correspond to the resonances of the stuck region behaving as a fixed–fixed or a free–free bar. For a stiffness of 1.0×10^4 N/m $/m$, the zeros occur at integral multiples of 85 Hz as can be seen in figure 5-3.

For large values of the distributed stiffness (say, 1.0×10^8 N/m $/m$),

$$\begin{array}{lll} \left(\frac{S}{EA}\right) \gg \left(\frac{n\pi}{L}\right)^2 & \text{for small } n & \\ \left(\frac{S}{EA}\right) \approx \left(\frac{n\pi}{L}\right)^2 & \text{for moderately large } n & (5.37) \\ \left(\frac{S}{EA}\right) \ll \left(\frac{n\pi}{L}\right)^2 & \text{for large } n & \end{array}$$

In such a case, the spacing between the zeros approaches 85 Hz for large values of n ($n \approx 10$ for a stiffness of 1.0×10^8 N/m $/m$). For small values of n, the distributed stiffness value plays an important role in determining the locations of the zeros as well as the spacing between them. From the phase curve shown in figure 5-4, it can be seen that transitions of π *rads* occur at the locations of the zeros.

A more realistic situation is now considered, where a jar placed some distance (100 m) above the stuck location delivers a *unit impulse* which is modeled as

described in section (4.2.1)[4] This impulse travels down to the stuck region where some of the energy is reflected and some of it is transmitted. The shapes of the reflected and the transmitted pulses in the time domain depend on the nature of the stuck region (governed by the value of the distributed stiffness), and hence on the reflection and transmission coefficients, for a given stuck length. Figure 5-7 shows the reflected wave form in the BHA, 50 m from the top of the stuck region, for various levels of distributed stiffness. Also shown in the same figure for comparison, is the input wave form, both at the jar location and at a location infinitesimally close to the boundary between the free and the stuck regions, just before it is incident on the interface. Similarly, figure 5-8 shows the transmitted waveform 50 m from the bottom of the stuck region for different levels of distributed stiffness, along with the input waveform.

5.1.3 Example 5.2 – Distributed Damping model of the Stuck Region

The case considered here represents a similar situation as was analyzed in section (5.1.2), except that the stuck region is now modeled as *distributed damping.* This can be seen from figure 5-9 on page 105.

The data is the same as in example 5.1, but for the values of distributed damping and stiffness. The details are presented in the following tables.

$E = 2.0417 \times 10^{11}\ N/m^2$	Young's modulus for steel
$\rho = 7.850 \times 10^3\ kg/m^3$	Density of steel
$K = 0.0\ N/m\ /m$	Distributed stiffness in drillstring
$c = 5100\ m/s$	Axial wave propagation speed in steel
$L = 30\ m$	Length of the stuck region
$A = 0.01579\ m^2$	Area of cross-section of BHA (6.25 " DC)

[4]The width of the impulse is $\sim 6.1\ ms$.

Distributed Damping $N-s/m\ /m$				
	Region I	Region II	Symbol	Region III
case (a)	1.1×10^2	1.1×10^3	-	1.1×10^2
case (b)	1.1×10^2	1.1×10^4	-·	1.1×10^2
case (c)	1.1×10^2	1.1×10^5	--	1.1×10^2
case (d)	1.1×10^2	1.1×10^6	_	1.1×10^2

Discussion :

Figure 5-10 shows the magnitude of the reflection coefficient for various levels of distributed damping in the stuck region. It is clear that the value of the reflection coefficient is very small for small values of damping ($R = 1.1 \times 10^3\ N-s/m\ /m$ and $R = 1.1 \times 10^4\ N-s/m\ /m$), which means that most of the energy is transmitted into the stuck region. At the same time, the magnitude of the transmission coefficient is almost unity and the phase is zero, as can be seen from figures 5-12 and 5-13. This shows that there is negligible dispersion, and consequently the shape of the incident pulse is preserved as it travels through the stuck region.

The magnitude of the reflection coefficient increases with an increase in damping due to a greater impedance mismatch now existing between the free and the stuck regions. Also, for high values of the damping constant ($R = 1.1 \times 10^6\ N-s/m\ /m$), the magnitude of the transmission coefficient decreases much more steeply with frequency than the reflection coefficient. This is because the high frequency components get absorbed in the stuck region resulting in a dissipation of energy. Thus the stuck region in this case behaves as a lowpass filter. From the phase curve shown in figure 5-13, it is apparent that with increasing frequency, the various frequency components of the transmitted wave become increasingly out of phase relative to one another causing a significant distortion of the incident pulse shape as it propagates through the stuck region.

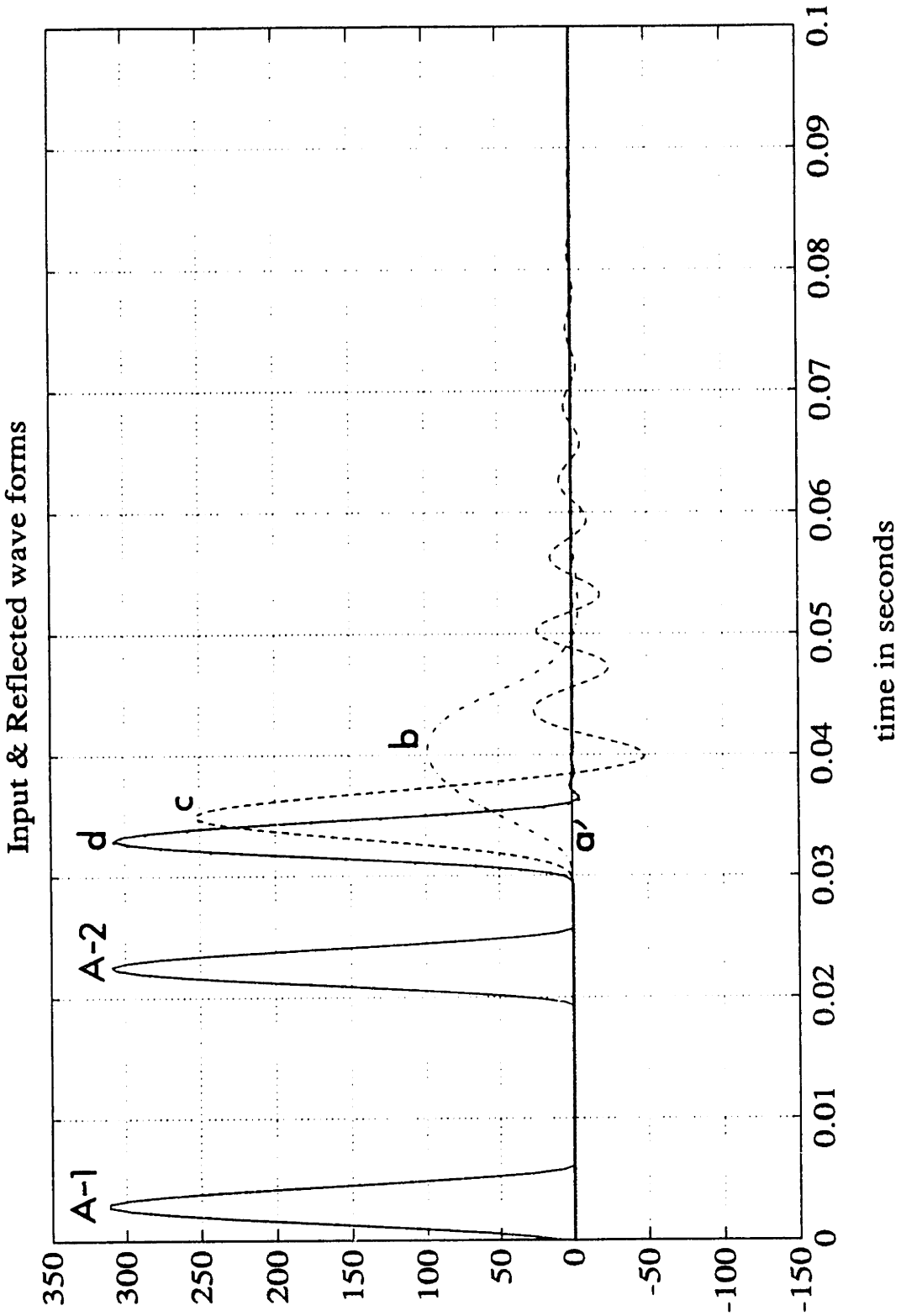

Figure 5-7: A. – Time domain representation of the *input pulse* 100 m from the interface (A-1) and at the interface (A-2) between the free & the stuck regions. (6.25″ *DC*)

B. Time domain representation of the *reflected waveform* 50 m above the interface for a stuck region of length ($L = 30\ m$), for various levels of distributed stiffness. (6.25″ *DC*)

a) – $K = 1.0 \times 10^4 N/m\ /m$ b) –· $K = 1.0 \times 10^7 N/m\ /m$

c) –– $K = 1.0 \times 10^8 N/m\ /m$ d) ▬ $K = 1.0 \times 10^9 N/m\ /m$

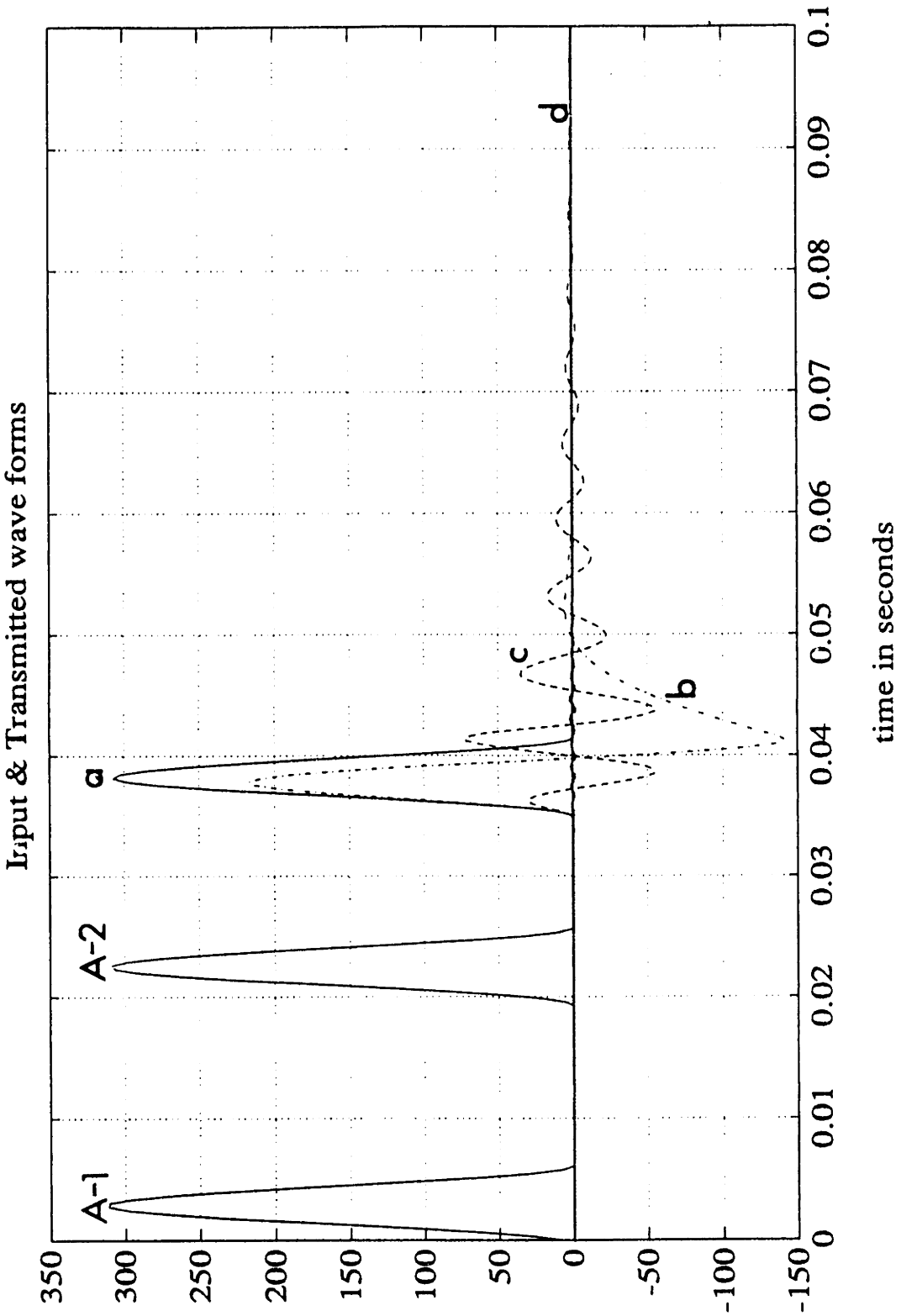

Figure 5-8: A. – Time domain representation of the *input pulse* 100 m from the interface (A-1) and at the interface (A-2) between the free & the stuck regions. (6.25″ *DC*)

B. Time domain representation of the *transmitted waveform* 50 m below the bottom of the stuck region for a stuck length (L = *30 m*), for various levels of distributed stiffness. (6.25″ *DC*)

a) – $K = 1.0 \times 10^4 N/m\ /m$ b) –· $K = 1.0 \times 10^7 N/m\ /m$

c) – – $K = 1.0 \times 10^8 N/m\ /m$ d) ▬ $K = 1.0 \times 10^9 N/m\ /m$

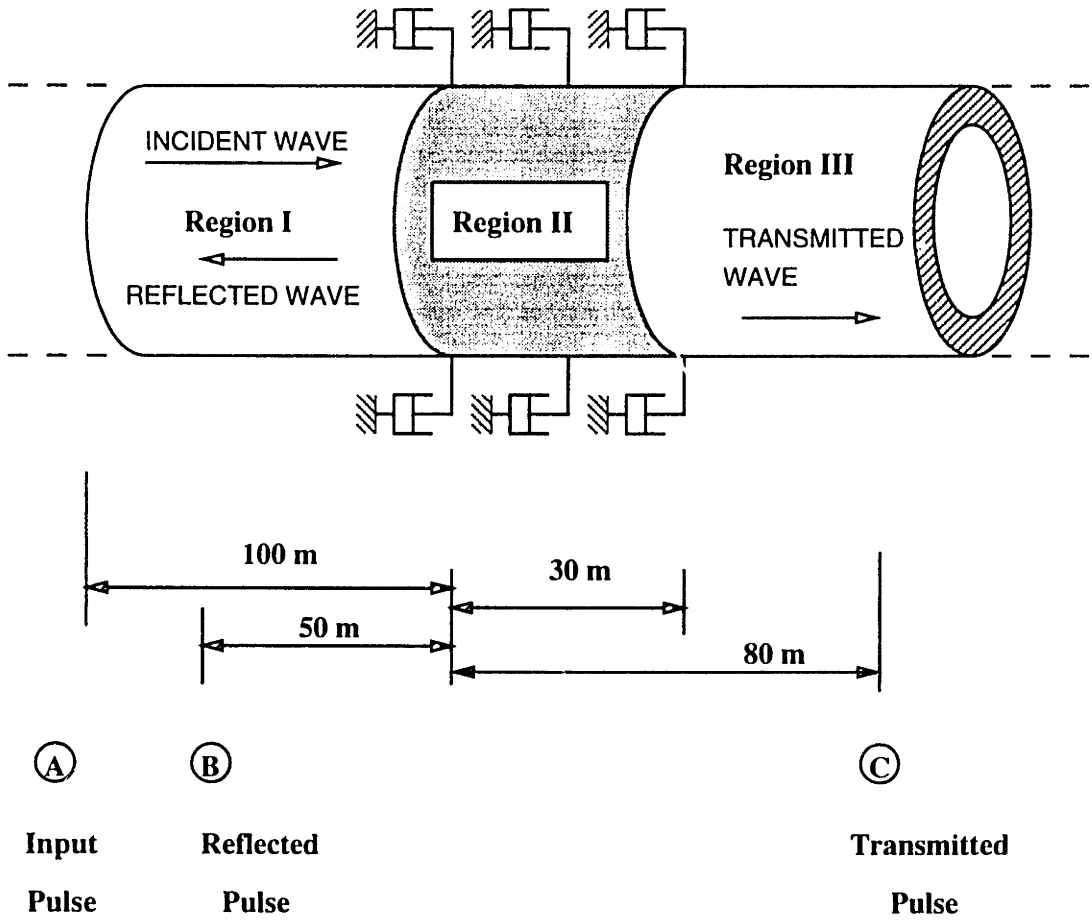

Figure 5-9: Reflection and Transmission of a Force Impulse at a barrier modeled as distributed damping

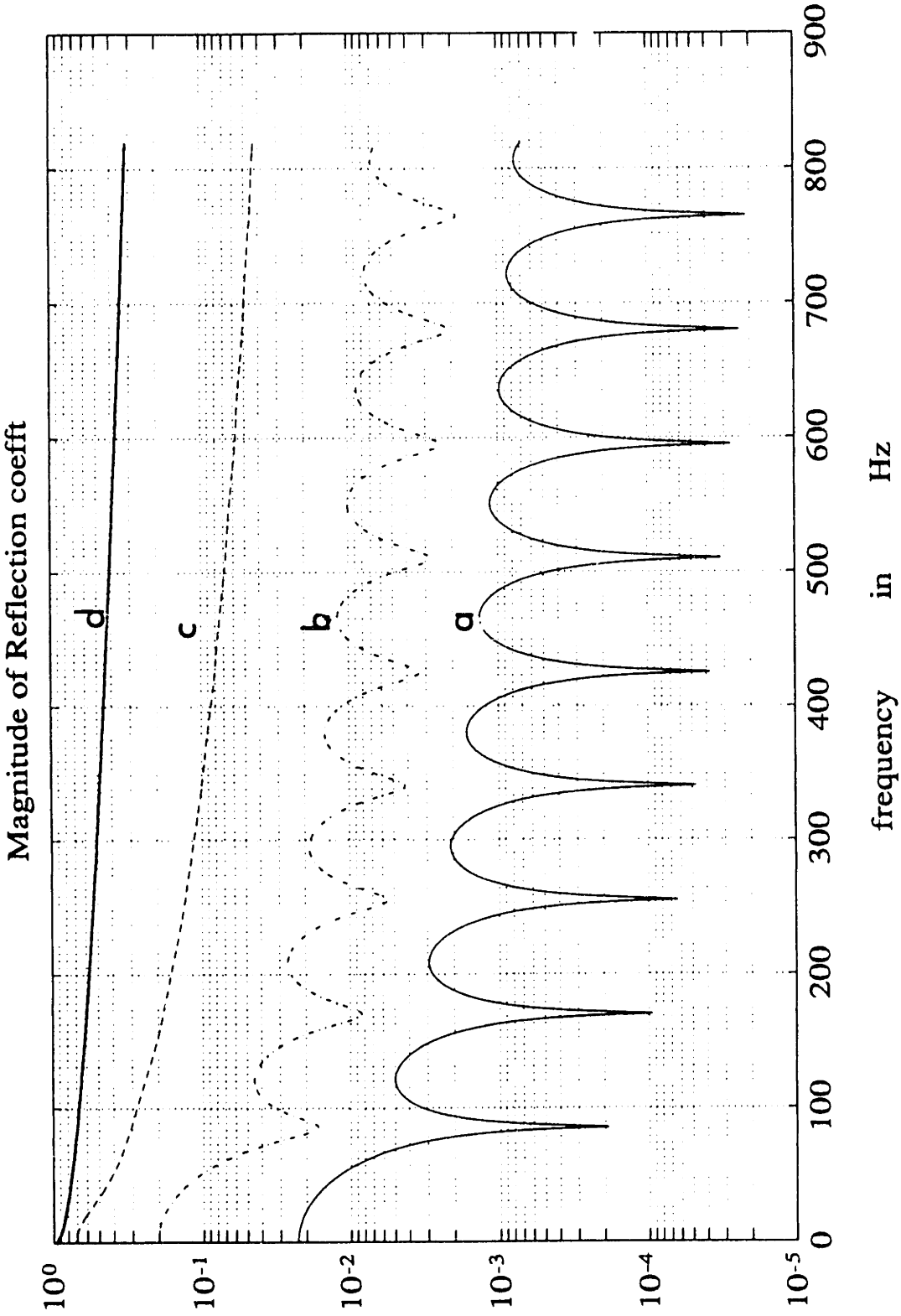

Figure 5-10: Magnitude of *Force Reflection coefficient* $\tilde{R}_f$ for a stuck region of length (L = 30 m) for various levels of distributed damping $(6.25''\ DC)$

a) – $R = 1.1 \times 10^3 N - s/m\ /m$ b) –· $R = 1.1 \times 10^4 N - s/m\ /m$

c) –– $R = 1.1 \times 10^5 N - s/m\ /m$ d) ▬ $R = 1.1 \times 10^6 N - s/m\ /m$

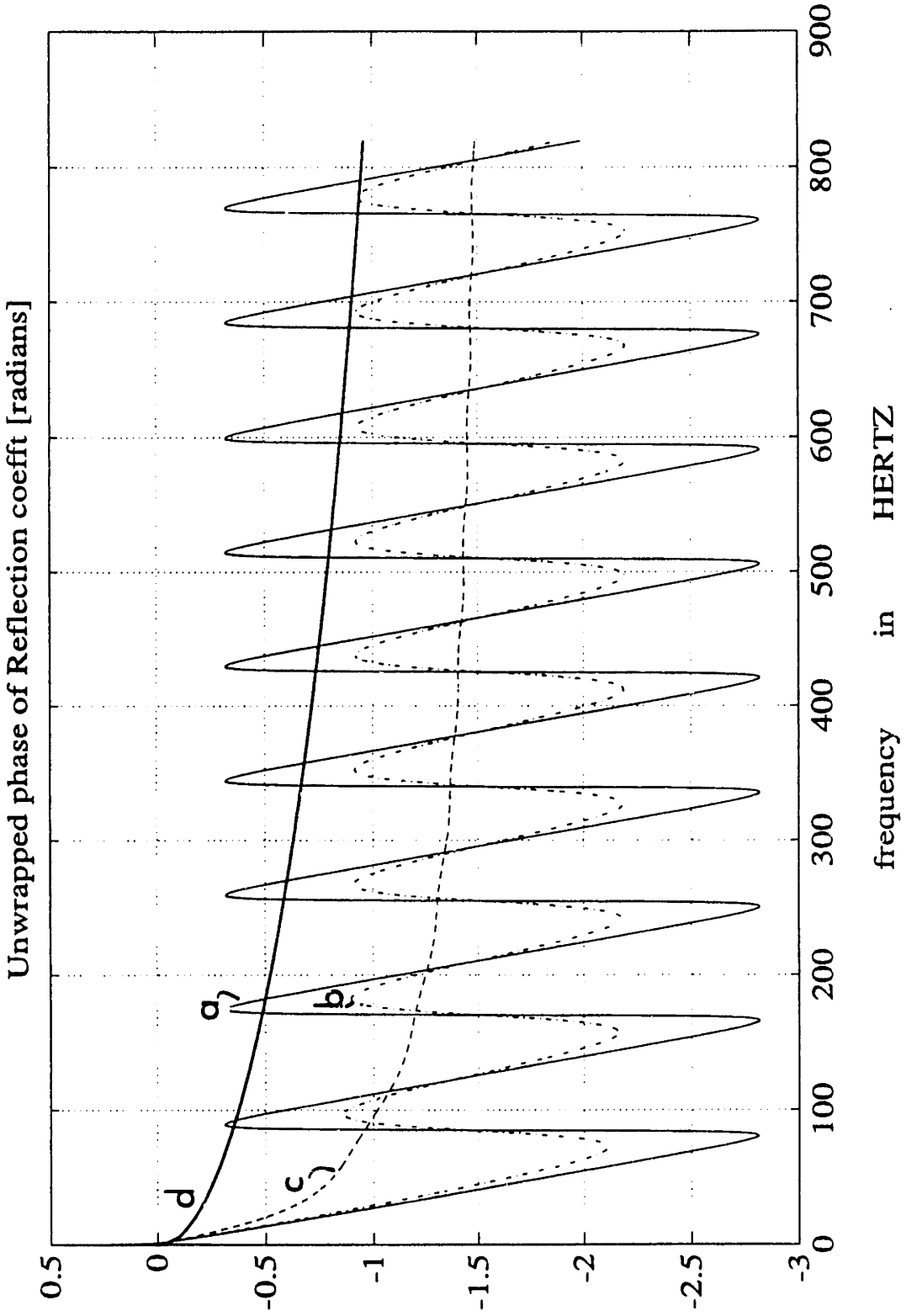

Figure 5-11: Unwrapped phase of *Force Reflection coefficient* $\tilde{R}_f$ for a stuck region of length (L = 30 m) for various levels of distributed damping $(6.25''\ DC)$

a) – $R = 1.1 \times 10^3 N - s/m\ /m$ b) –· $R = 1.1 \times 10^4 N - s/m\ /m$

c) – – $R = 1.1 \times 10^5 N - s/m\ /m$ d) ▬ $R = 1.1 \times 10^6 N - s/m\ /m$

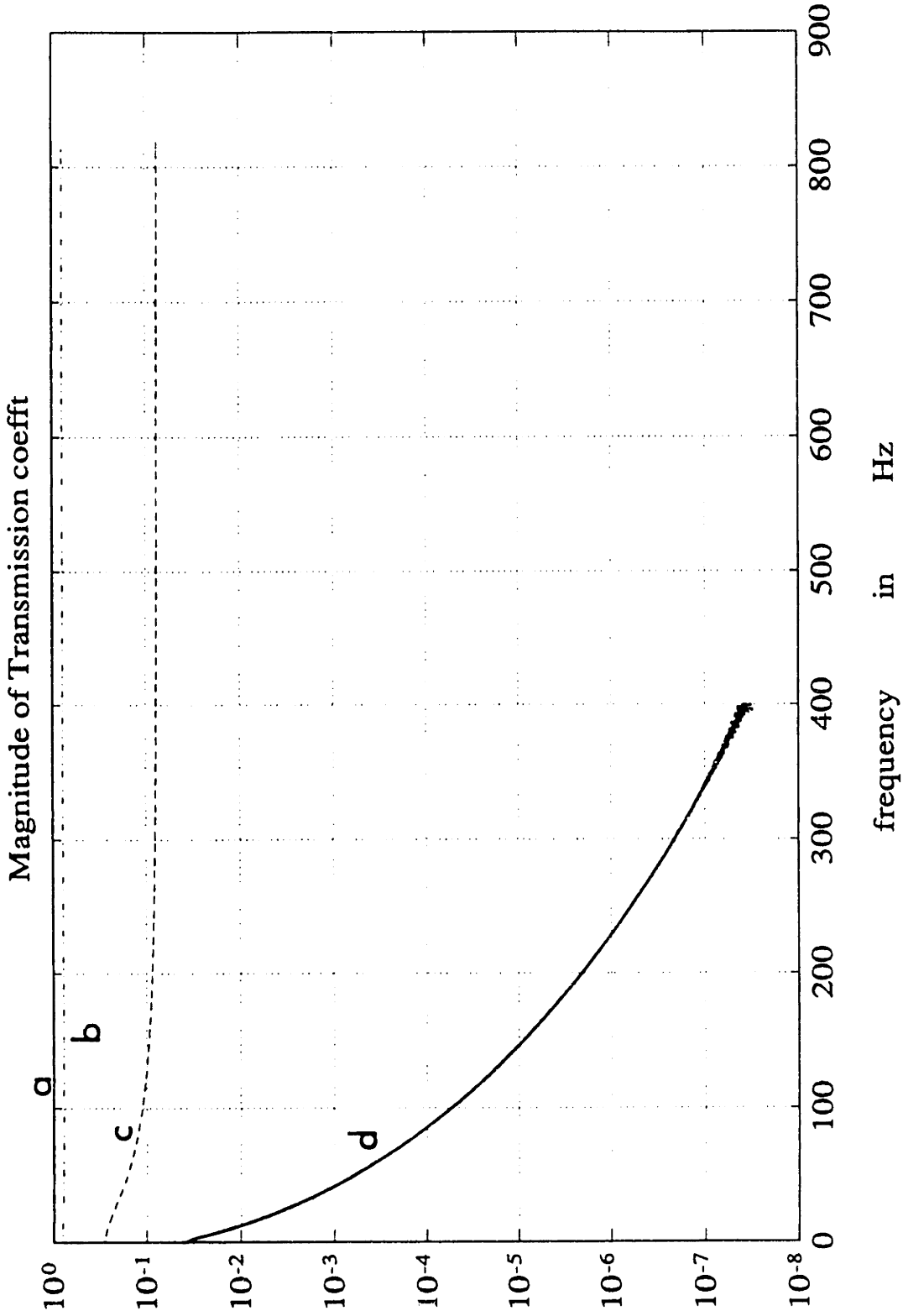

Figure 5-12: Magnitude of *Force Transmission coefficient* $\tilde{T}_f$ for a stuck region of length (L = 30 m) for various levels of distributed damping (6.25″ *DC*)
a) - $R = 1.1 \times 10^3 N - s/m\ /m$ b) -· $R = 1.1 \times 10^4 N - s/m\ /m$
c) -- $R = 1.1 \times 10^5 N - s/m\ /m$ d) — $R = 1.1 \times 10^6 N - s/m\ /m$

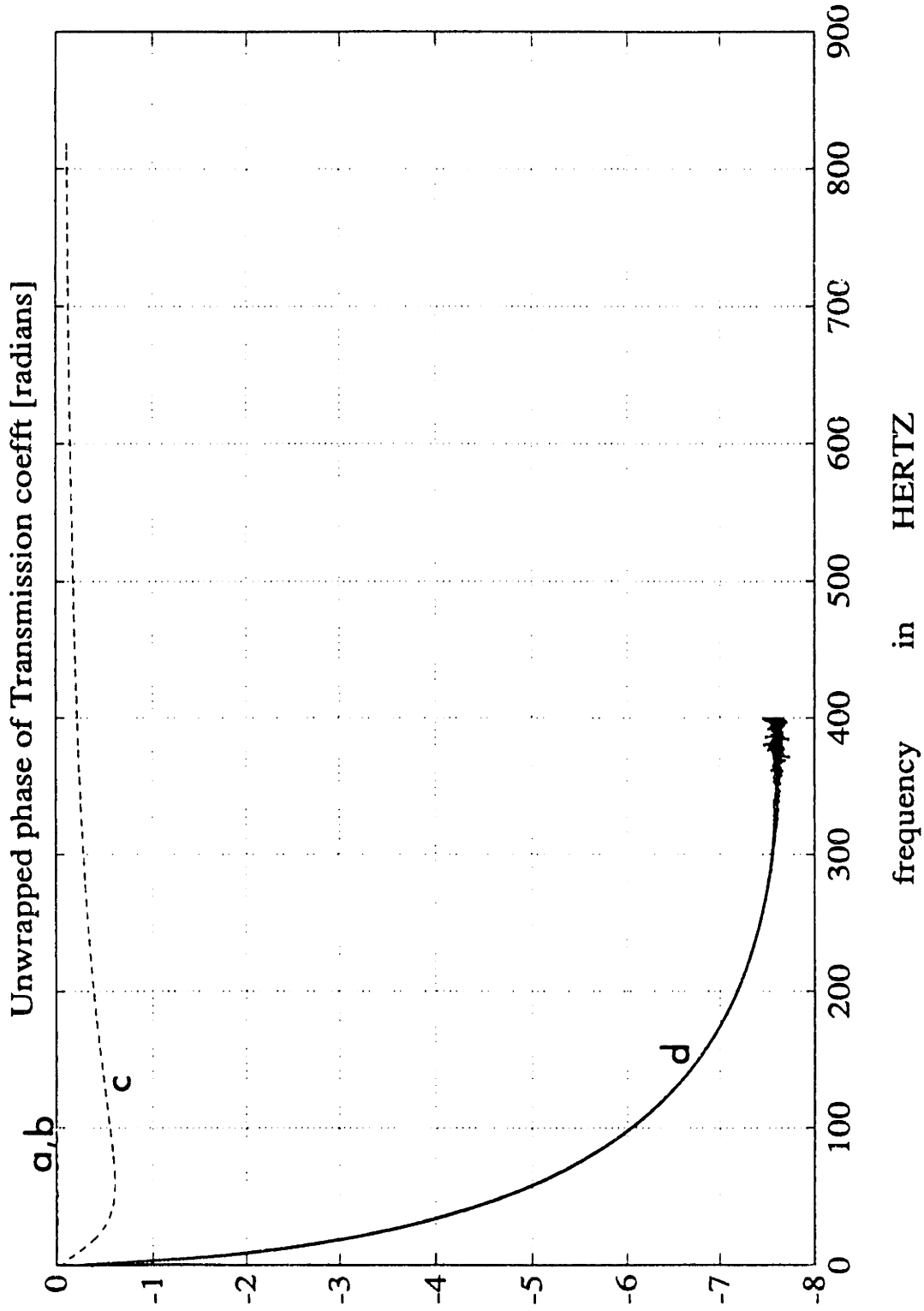

Figure 5-13: Unwrapped phase of *Force Transmission coefficient* $\tilde{R}_f$ for a stuck region of length (L = 30 m) for various levels of distributed damping $(6.25''\ DC)$

a) – $R = 1.1 \times 10^3 N - s/m\ /m$ b) –· $R = 1.1 \times 10^4 N - s/m\ /m$

c) – – $R = 1.1 \times 10^5 N - s/m\ /m$ d) ▬ $R = 1.1 \times 10^6 N - s/m\ /m$

For small values of distributed damping ($1.1 \times 10^3\ N - s/m\ /m$ and $1.1 \times 10^4\ N - s/m\ /m$), the imaginary part of the wave number in the stuck region (k_2) is very small and the zeros of the reflection coefficient occur when

$$\begin{aligned} \sin k_2 L &= 0 \\ f_n &= \frac{nc}{2\pi} \qquad\qquad n = 1, 2, 3 \ldots \end{aligned}$$

However, when the damping in the stuck region is substantial ($1.1 \times 10^5\ N - s/m\ /m$ and $1.1 \times 10^6\ N - s/m\ /m$), the wave number k_2 is complex and the reflection coefficient does not have any zeros. This is readily observed in figure 5-10.

Figures 5-14 and 5-15 show the reflected and the transmitted wave forms 50 m above the top of the stuck region and at an equal distance from below the bottom of the stuck region respectively, for a unit pulse input, 100 m from the top of the stuck region. It can be noticed that, with increasing values of damping, the reflected and the transmitted waveforms develop a distinct *tail* caused by dispersion of the incident pulse.

The distinction between the reflected and the transmitted waveforms for the DDM (Distributed Damping Model) and the DSM (Distributed Stiffness Model) is quite conspicuous. The main feature of the DSM is the presence of cut-off frequencies above which, wave propagation through the stuck region proceeds unimpeded. For large values of stiffness, the cut-off frequencies are large and as a result the transmitted waveform consists only of high frequency components. On the other hand, for large values of damping in the DDM, high frequency components in the the incident pulse are greatly attenuated as they pass through the stuck region. The transmitted waveform in this case is thus chiefly comprised of low frequency components.

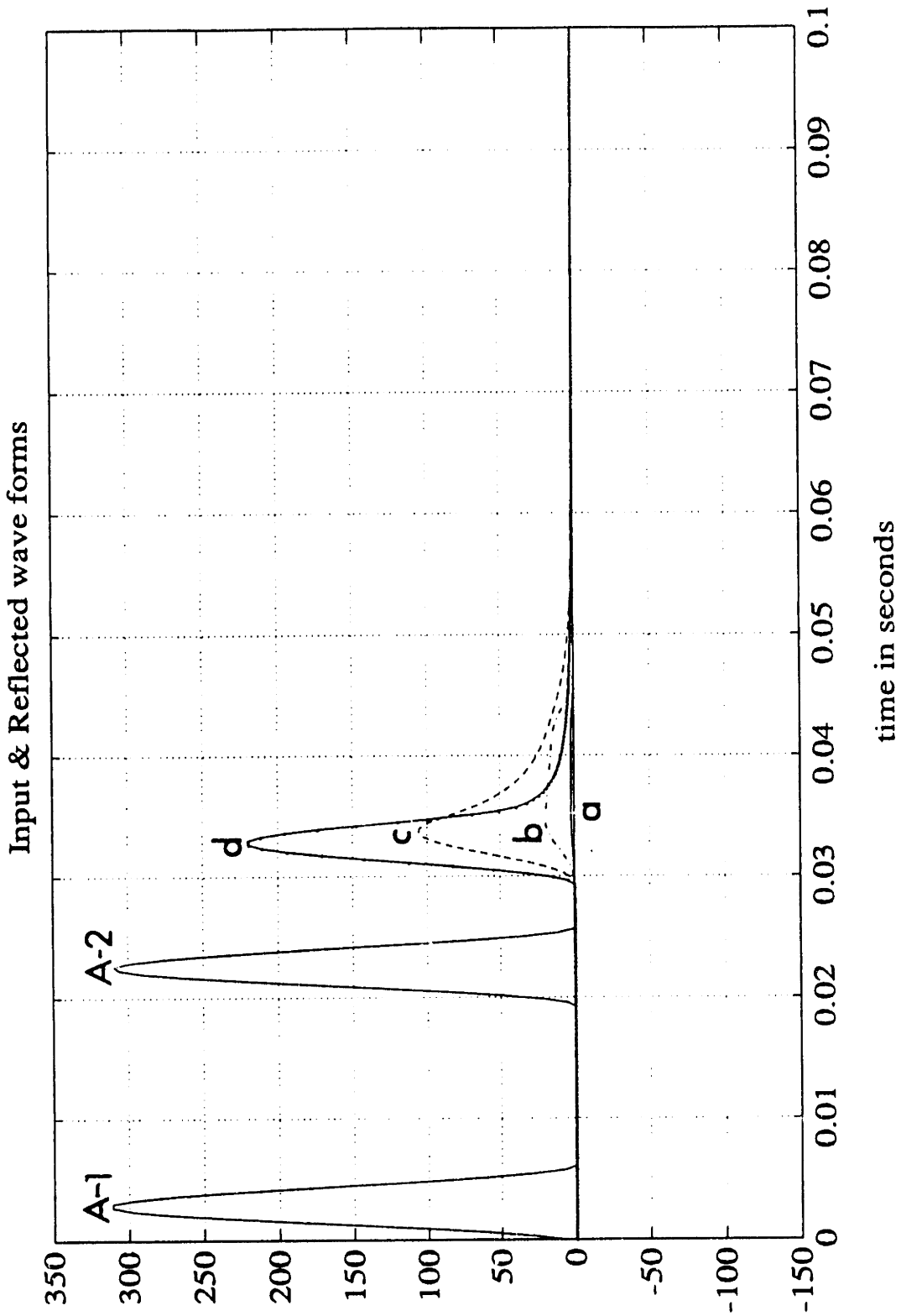

Figure 5-14: A. – Time domain representation of the *input pulse* 100 m from the interface (A-1) and at the interface (A-2) between the free & the stuck regions. (6.25″ *DC*)

B. Time domain representation of the *reflected waveform* 50 m above the interface for a stuck region of length ($L = 30\ m$), for various levels of distributed damping. (6.25″ *DC*)

a) – $R = 1.1 \times 10^3 N - s/m\ /m$ b) –· $R = 1.1 \times 10^4 N - s/m\ /m$

c) –– $R = 1.1 \times 10^5 N - s/m\ /m$ d) ▬ $R = 1.1 \times 10^6 N - s/m\ /m$

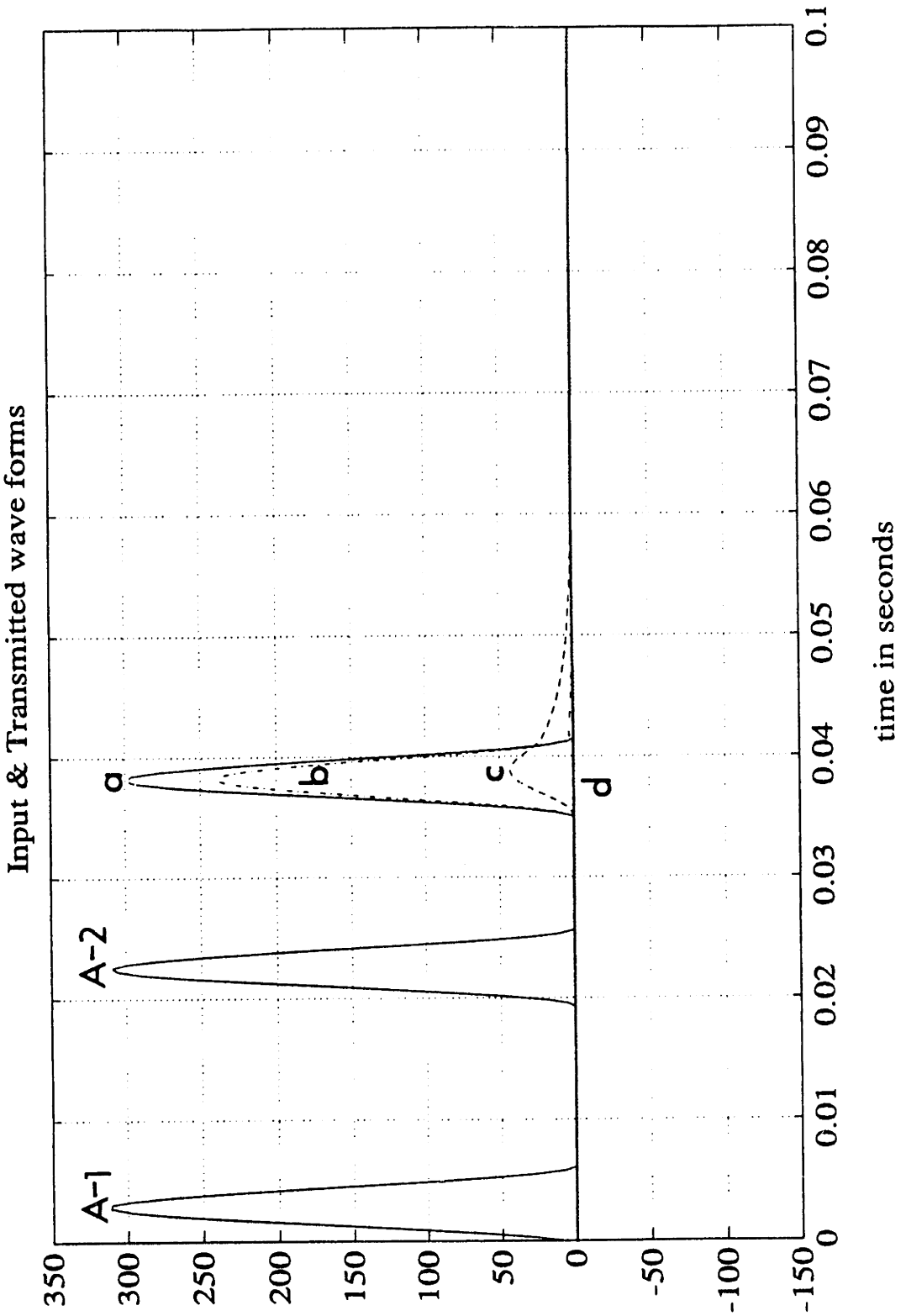

Figure 5-15: A. – Time domain representation of the *input pulse* 100 m from the interface (A-1) and at the interface (A-2) between the free & the stuck regions. (6.25″ *DC*)

B. Time domain representation of the *transmitted waveform* 50 m above the interface for a stuck region of length ($L = 30\ m$), for various levels of distributed damping. (6.25″ *DC*)

a) – $R = 1.1 \times 10^2 N - s/m\ /m$ b) –· $R = 1.1 \times 10^4 N - s/m\ /m$

c) –– $R = 1.1 \times 10^5 N - s/m\ /m$ d) ▬ $R = 1.1 \times 10^6 N - s/m\ /m$

5.2 Realistic case – Examples

Consider the following scenario which is a common occurence at any rig site.

Drilling operation has been proceeding smoothly for some hours, when the driller realizes that he has drilled into a break (sudden increase in penetration rate, usually indicative of a permeable formation). Under such a situation, a routine flow check is performed to check for gas leaks. Drilling is stopped to perform the flow check. Before recommencing drilling, the driller picks up a little to work the pipe and to his dismay, finds that the hook load has shot way up. This is a typical indication of stuck pipe, a problem which costs the oil industry millions of dollars each year, and is currently gaining industry–wide attention.

We now have developed the background necessary to analyze a realistic case. In the following sections, two specific examples are considered. In the first example (Example 5.3), we consider a case wherein the drillstring gets stuck while tripping out. This case is analyzed for distributed damping as well as distributed stiffness models of the stuck region. Transfer functions (Force response as a function of frequency at a surface location, due to a unit force impulse at the jar location) are compared for various levels of distributed damping and distributed stiffness in the stuck region, as a means of establishing an indicator for jarring effectiveness. Furthermore, a non–linear signal processing technique known as *cepstral analysis* is introduced and used to identify the exact location of the stuck region, to compare and contrast the signatures obtained in the two different models used for representing the stuck region, and to establish criteria for effective jarring.

The second example (Example 5.4) is the same as the earlier example except that it differs from the former in the location of the input force impulse. The input in this case is assumed to be at a surface location, as is the response (The

input and response locations are however, separated by a finite distance). The rationale behind analyzing this case is that it lends itself to field experimentation and one can, in addition to locating and characterizing the stuck region (whether the stuck region behaves as distributed stiffness or distributed damping), also obtain the signature of a free drillstring. This is not physically realizable with a jar in the BHA as a source of force impulse, since most of the jars can be tripped only when the drillstring is stuck.

5.3 Example 5.3

5.3.1 Drillstring description

The following example considers a situation where the drillstring is stuck along a certain length of the BHA. Figure 5-16 on page 116 shows the analytical model of the drillstring during normal drilling operation, and when it is stuck. The drillstring considered is the same as the one used for the **Shell–NL** field tests in 1984 [11]. The drillstring particulars are provided in the following table.

Data for figure 5-16	
Equivalent mass of surface equipment	$M_{eq} = 9100.0\ Kg$
Equivalent spring constant of surface equipment	$K_{eq} = 9 \times 10^6\ N/m$
Damping constant of surface equipment	$R_s = 4 \times 10^4\ N - s/m$
Damping constant in drillstring	$R = 1.1 \times 10^2\ N - s/m\ /m$
Total length of drill pipe	$L_{DP} = 1874.5\ m$
Total length of BHA (drill collars)	$L_{BHA} = 230.0\ m$
Total length of drillstring	$L_{DS} = 2104.5\ m$
Area of cross-section of Drill pipe (4.64 " DP)	$A_{DP} = 0.00349\ m^2$
Area of cross-section of BHA (6.25 " DC)	$A_{BHA} = 0.01579\ m^2$
Young's modulus for steel	$E = 2.0417 \times 10^{11}\ N/m^2$
Density of steel	$\rho = 7.850 \times 10^3\ kg/m^3$
Axial wave propagation speed in steel	$c = 5100\ m/s$

Equivalent mass, M_{eq} : It is the total mass of the travelling block, power swivel and other equipment between the measurement point and the connection point of the cables to the travelling block.

Equivalent spring constant, K_{eq} : This is largely governed by the cable diameter, lengths, and number of passes between the crown block and the travelling block.

The damping constant of the surface equipment R_s was chosen to provide a good match in the amplitudes of the simulated and measured transfer functions (Surface Acceleration to Surface Force, for a unit relative bit displacement excitation). The values of the equivalent mass, the equivalent stiffness and the damping constant for the drillstring under consideration are given in [16] and [9].

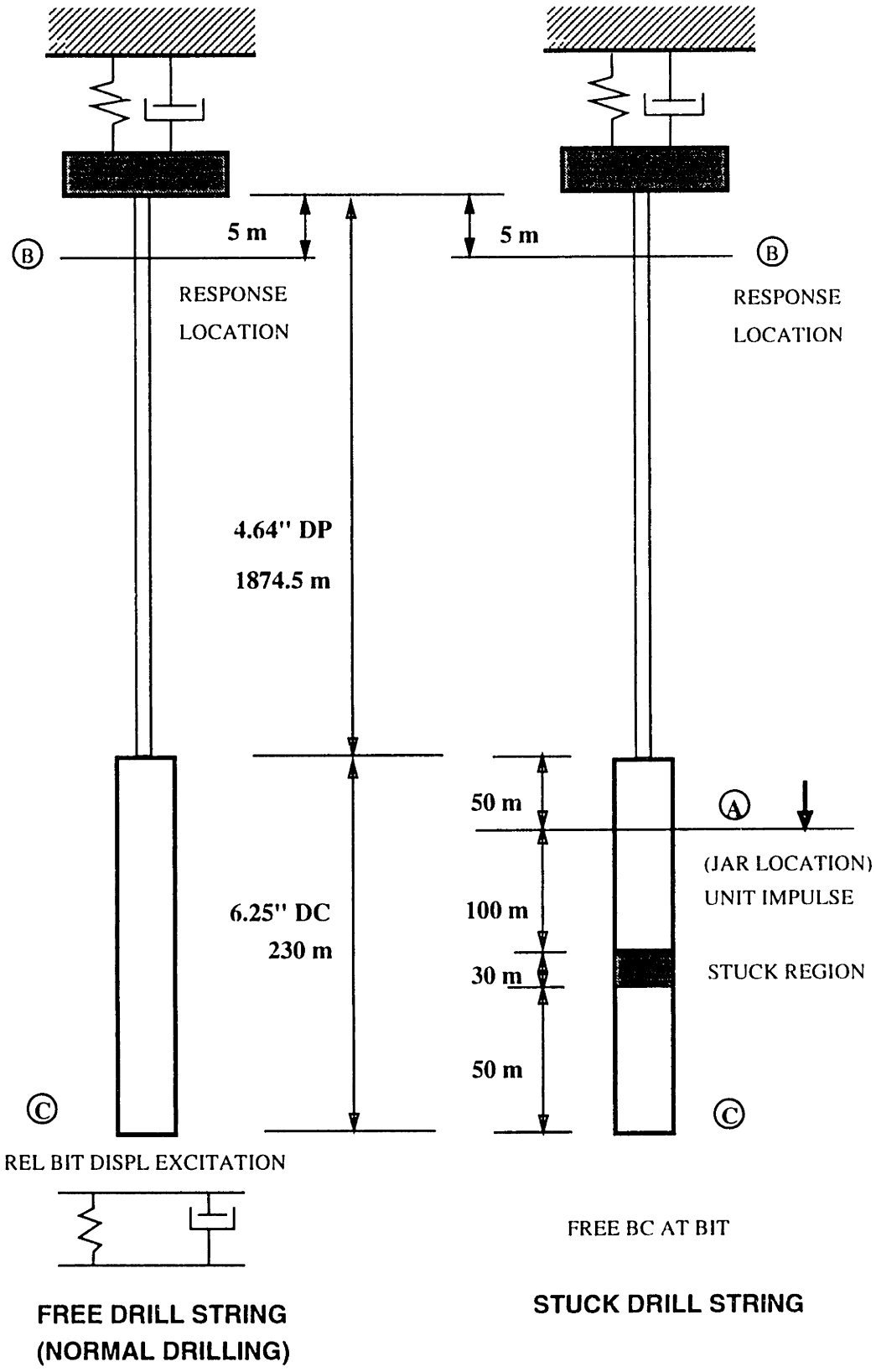

Figure 5-16: Analytical model of the drillstring under normal drilling operation and in the stuck condition

5.3.2 Normal Drilling Operation

Excitation : During normal drilling operation, the chief source of excitation is from the bit (position (C) in figure 5-16). This is modeled as a *unit relative bit displacement* excitation.

Response : *Force* at a surface location 5 m below the surface mass–spring–damper subsystem (position (B) in figure 5-16).

Bottom b.c.[5] **:** Rock stiffness $= 3.0 \times 10^5\ N/m$
Rock damping $= 7.5 \times 10^7\ N - s/m$

Discussion :

Figure 5-17 shows the magnitude and unwrapped phase of the predicted transfer function between the force at the surface (location B in figure 5-16) and a unit relative bit displacement excitation between the bit and the bottom boundary (location C in figure 5-16). The small, closely spaced peaks in the magnitude of the transfer function represent the resonances of the drillpipe behaving as a free–free bar. The spacing between the peaks correspond to $\frac{c}{2L_{DP}}$. Also seen, are the resonances of the BHA which are spaced farther apart and are very conspicuous. These peaks correspond to the resonances of the BHA behaving as a fixed–free bar. This is because the bottom boundary has a displacement excitation source. The transfer function then has peaks at the resonances of the BHA as if it had a fixed boundary condition at the bit [8]. At the same time, due to the large cross–sectional discontinuity at the BHA/drillpipe junction, this interface behaves predominantly as a free boundary. The BHA resonances occur at frequencies given by

$$f_n = (2n - 1)\frac{c}{4L} \qquad n = 1, 2, 3 \ldots$$

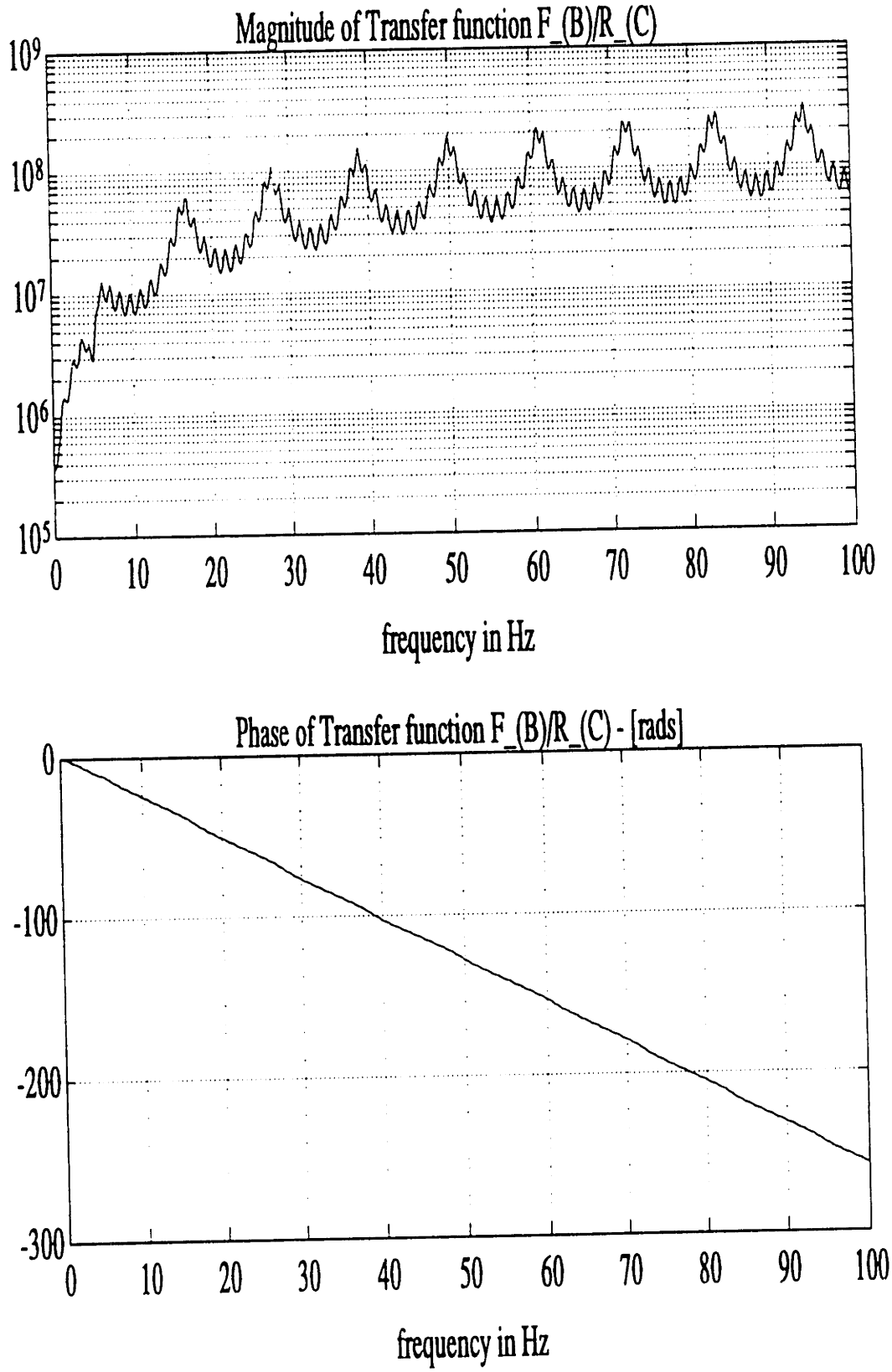

Figure 5-17: Magnitude and Unwrapped phase of the simulated transfer function between the *force* measured at the surface (5 m below the mass–spring–damper subsystem) and a *unit relative bit displacement* excitation between the bit and the bottom.

Thus the resonances of the BHA occur at 16.83 Hz, 27.85 Hz, 38.75 Hz and so on.

The unwrapped phase of the transfer function is a measure of the propagation delay between the input and the output locations. Though the damping in the system is small, it is sufficient to smoothen out the phase transitions due to poles (resonances of the system) resulting in a continuous phase curve. From the plot of the unwrapped phase as a function of frequency, it is possible to obtain the *group delay* at any frequency by taking the negative of the local slope of the phase curve. The group delay is defined as

$$\tau_g(f) = -\frac{1}{2\pi}\left(\frac{d\theta}{df}\right) \tag{5.38}$$

where

τ_g : Group delay

θ : Unwrapped phase angle [radians]

Thus, we see that a phase which continuously increases with frequency produces a group delay which is proportional to the slope of the phase curve. In our case, since the damping is very small, the phase curve is linear. The mean group delay calculated from the phase curve, over a frequency band from 0.2–819.2 Hz was found to be

$$\tau_g|_{\text{ from phase curve}} = 0.4113 \; secs \tag{5.39}$$

Since the separation between the source and response locations is known (2099.5 m), one can estimate the group delay by assuming the group speed of longitudinal waves in steel to be the same as the phase speed (5100 m/s), since damping is small.

$$\tau_g = \frac{2099.5}{5100} = 0.4117\ secs \tag{5.40}$$

The group delay calculated from the phase curve agrees with that calculated with a knowledge of the source–receiver separation distance (assuming a group speed of 5100 m/s).

5.3.3 Stuck condition – Input Force Impulse at Jar location

Figure 5-16 on page 116 shows the mechanical model of the drillstring in the stuck condition. Two cases are studied in particular.

1. Distributed damping model of the stuck region
2. Distributed stiffness model of the stuck region

The data relevant to the stuck case is presented in the following table. Other drillstring particulars are the same as described in section (5.3.1)

Data for figure 5-16 & 5-27 – Stuck case	
Jar location (L_{IJ} : distance below DP/BHA interface)	50 m
Stuck region (L_{IS} : distance below DP/BHA interface)	150 m
Stuck region (L_{JS} : distance below jar)	100 m
Stuck length (L_S)	30 m
BHA length between bottom of stuck region and bit (L_{SB})	50 m
BHA length between jar location and bit (L_{JB})	180 m
Total length of BHA (L_{BHA})	230 m

5.3.4 Case 1) – Distributed stiffness model of the stuck region

In this case, the stuck region is modeled as a distributed stiffness. One can interpret this model as, the drillstring being restrained from moving axially. This is achieved by a set of springs distributed in a continuous manner between the BHA and the surrounding formation, along the entire length of the stuck region. This can be seen in figure 4-2 on page 61. The degree of restraint is governed by the value of the distributed stiffness.

Input : When the drillstring is stuck, there is no longer a relative bit displacement excitation. The source of excitation then, is from the jarring action. This is modeled as a *unit force impulse* in the time domain, at the jar location (position (A) in figure 5-16).

Response : *Force* at a surface location 5 m below the surface mass–spring–damper subsystem (position (B) in figure 5-16).

Bottom b.c : The drillstring is assumed to get stuck while tripping out. Under such circumstances, the bit is off–bottom and the boundary condition at the bottom is free.

Discussion :

Figure 5-18 shows the magnitude of the simulated transfer functions between the force at the surface (position B in figure 5-16) and a unit harmonic force excitation at the jar location (position A in figure 5-16) for different levels of distributed stiffness in the stuck region. The transfer functions are calculated over a frequency range from 0.2–819.2 Hz, with a step size of 0.2 Hz, but results are presented only upto 100 Hz for the sake of clarity. The values of distributed

stiffness used are given in the following table.

Data for figure 5-18 (DSM[6])		
Distributed Stiffness N/m $/m$		
	Stuck region	Elsewhere in drillstring
case a)	1.0×10^9	0.0
case b)	1.0×10^8	0.0
case c)	1.0×10^7	0.0
case d)	0.0	0.0
Elastic stiffness of stuck length of BHA $K_{SL} = \frac{EA_{BHA}}{L_S} = 1.0746 \times 10^8\ N/m$		

Case a) : Firmly stuck situation

This can be taken to represent the worst case scenario of the stuck pipe condition, since the force (per unit length of the stuck region) needed to cause a unit displacement of the stuck portion of the BHA, is the maximum in this instance owing to the high value of distributed stiffness. The distributed stiffness in the stuck region is much larger than the elastic stiffness of the stuck length of the BHA. This might be the condition a driller would start out with, when he first encounters stuck pipe (if the sticking mechanism behaves as a stiffness or a conservative restraint on the BHA). Figure 5-18 a) shows the surface force response as a function of frequency, due to a unit harmonic force input at the jar location. The sharp dips (zeros) of the transfer function indicate that the response location behaves as a node[7] for the measured **force** at those frequencies. Hence, for a finite harmonic force excitation at the jar location, the surface *force* response is negligible at frequencies corresponding to the zeros of the transfer function.

[7] A *small force* implies a *large displacement* and vice–versa

The first zero occurs at 5 Hz. This corresponds to the natural frequency of the mass–spring–damper subsystem at the top boundary, given by

$$\begin{aligned} f_0 &= \sqrt{\frac{K_{eq}}{M_{eq}}} = \sqrt{\frac{9\times10^6}{9100.0}} \\ &= 5.0\ Hz \end{aligned}$$

Thus, when the excitation frequency at the jar location is 5 Hz, the mass–spring–damper subsystem is forced at its resonant frequency. This causes large amplitude oscillations of the mass and a zero in the transfer function at that frequency (since the response location is at the surface). The position of this zero strongly depends on the force measurement location and the characteristics of the MSD[8] subsystem.

The subsequent zeros of the transfer function are of greater relevance and occur at frequencies 24.6, 49.8, 73.8 Hz.... These are nodal points due to standing waves which form in the section of the BHA between the jar and the top of the stuck region. The jar location and the top of the stuck region behave as fixed boundaries in this case. These frequencies are given by

$$\begin{aligned} f_n &= \frac{nc}{2L_{JS}} \qquad n = 1, 2, 3 \ldots \\ &= \frac{n\,5100}{2\times100} \qquad n = 1, 2, 3 \ldots \\ &= 25.5,\ 51.0,\ 76.5\ Hz\ldots \end{aligned} \tag{5.41}$$

where

L_{JS} is the BHA length between the jar and the top of the stuck region.

Thus, in this case, the top of the stuck region behaves as a rigid boundary. It should be noted that the stiffness due to external restraints over the stuck

[8]Mass–spring–Damper

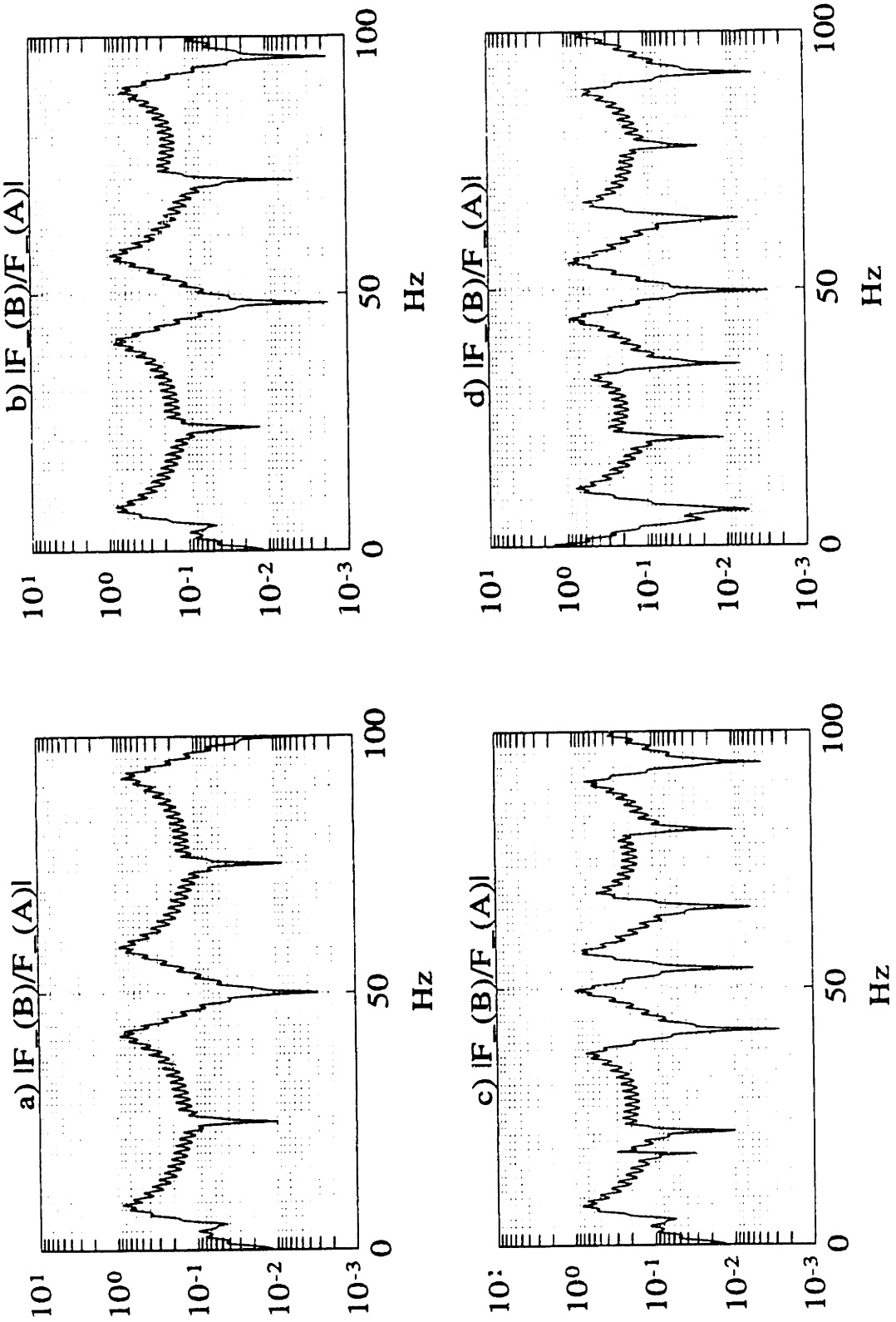

Figure 5-18: Magnitude of the simulated transfer function between the *force* measured at the surface (5 m below the mass–spring–damper subsystem) and a *unit harmonic force* excitation at the jar location, for different levels of distributed stiffness

a) $K = 1.0 \times 10^{9} N/m\ /m$ b) $K = 1.0 \times 10^{8} N/m\ /m$

c) $K = 1.0 \times 10^{7} N/m\ /m$ d) $K = 0.0\ N/m\ /m$

length ($(1.0 \times 10^9\ N/m\ /m) \times 30\ m$) is greater than the elastic stiffness of the stuck length of the BHA ($\sim 1.0 \times 10^8\ N/m$) by a factor of 300.

The peaks of the transfer function occur at frequencies 8.76, 41.8, 59.18 Hz.... These correspond to the resonances of the section of the BHA between the top of the stuck region and the BHA/drillpipe interface, behaving as a bar with *fixed-free* boundary conditions. These resonant frequencies are given by

$$\begin{aligned} f_n &= \frac{n\,c}{4\,L_{IS}} & n &= 1,\ 3,\ 5\ ... \\ &= \frac{n\ 5100}{4 \times 150} & n &= 1,\ 3,\ 5\ ... \\ &= 8.5,\ \ 25.5,\ \ 42.5\ Hz... \end{aligned} \tag{5.42}$$

where

L_{IS} is the BHA length between the BHA/drillpipe interface and the top of the stuck region.

Note that the resonances at 25.5 and 76.5 Hz are not excited because the jar is located at a node for these frequencies. It can also be observed that, in the absence of a resonance, the zero at 51.0 Hz becomes conspicuous. The small, closely spaced peaks in the figure represent the resonances of the drillpipe. These peaks have a frequency spacing given by $\frac{c}{2\,L_{DP}}$, where L_{DP} is the length of the drillpipe.

With a knowledge of the locations of the poles and zeros of the transfer function, one can determine the location of the stuck region from force measurements at the surface.

Cases b) & c) : Transition from a stuck to a free drillstring

Figures 5-18 b) & c) show the force at a surface location due to a unit harmonic force input at the jar location for distributed stiffness values of $1.0 \times 10^8\ N/m\ /m$

and 1.0×10^7 N/m $/m$ in the stuck region respectively. These represent stiffness values over the stuck length that are greater than the elastic stiffness of the stuck portion of the BHA by factors of 30 and 3 for the two cases. The position of the first zero stays at 5 Hz, since it represents the resonance of the mass–spring–damper subsystem and, as was pointed out earlier, its position depends on the response location and the characteristics of the mass–spring–damper subsystem.

Figure 5-18 b) differs from figure 5-18 a) in the location of the poles and zeros which have been slightly shifted to the left. The zeros now occur at frequencies 24.2, 48.17, 72.16 Hz.... These can be interpreted as nodal points due to standing waves which form in an effective length of the BHA between the jar and some point *within* the stuck region. At this point, the equivalent boundary condition is fixed. These resonant frequencies, which have nodes at the jar location are given by

$$\begin{aligned} f_n &= \frac{n\,c}{2\,L_{JS}^{eff}} \qquad n = 1,\ 2,\ 3\ \ldots \\ &= \frac{n\ 5100}{2 \times 106} \qquad n = 1,\ 2,\ 3\ \ldots \\ &= 24.1,\ \ 48.1,\ \ 72.16\ Hz\ldots \end{aligned} \tag{5.43}$$

where

L_{JS}^{eff} is the effective length of the BHA between the jar and an effective point within the stuck region, which behaves as if it were fixed.

The peaks of the transfer function occur at frequencies 8.20, 40.45, 57.60 Hz.... These correspond to the resonances of an effective section of the BHA between the BHA/drillpipe interface and a point within the stuck region, behaving as a bar with *free–fixed* boundary conditions. These resonant frequencies are given by

$$
\begin{aligned}
f_n &= \frac{nc}{4L_{IS}^{eff}} \qquad n = 1, 3, 5 \ldots \\
&= \frac{n\,5100}{4\times 156} \qquad n = 1, 3, 5 \ldots \\
&= 8.17,\ 24.5,\ 40.8\ Hz\ldots
\end{aligned}
\tag{5.44}
$$

where

L_{IS}^{eff} is the effective BHA length between the BHA/drillpipe interface and a point within the stuck region, which behaves as if it were fixed.

The difference between figures 5-18 b) and 5-18 c) is quite distinct due to the closer spacing between the zeros of the transfer function. Also, the modal force zeros which were obscuring the display of the resonances in cases a) and b) have moved sufficiently to unveil the peaks.

Case d) : Free drillstring

The force response at the surface due to a unit harmonic force input at the jar location is shown in figure 5-18 d) for a free drillstring. The zeros of the transfer function occur at frequencies 7.03, 21.2, 35.40 Hz.... These correspond to standing wave nodes of the BHA between the jar location and the bit, which has a free boundary condition. There are no displacement nodes at the jar location at these frequencies. These frequencies are given by

$$
\begin{aligned}
f_n &= \frac{nc}{4L_{JB}} \qquad n = 1, 3, 5 \ldots \\
&= \frac{n\,5100}{4\times 180} \qquad n = 1, 3, 5 \ldots \\
&= 7.08,\ 21.25,\ 35.41\ Hz\ldots
\end{aligned}
\tag{5.45}
$$

where

L_{JB} is the BHA length between the jar location and the bit.

The poles of the transfer function occur at 11.4, 23.4, 32.42 Hz.... These correspond to the resonances of the BHA behaving as a bar with *free–free* boundary conditions. These resonant frequencies are given by

$$\begin{aligned} f_n &= \frac{n\,c}{2\,L_{BHA}} \qquad n = 1,\ 2,\ 3\ ... \\ &= \frac{n\ 5100}{2 \times 230} \qquad n = 1,\ 2,\ 3\ ... \\ &= 11.08,\ 22.17,\ 33.26\ Hz... \end{aligned} \tag{5.46}$$

where

L_{BHA} is the length of the BHA.

Conclusions :

The sequence of transfer functions shown in figures 5-18 a) through 5-18 d) simulates the progress made in freeing a stuck drillstring, in the event of the sticking mechanism behaving as a conservative restraint preventing the stuck length of the BHA from moving axially. In case c), we saw that the top of the stuck region behaved as a rigid boundary and the length of the BHA below the stuck region had no bearing on the zeros and poles of the transfer function. This agrees with figure 5-5 on page 97, where the force transmission coefficient is shown as a function of frequency, through a barrier modeled as a distributed stiffness. It can be seen that the transmission coefficient is unity only *above the cut–off* frequency which for a distributed stiffness of $1.0 \times 10^9\ N/m\ /m$ is 452 Hz. Below the cut–off frequency, the transmission coefficient can be seen to drop–off very steeply. Thus, for the frequency range over which the transfer function is shown (0–100 Hz), there is no transmission into the stuck region.

Case b) simulates a situation where, due to continuous jarring, the distributed stiffness over the stuck length has reduced to 1.0×10^8 N/m $/m$. The corresponding cut–off frequency is 143 Hz. The transmission coefficient in this case though small (figure 5-5), is not insignificant for the frequency range 0–100 Hz. This causes a slight shift to the left, of the poles and zeros of the transfer function which indicates that some energy is being transmitted into the stuck region below 100 Hz.

Case c) indicates further progress towards freeing the stuck drillstring, where the stiffness in the stuck region is now 1.0×10^7 N/m $/m$. The corresponding cut–off frequency is $\sim$ 45 Hz. Thus, a significant amount of energy is transmitted through the stuck region below 100 Hz and this causes additional zeros to appear in the transfer function (in the frequency range $0 - 100$ Hz.)

Finally in case d), the zeros correspond to nodes at the jar location, when the bit has a free boundary condition, indicating that the jarring operation has indeed been successful.

Impulse Response :

Figures 5-19 a) through 5-19 d) show the impulse responses (*force* at the surface due to a *unit force impulse* at the jar location) for various levels of distributed stiffness. The impulse responses are obtained by inverse fourier transforming the transfer functions ($0 - 819.2$ Hz), followed by *smoothening using a* 3 ms *blackman window.* The impulse responses correspond to the cases shown in figure 5-18 in the same order, and simulate the force measurements at the surface during jarring, in proceeding from a stuck to a free drillstring.

The first peak in all of the four cases corresponds to the direct arrival (0.3766 $secs$) of the input force pulse. The subsequent peaks represent echoes/superposition of echoes, a result of reflections at boundaries and consequent ringing effects. The second peak in the free drillstring, (case d)) is the reflection off the bottom

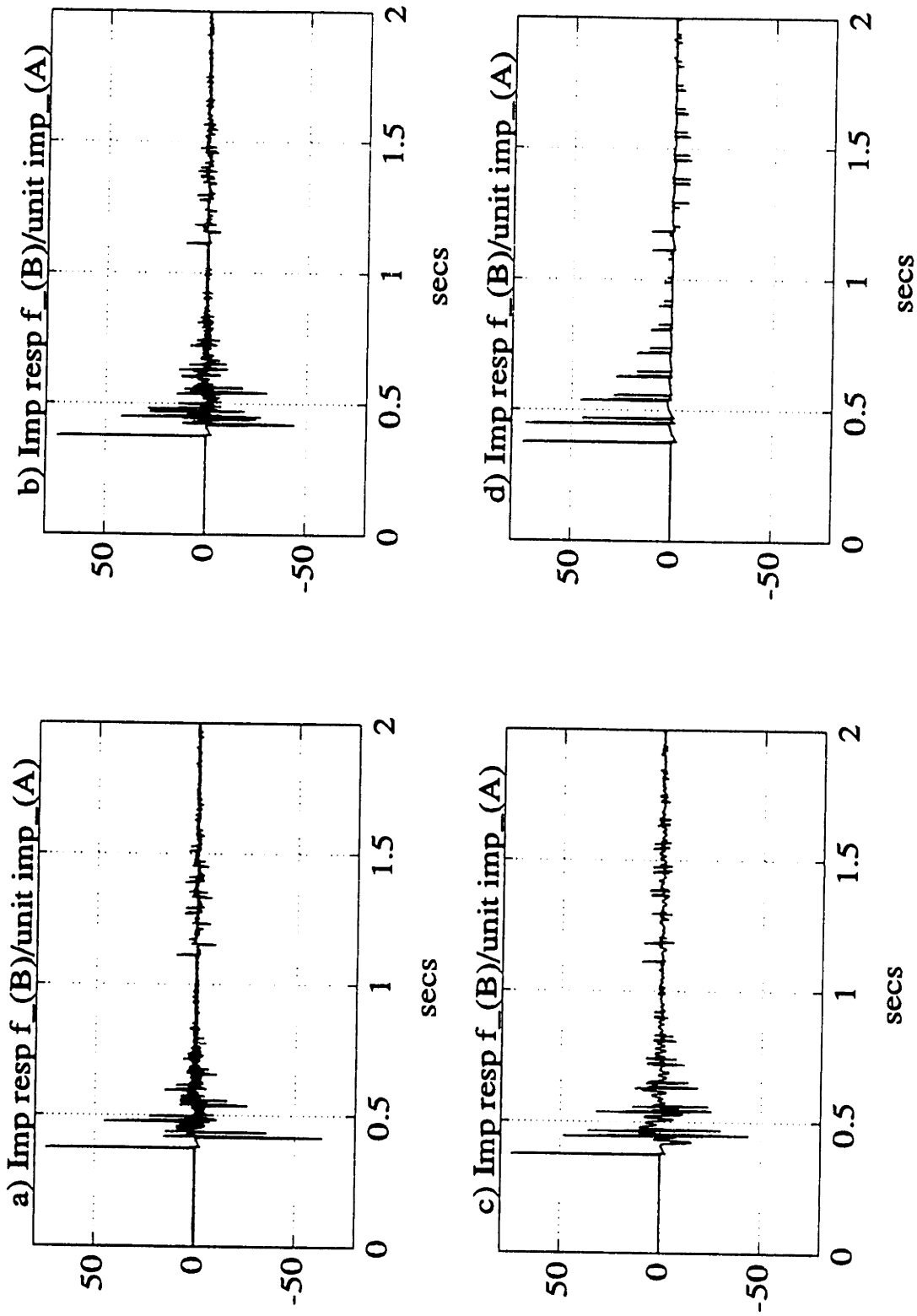

Figure 5-19: *Force* response at the surface (5 m below the mass-spring-damper subsystem) due to a *unit force impulse* at the jar location, for different levels of distributed stiffness

a) $K = 1.0 \times 10^9 N/m\ /m$ b) $K = 1.0 \times 10^8 N/m\ /m$

c) $K = 1.0 \times 10^7 N/m\ /m$ d) $K = 0.0\ N/m\ /m$

boundary; the bit being a free end causes the force signal to flip signs. In cases a), b) and c) the second arrival corresponds to the reflection from the stuck region (The force signal does not change signs in this case). The impulse response dies out eventually due to internal damping in the drillstring. In the presence of a stuck region, it is generally not possible to distinguish between signal arrivals in plots of impulse responses, due to the complex nature of the reflected and transmitted waveforms at the stuck region.[9] Hence assessment of jarring effectiveness from impulse response calculations, is not the best approach in the distributed stiffness model of the stuck region. To overcome this problem, a different technique, the *cepstral analysis* is employed. This will be discussed in section (5.3.6).

5.3.5 Case 2) – Distributed damping model of the stuck region

The stuck region is modeled as a dissipative region by a series of viscous dashpots continuously distributed between the BHA and the surrounding formation. This is shown in figure 4-3 on page 62. The instantaneous power dissipated at any point in the stuck region is given by the product of the instantaneous dashpot force and the instantaneous velocity at that point. The power dissipated is governed by the value of the distributed damping constant.

Input : A *unit force impulse* in the time domain, at the jar location (position (A) in figure 5-16).

Response : *Force* at a surface location 5 m below the surface mass–spring–damper subsystem (position (B) in figure 5-16).

Bottom b.c : Free boundary condition at the bit.

[9] shown in figure 5-7 and figure 5-8. The reflected and transmitted waveforms no longer retain the shape of a pulse, leading to a superposition of the various arrivals at the surface

Discussion :

The simulated surface response (position B in figure 5-16) for a unit harmonic force excitation at the jar location (position A in figure 5-16) is shown in figure 5-20 for various levels of distributed damping in the stuck region. The transfer functions are presented only up to 100 Hz. The values used for distributed damping are given in the following table.

Data for figure 5-18 (DDM[10])		
Distributed Damping $N - s/m\ /m$		
	Stuck region	Elsewhere in drillstring
case a)	1.1×10^6	1.1×10^2
case b)	1.1×10^5	1.1×10^2
case c)	1.1×10^4	1.1×10^2
case d)	1.1×10^2	1.1×10^2

The worst case scenario in the event when the stuck region behaves as an absorptive medium is illustrated in figure 5-20 a). With effective jarring, one would see a shift to the left, of the frequencies at which the poles and zeros of the transfer function occur, as shown in figure 5-20 b). As the drillstring approaches the free case, the spacing between the zeros decreases (figure 5-20 c)) due to energy being transmitted through the stuck region and being reflected off the free boundary at the bit. The completely free case is shown in figure 5-20 d). The locations of the zeros and poles in cases a) and d) are the same as was for the distributed stiffness model (DSM). However, it can be seen that the peaks and valleys are not as sharp, due to damping.[11]

[11]The zero at 5 Hz is not affected by damping in the stuck region since it represents the natural

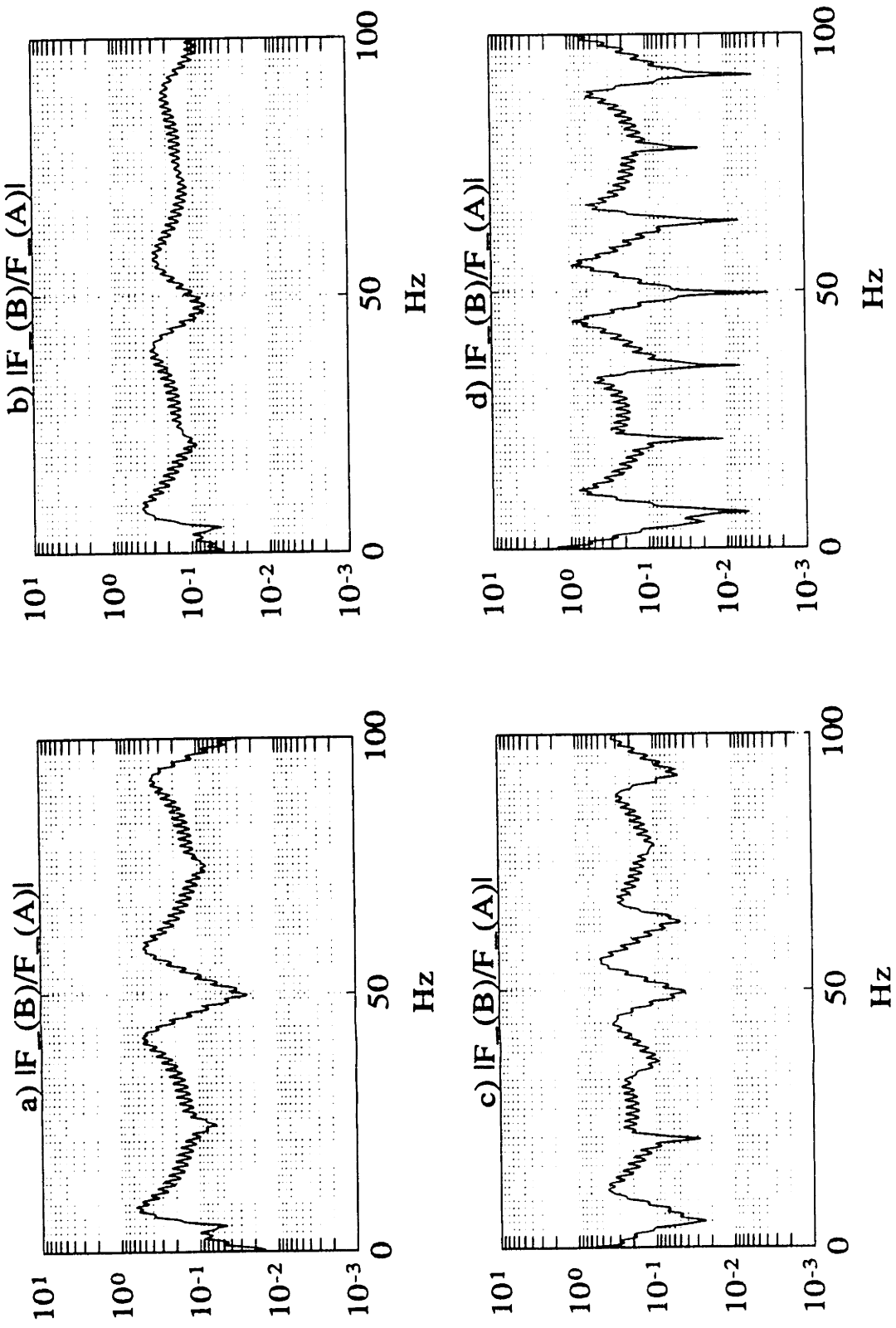

Figure 5-20: Magnitude of the simulated transfer function between the *force* measured at the surface (5 m below the mass–spring–damper subsystem) and a *unit harmonic force* excitation at the jar location, for different levels of distributed damping

a) $R = 1.1 \times 10^6 N - s/m\ /m$ b) $R = 1.1 \times 10^5 N - s/m\ /m$

c) $R = 1.1 \times 10^4 N - s/m\ /m$ d) $R = 1.1 \times 10^2 N - s/m\ /m$

Conclusions :

The transfer functions in figures 5-20 a) through figure 5-20 d) simulate the force response at the surface to jarring, for the cases when the stuck region is modeled as distributed damping. In case a), it was noted that the poles and zeros of the transfer function occur at the same frequencies for both the DSM and the DDM for the frequency range over which the transfer functions are plotted. This is consistent with figure 5-12 on page 108, where the force transmission coefficient through a barrier modeled as distributed damping is shown. It can be seen that the transmission coefficient is extremely small and a monotonically decreasing function of frequency. There is thus, negligible transmission of energy into the stuck region. Differences between the two models would become apparent for frequencies above the cut–off frequency (452 Hz), when there is near total transmission through the stuck region in the DSM resulting in a decrease in the frequency spacing between the zeros of the transfer function.

Cases b) & c) represent the transition from the stuck to the free case. The transmission coefficient is significant in the range $0 - 100\ Hz$ for a distributed damping value of $1.1 \times 10^5\ N - s/m\ /m$ (case b)), and is close to unity when the distributed damping is $1.1 \times 10^4\ N - s/m\ /m$ (case c)), as can be seen from figure 5-12. For cases b) & c), energy is transmitted through the stuck region over the entire frequency band considered ($0 - 100\ Hz$), resulting in a closer spacing between the poles and zeros of the transfer function.[12]

Case d) represents the free drillstring and was analyzed in section 5.3.4.

Impulse Response :

---

frequency of the mass–spring–damper subsystem atop the drillstring and is therefore, independent of the stuck region.

[12]The frequencies at which the zeros occur can be interpreted as resonances of an effective length of the BHA between the jar location and some point in the stuck region behaving as a fixed–fixed bar. As energy transmitted through the stuck region increases, this effective BHA length also increases, causing the zeros to be spaced closer to each other. A similar argument holds for the poles of the transfer function.

The *force* response at the surface due to a *unit force impulse* at the jar location is shown in figures 5-21 a) through d) for various levels of distributed damping. The first peak corresponds to the direct arrival. The subsequent arrivals correspond to reflections from the stuck region in cases a) & b); the peak at 1.11 *secs* is due to the ringing of the pulse in the drillpipe. The area under the reflected force pulse from the stuck region in case b), as seen at the surface is very small; at the same time no reflections from the bottom boundary are observed.[13] With a knowledge of the difference in momentum (as given by the difference in areas under the input pulse and reflected pulse from the stuck region), a measure of the power dissipated in the stuck region can be obtained.

Figure 5-21 c) shows that, with a decrease in damping, strong reflections from the free end at the bit are also seen in addition to weak reflections from the stuck region, indicating that most of the energy is transmitted through the stuck region. Finally, in case d), the peaks represent reflections from the bit and the BHA/drillpipe interface.

It should be noted that though it is possible to distinguish between the various arrivals by looking at the impulse response in a DDM (for a relatively simple drillstring), this is not true in the DSM of the stuck region.

5.3.6 Cepstral Analysis in Waveform Recovery

It was pointed out with reference to the distributed stiffness model that the it is not easy to distinguish between arrivals from various boundaries, from the impulse response function. The cepstral analysis is mainly used, when the impulse response of a system becomes folded with the input such that separate extraction of the source and path information becomes virtually impossible in

[13]If reflections had been observed, distinct resonances would have been observed in the surface response corresponding to the section of the BHA between the stuck region and the bit, which is not so.

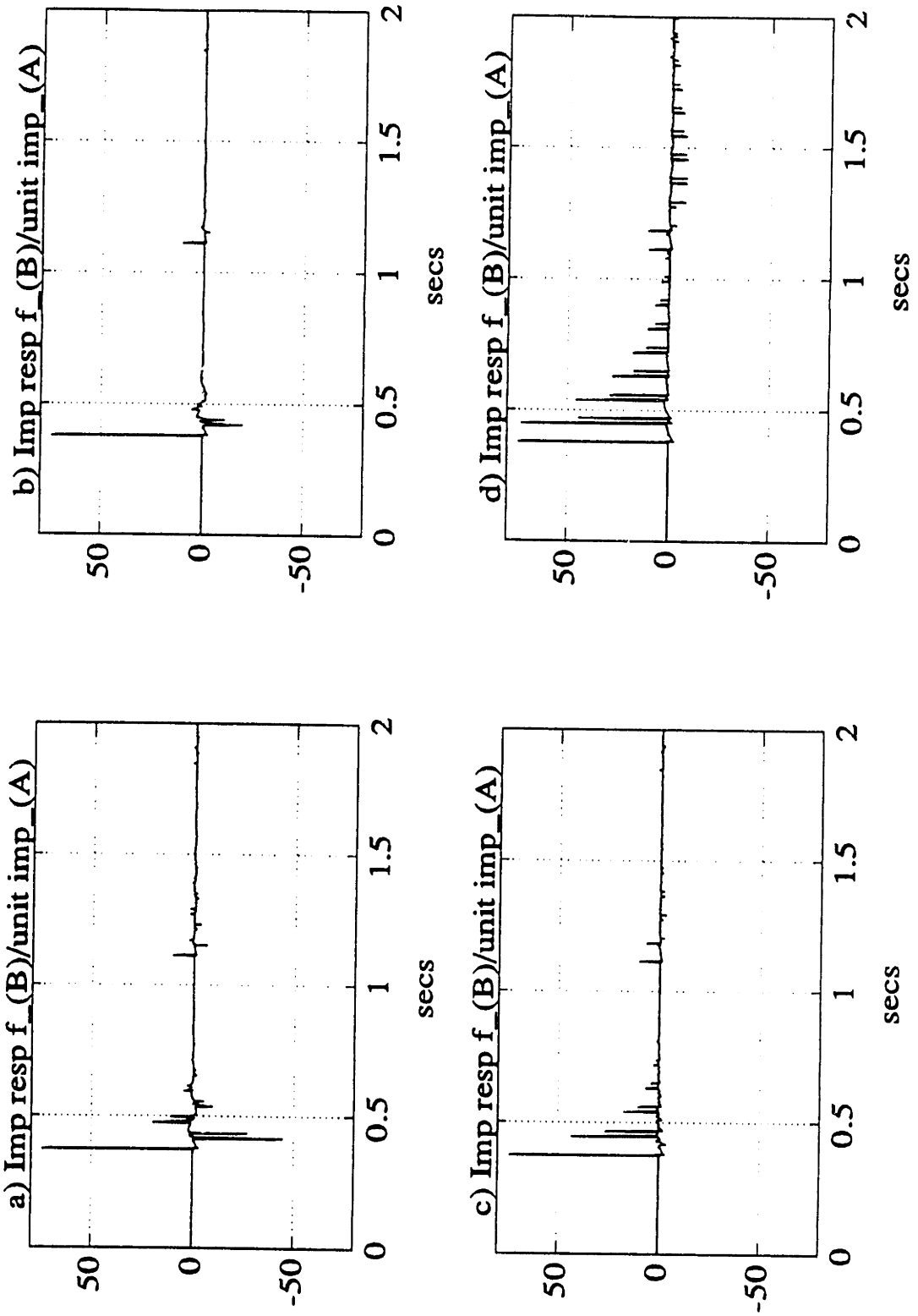

Figure 5-21: *Force* response at the surface (5 m below the mass–spring–damper subsystem) due to a *unit force impulse* at the jar location, for different levels of distributed damping

a) $R = 1.1 \times 10^6 N - s/m\ /m$ b) $R = 1.1 \times 10^5 N - s/m\ /m$

c) $R = 1.1 \times 10^4 N - s/m\ /m$ d) $R = 1.1 \times 10^2 N - s/m\ /m$

the time domain. In our case, the input is an impulse and the output is the impulse response; hence the question of folding with the input does not arise. However, we shall see that, identification of various arrivals becomes much easier in the cepstral domain. This is because the peaks in the power cepstrum, in spite of having the same time periodicity as the impulse response, die away much more quickly. The main premise behind cepstral analysis is that the logarithm of the Fourier transform of a signal containing an echo has an additive periodic component due to the echo, and hence the inverse fourier transform of the log magnitude (of the fourier transform of the signal) exhibits a peak at the echo delay. This function is called the *real* or the *power cepstrum.* In mathematical terms,

$$H(\omega) = \int_0^\infty h(t)e^{-j\omega t}dt \tag{5.47}$$

The power or real cepstrum is then defined as :

$$C_{\hat{h}} = \frac{1}{2\pi}\int_{-\infty}^{\infty} \log \mid H(\omega) \mid e^{j\omega t}d\omega \tag{5.48}$$

where

$h(t)$	:	Impulse response of the system
$H(\omega)$	:	Transfer function of the system
$C_{\hat{h}}$	:	Power or real cepstrum of the impulse response

A more rigorous discussion on cepstral analysis can be found in [13] and [10].

5.3.7 Cepstral Analysis: Application to Distributed Stiffness and Distributed Damping Models of the stuck region

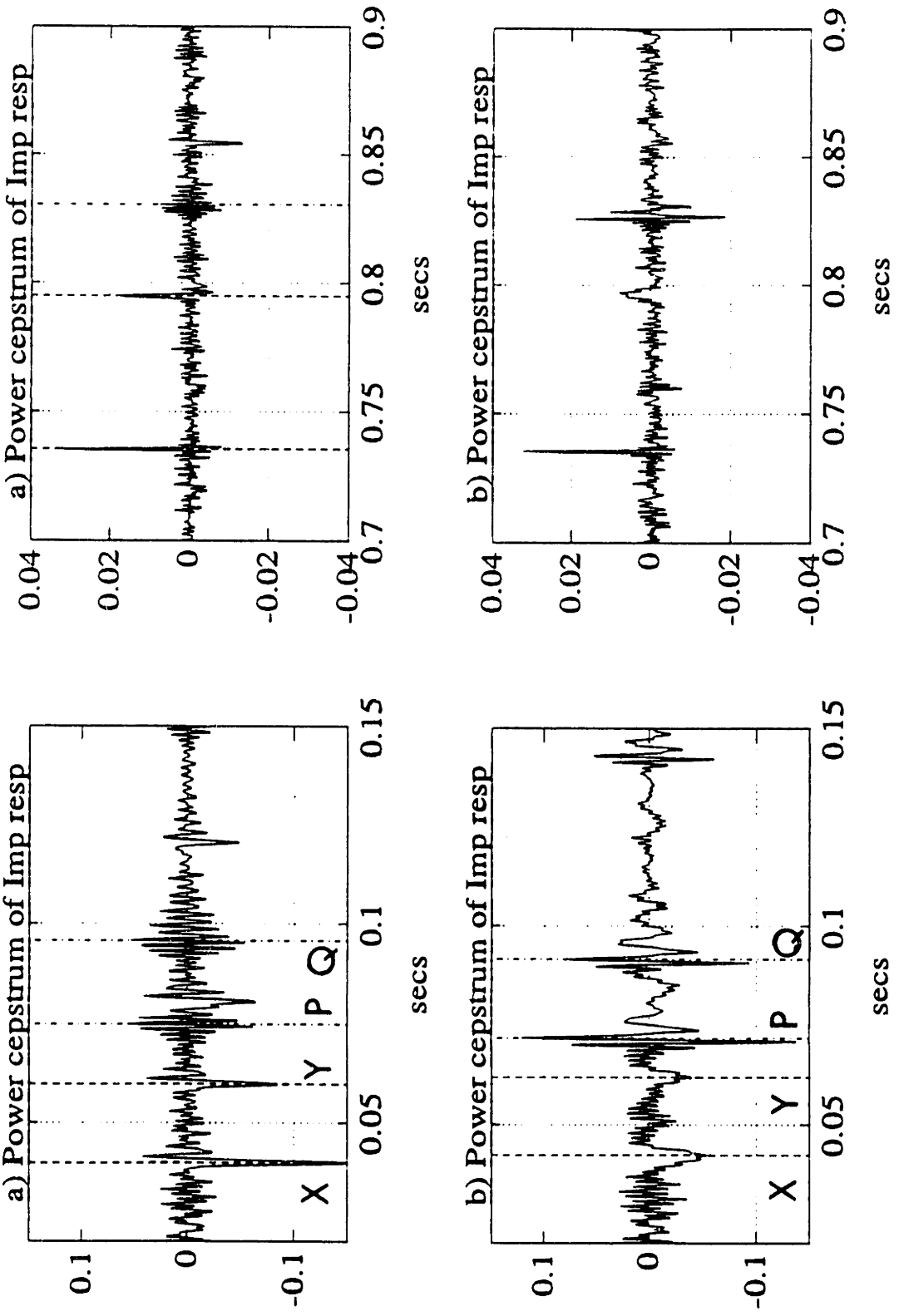

Figure 5-22: *Power cepstrum of response* at the surface (5 m below the mass–spring–damper subsystem) due to a *unit force impulse* at the jar location, for different levels of distributed stiffness

a) $K = 1.0 \times 10^9 N/m\ /m$

b) $K = 1.0 \times 10^8 N/m\ /m$

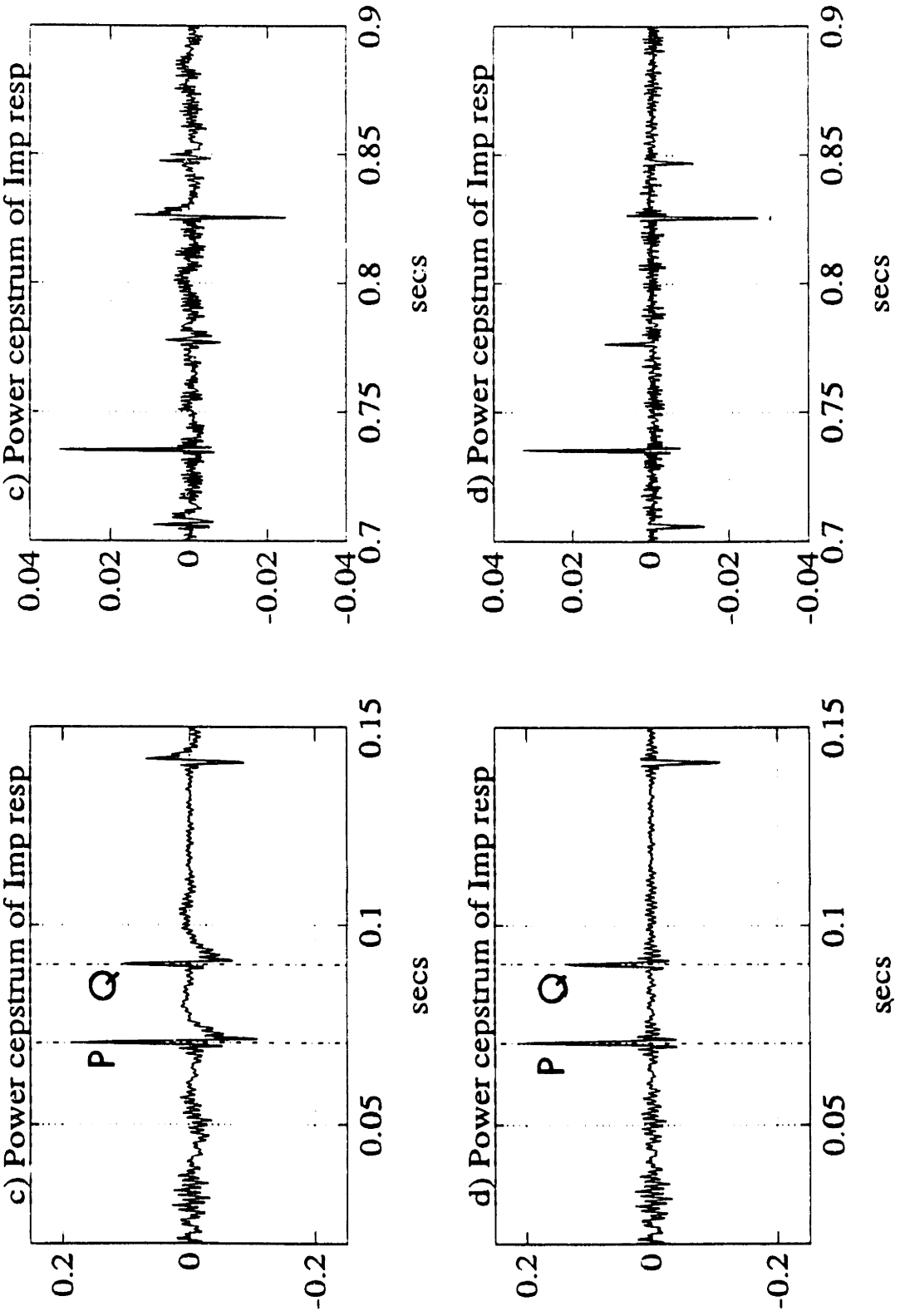

Figure 5-23: *Power cepstrum of response* at the surface (5 m below the mass–spring–damper subsystem) due to a *unit force impulse* at the jar location, for different levels of distributed stiffness

c) $K = 1.0 \times 10^7 N/m\ /m$

d) $K = 0.0\ N/m\ /m$

Distributed Stiffness Model (DSM) :

The impulse response at the surface due to a unit force impulse at the jar location was shown in figures 5-19 a) through d) for various levels of distributed stiffness. Figures 5-22 a) & b) and 5-23 c) & d) represent the power cepstrum of the impulse response for the corresponding cases. The power cepstrum is plotted from 0.02-0.15 *secs* and again from 0.7-0.9 *secs* for easy comparison and interpretation of results, as it is during these time intervals that echoes of primary interest are observed.

Case a) represents the firmly stuck case with a distributed stiffness value of 1.0×10^9 N/m $/m$ in the stuck region. It can be seen that strong echoes occur at times 0.0400 *secs* and 0.0597 *secs*. These represent time delays of subsequent arrivals relative to the direct arrival[14]. The peak at 0.0400 *secs* is the delay corresponding to the reflection of the pulse[15] (**X**) from the stuck region, whereas that at 0.0597 *secs* is the delay that corresponds to a pulse (**Y**) which undergoes reflections at the BHA/drillpipe interface and at the stuck region before making its way to the surface. The delays correspond to propagation distances of 204 m and 305 m respectively. In addition, strong peaks also occur at 0.0748 *secs* and 0.0958 *secs*.[16] 0.0748 *secs* is the delay corresponding to the reflection of the transmitted waveform (**P**) at the bottom free boundary; the peak at 0.09576 *secs* represents the time delay corresponding to the case where the pulse (**Q**) undergoes reflections at the BHA/drillpipe interface and at the bit before reaching the surface. Assuming that these peaks are representative of the wave group, the group velocity in the stuck region can be calculated as

$$\frac{2\,L_S}{c_g} + \frac{2(L_{JS} + L_{SB})}{5100} = 0.07476 \qquad (5.49)$$

[14]All time delays in the cepstral plots are with reference to the direct path arrival

[15]The various pulses and waveforms will be identified by the bold face letters in parentheses next to them, in the remainder of this chapter

[16]Above the *cut-off* frequency (452 Hz), there is propagation through the stuck region.

$$\frac{60}{c_g} + \frac{300}{5100} = 0.0746$$
$$c_g \sim 3765\ m/s \qquad (5.50)$$

The peaks at 0.7352 *secs* and 0.7949 *secs* represent echoes which occur every 3750 m and 4053 m respectively. These correspond to propapagation distances of $2\,L_{DP}$ and $2(L_{DP} + L_{IS})$ and indicate the ringing of the pulse in the drillpipe and in the length of the drillstring, which includes the drillpipe and the BHA above the stuck region. The echo at 0.8304 *secs* corresponds to a propagation distance equal to twice the length of the drillstring. Thus, the cepstrum produces peaks at time delays corresponding to signal arrivals which have a strong periodicity. In the rest of the discussion, only the time interval 0.02–0.15 *secs* will be analyzed.

The distributed stiffness in the stuck region in case b) is lower by a factor of 10 ($1.0 \times 10^8\ N/m\ /m$) than in case a) (as a result of jarring being effective to some extent). The first two strong echoes correspond to **X** and **Y**. The echoes corresponding to reflections from the stuck region are no longer as strong or as sharp as was seen in case a). The subsequent peaks at 0.0719 *secs* and 0.0916 *secs* represent **P** and **Q**. The peaks are much sharper since a wider band of frequencies now propagate through the stuck region owing to a lower cut–off frequency. The group velocity in the stuck region is calculated to be $\sim 4570\ m/s$.

In case c), the distributed stiffness is further reduced to $1.0 \times 10^7\ N/m\ /m$. Here, there is no echo corresponding to reflections from the stuck region. Most of the energy is transmitted through the stuck region. The peaks at 0.0705 *secs* and 0.0900 *secs* correspond to **P** and **Q** respectively. It can be observed that the shape of the echoes due to reflection from the bottom boundary bears a resemblance to the transmitted waveform through a barrier modeled as a distributed stiffness and shown in figure 5-8 on page 104.

The power cepstrum of the impulse response for a free drillstring is shown in case

d). The peaks at 0.0705 *secs* and 0.0903 *secs* represent **P** and **Q** respectively. The peaks are very sharp due to absence of any significant dispersive effects. The group velocity ($\sim$ 5100 m/s) in this case, is the same throughout the drillstring since damping is negligible.

Distributed Damping Model (DDM) :

Figures 5-24 a) & b) and 5-25 c) & d) show the power cepstrum of the impulse response for various levels of distributed damping (shown for the same time intervals as was plotted in figures 5-22 and 5-23).

Case a) represents the firmly stuck case with the stuck region modeled as a distributed damping of value $1.1 \times 10^6\ N-s/m\ /m$. It can be seen that strong echoes occur at times 0.0393 *secs* and 0.0592 *secs*. These represent time delays of subsequent arrivals relative to the direct arrival. The peak at 0.0393 *secs* corresponds to the reflection of the pulse (**X**) from the stuck region, whereas that at 0.0592 *secs* corresponds to the pulse (**Y**) that undergoes reflections at the BHA/drillpipe interface and at the stuck region before making its way to the surface. The delays correspond to propagation distances of 201 m and 301 m respectively. It should be noted that this differs from case a) of the DSM in that there is no transmission through the stuck region and hence no echo corresponding to reflection from the free boundary at the bit, is seen.

The distributed damping in case b) is lower ($1.1 \times 10^5\ N/m\ /m$) by a factor of 10 than that in case a). From figure 5-24 b), it can be noticed that there are no strong echoes, though weak reflections from the stuck region can be seen. This implies that most of the energy is being dissipated in the stuck region, which is a sign of effective jarring operation.

Figure 5-25 c) represents a case where the damping is further reduced to $1.1 \times 10^5\ N/m\ /m$. In this case, there are no echoes associated with reflections from the stuck region. Echoes however occur at times 0.0705 *secs* and 0.0904 *secs* corresponding to reflections from the free boundary at the bit. This indicates

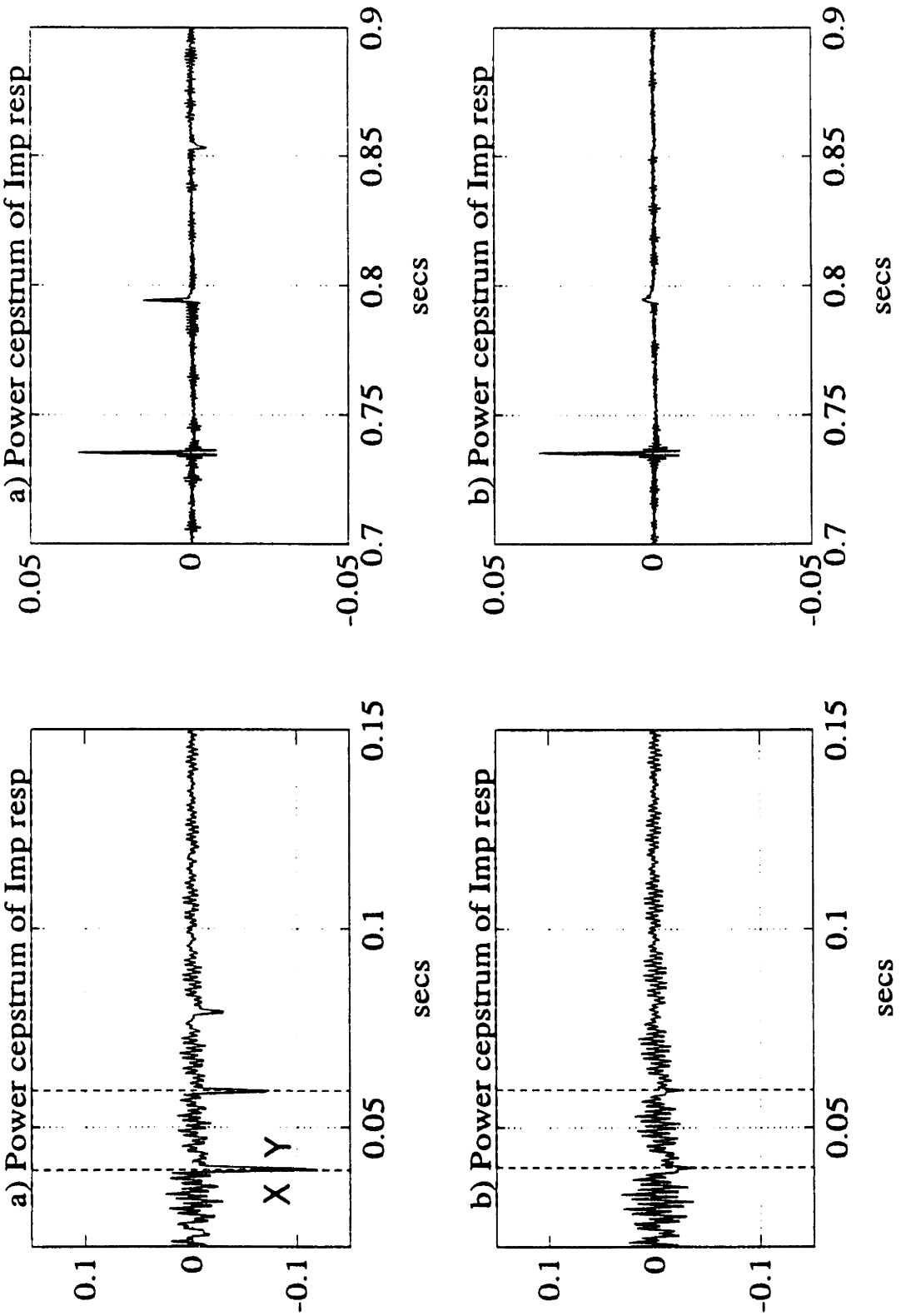

Figure 5-24: *Power cepstrum of response* at the surface (5 m below the mass–spring–damper subsystem) due to a *unit force impulse* at the jar location, for different levels of distributed damping

a) $R = 1.1 \times 10^6 N - s/m\ /m$

b) $R = 1.1 \times 10^5 N - s/m\ /m$

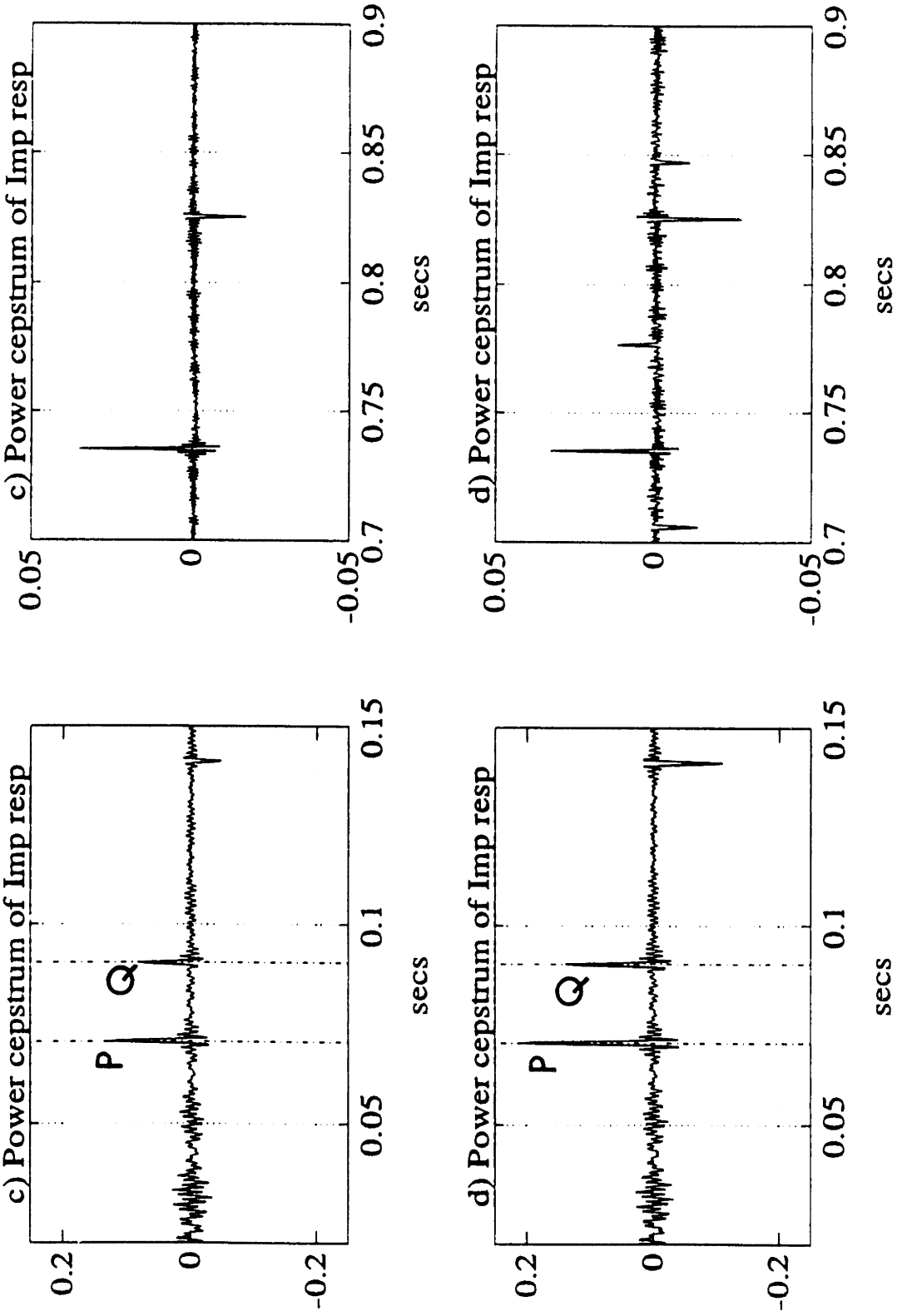

Figure 5-25: *Power cepstrum of response* at the surface (5 m below the mass–spring–damper subsystem) due to a *unit force impulse* at the jar location, for different levels of distributed damping

c) $R = 1.1 \times 10^4 N - s/m\ /m$

d) $R = 1.1 \times 10^2 N - s/m\ /m$

that some of the energy is dissipated and some of it transmitted through the stuck region. The group velocity of the pulse through the stuck region can be calculated as

$$\frac{2\,L_S}{c_g} + \frac{2(L_{JS} + L_{SB})}{5100} = 0.0705 \tag{5.51}$$

$$\frac{60}{c_g} + \frac{300}{5100} = 0.0705$$

$$c_g \sim 5150\ m/s \tag{5.52}$$

Figure 5-25 d) shows the cepstrum of the impulse response for a free drillstring. This differs from case c) in that the echoes are much stronger. The peaks at 0.0705 *secs* and 0.0903 *secs* represent reflections **P** and **Q** respectively.

Thus, we have seen how the cepstrum plots can be used as an analysis tool for evaluating jarring effectiveness. It must however be borne in mind, that most of the jars are uphit jars,[17] and hence can be tripped only when the drillstring is stuck. Therefore, in most of the situations, the signature of a free drillstring due to the tripping of the jar cannot be obtained. This is the motivation behind studying *example 5.4* where a force impulse is delivered to the drillpipe at the surface and the resulting response measured, also at a surface location.

5.4 Example 5.4 – Input impulse at surface location

A jar downhole, is usually tripped only under stuck conditions, whereas an impulse can be delivered to the drillpipe at the surface even when the drillstring is free. One can thus have a baseline measurement of the impulse response at the surface in the free case, which can then be used in the evaluation of jarring

[17] *trip under a tensile overpull at the surface*

effectiveness. A flowchart indicating the sequence of steps is shown in figure 5-26.

The drillstring considered is the same as the one used in example 5.3, and is described in section (5.3.1) on page 114. The analytical model of the drillstring is shown in figure 5-27 on page 148. Two cases are analyzed - the distributed stiffness and the distributed damping models of the stuck region. The data relevant to the stuck cases along with the nomenclature used is given in the table that follows

Data for figure 5-27 - Stuck case	
Stuck region (L_{IS} : distance below DP/BHA interface)	150 m
Stuck length (L_S)	30 m
BHA length between bottom of stuck region and bit (L_{SB})	50 m
Total length of BHA (L_{BHA})	230 m

5.4.1 Case 1) – Distributed stiffness model of the stuck region

Input : The input at the surface (position (A) in figure 5-27) is modeled as a unit force impulse in the time domain.

Response : *Force* at a surface location 2 m below the surface mass–spring–damper subsystem and 3 m above the input location (position (B) in figure 5-27).

Bottom b.c : The drillstring is assumed to be off–bottom when it gets stuck; the bottom boundary is therefore modeled as a free boundary.

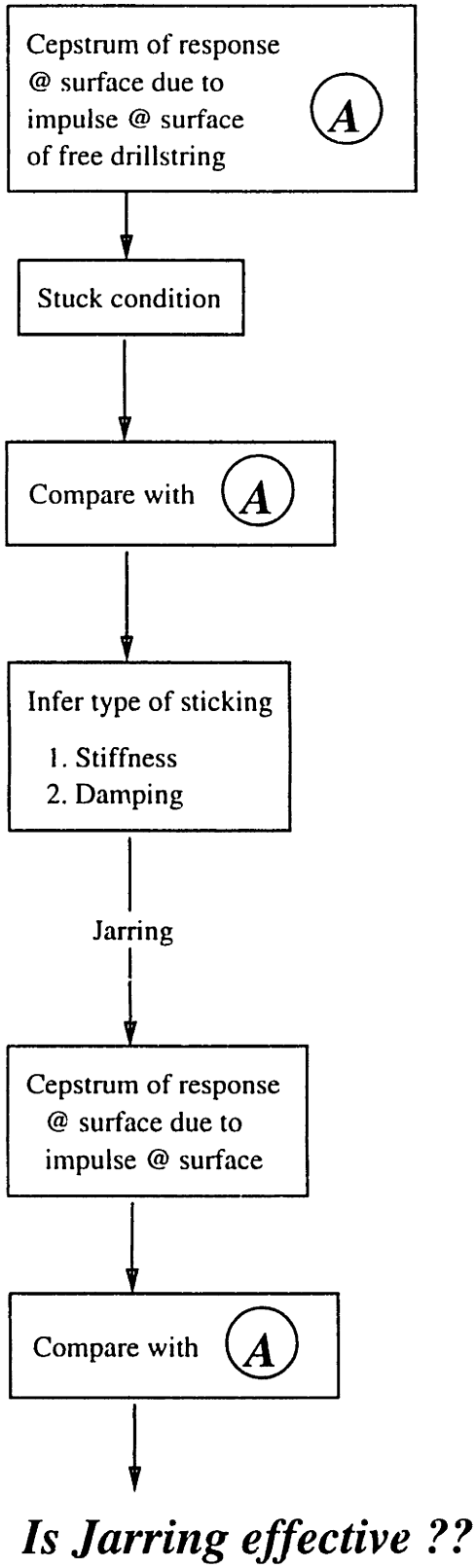

Figure 5-26: Flow chart for evaluation of jarring effectiveness

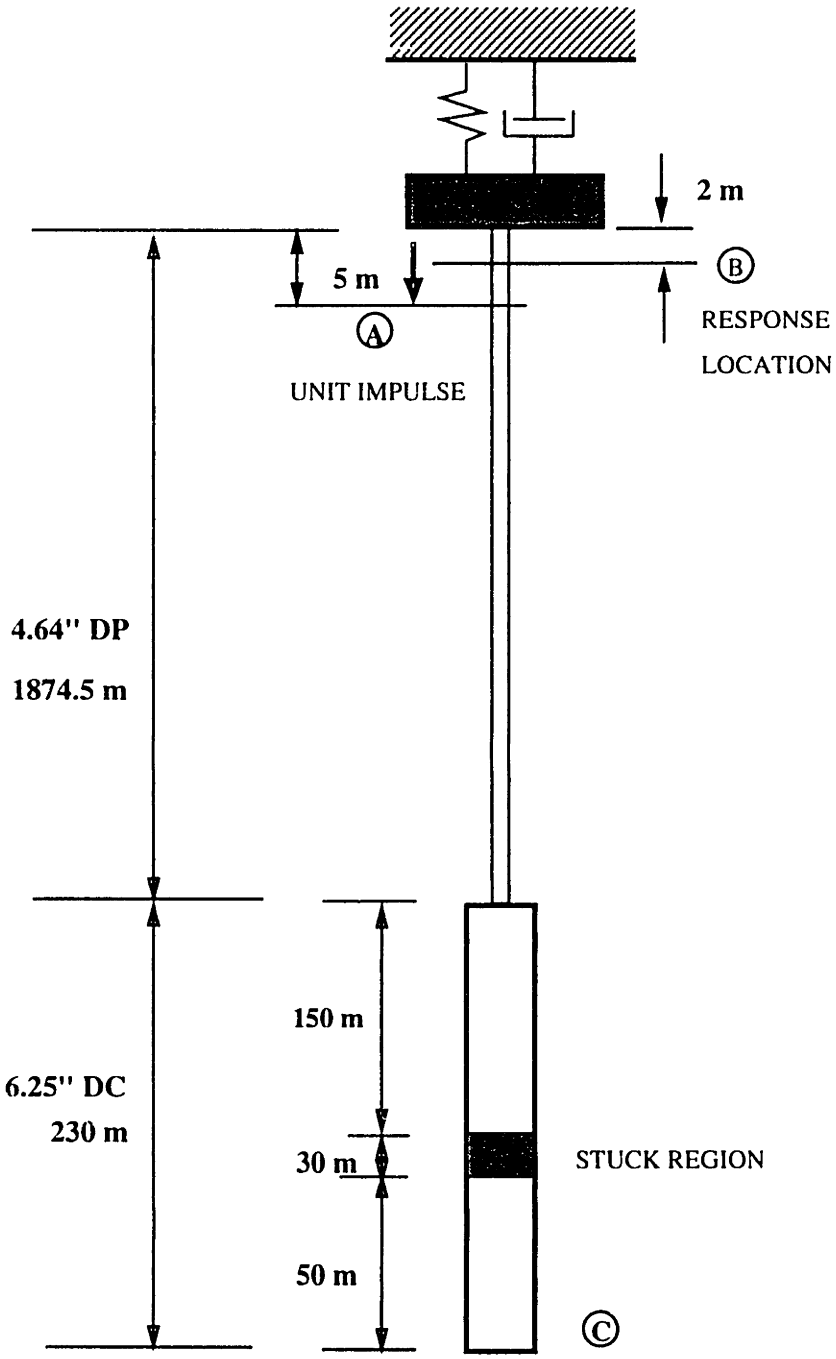

Figure 5-27: Analytical model of a stuck drillstring

Discussion :

Figure 5-28 shows the magnitude of the predicted transfer functions between the force at the surface (position B in figure 5-27) and a unit harmonic force excitation 3 m below (position A in figure 5-27) the response location. The transfer functions are calculated over a frequency band 0.2–819.2 Hz, with a step size of 0.2 Hz and are shown for various levels of distributed stiffness in the stuck region. The values of the distributed stiffness used are the same as the ones used in *example 5.3* and are given in section (5.3.4).

The zeros of the transfer function indicate that the response location acts as a node for the measured force at those frequencies. The first zero occurs at $\sim$ 5.2 Hz. This corresponds to the natural frequency of the mass–spring–damper subsystem at the top boundary. The position of this zero is dependent on the response location and the mass–spring system used to model the surface boundary condition. The next zero occurs at 638.8 Hz. This corresponds to a frequency for which there is a node in the standing wave of strain distribution formed between the input location and the mass–spring–damper subsystem. At this frequency, the mass acts as an approximately fixed boundary. These frequencies are given by

$$\begin{aligned} f_n &= \frac{nc}{4L_{SR}} \qquad n = 1, 3, 5 \ldots \\ &= \frac{n\,5100}{4\times 2} \qquad n = 1, 3, 5 \ldots \\ &= 637.5,\ 1912.5,\ Hz \ldots \end{aligned} \tag{5.53}$$

where

L_{SR} is the length of the drillpipe section between the response location and the mass–spring–damper subsystem.

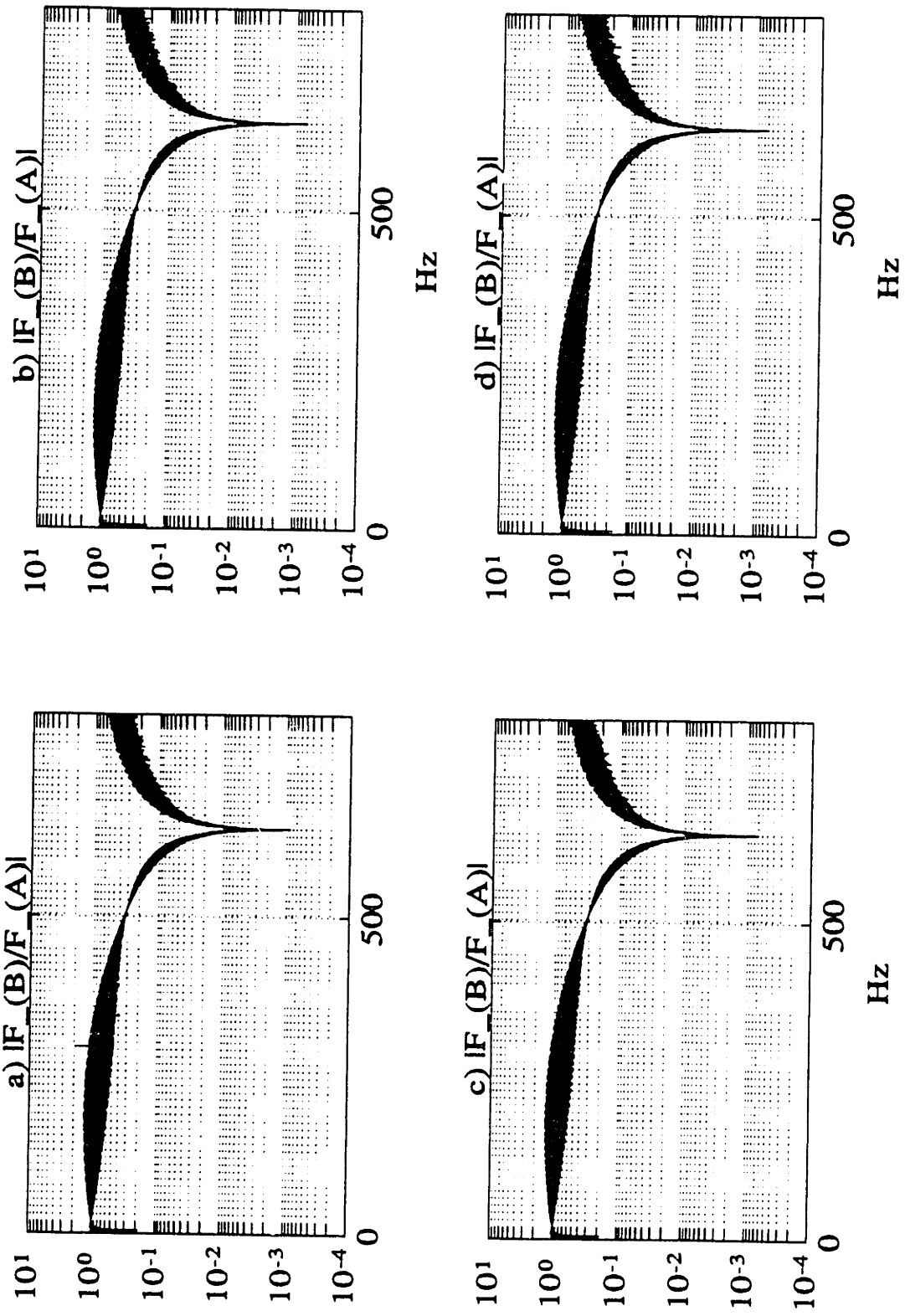

Figure 5-28: Magnitude of the simulated transfer function between the *force* measured at the surface (2 m below the MSD subsystem) and a *unit harmonic force* excitation at a surface location (5 m below the MSD subsystem), for different levels of distributed stiffness

a) $K = 1.0 \times 10^9 N/m\ /m$ b) $K = 1.0 \times 10^8 N/m\ /m$

c) $K = 1.0 \times 10^7 N/m\ /m$ d) $K = 0.0\ N/m\ /m$

It can be observed that there are no noticeable differences in the overall characteristics of the transfer functions as one proceeds from a stuck pipe to a free drillstring. This was not the case when the input was at the jar location. Hence, one cannot evaluate jarring effectiveness from plots of transfer functions directly.

5.4.2 Case 2) – Distributed damping model of the stuck region

Input : A *unit force impulse* in the time domain (position (A) in figure 5-27).

Response : *Force* at a surface location 2 m below the surface mass–spring–damper subsystem (position (B) in figure 5-16).

Bottom b.c : Free boundary condition at the bit.

Discussion :

The predicted response at the surface (position B in figure 5-27) due to a unit harmonic force excitation (position A in figure 5-27) 3 m below the response location is shown in figure 5-29 for various levels of distributed damping in the stuck region. The values of distributed damping used are given in section (5.4.2).

The first zero of the transfer function occurs at 5 Hz, which corresponds to the natural frequency of the MSD subsystem. The next zero occurs at 638.8 Hz and corresponds to the node in strain at the response location.

It was pointed out with regard to the DSM that the transfer functions by themselves donot provide any insight on the efficacy of the jarring operation.

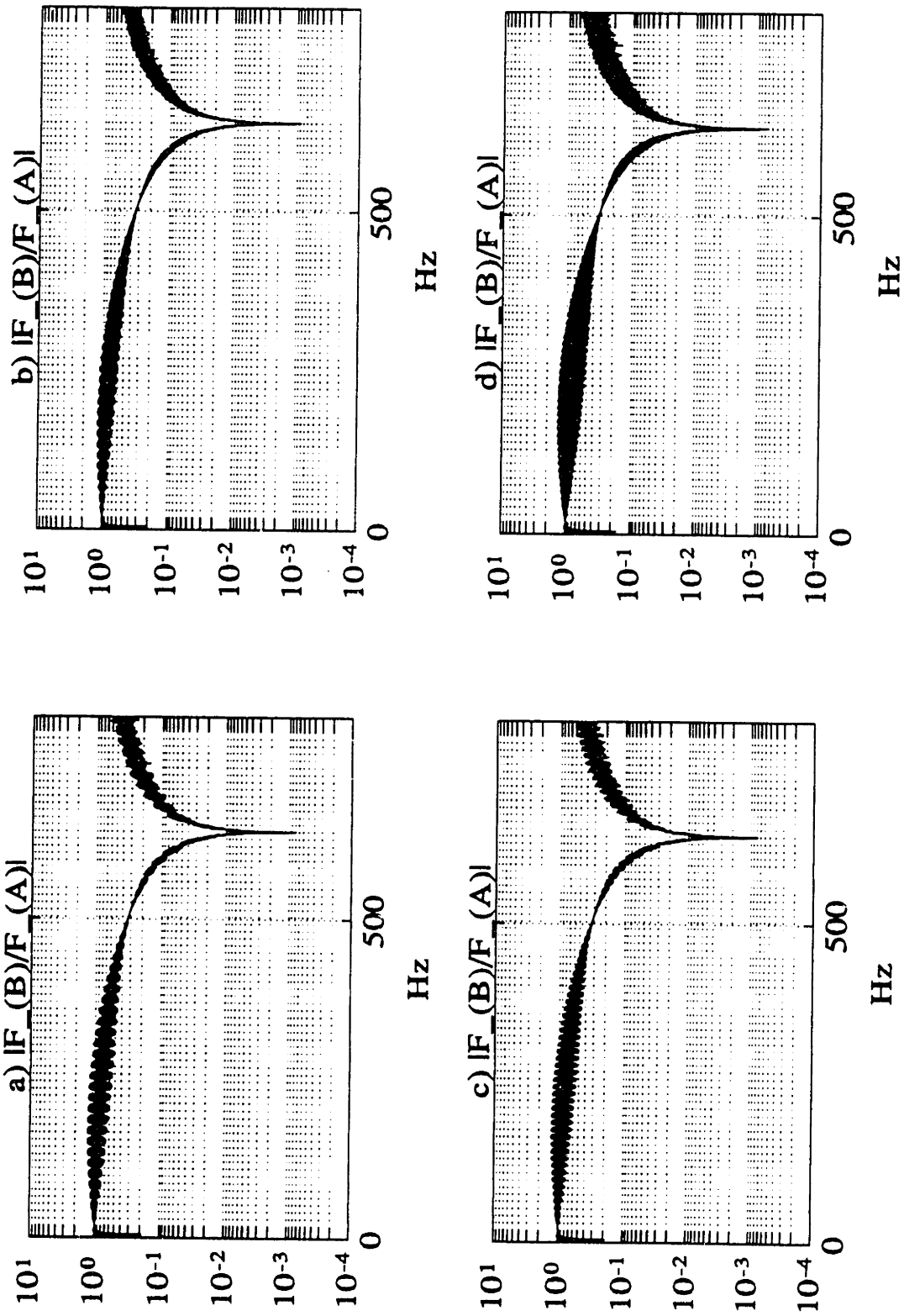

Figure 5-29: Magnitude of the simulated transfer function between the *force* measured at the surface (2 m below the MSD subsystem) and a *unit harmonic force* excitation at a surface location (5 m below the MSD subsystem), for different levels of distributed damping

a) $R = 1.1 \times 10^6\ N - s/m\ /m$ b) $R = 1.1 \times 10^5\ N - s/m\ /m$

c) $R = 1.1 \times 10^4\ N - s/m\ /m$ d) $R = 1.1 \times 10^2\ N - s/m\ /m$

This is also true in the case of the DDM. In section (5.4.3), the use of the cepstra of the impulse response functions to extract useful information about jarring effectiveness will be demonstrated.

5.4.3 Cepstral Analysis: Application to Distributed Stiffness and Distributed Damping Models of the stuck region

Distributed Stiffness Model (DSM) :

Figures 5-30 a) & b) and 5-31 c) & d) represent the power cepstrum of the impulse response for progressively decreasing levels of distributed stiffness in the stuck region.

Case a) represents the firmly stuck case ($K = 1.0 \times 10^9\ N/m\ /m$). Strong echoes can be seen corresponding to delay times[18] 0.7334 *secs* and 0.7930 *secs*. The peak at 0.7334 *secs* is the delay corresponding to the reflection of the pulse[19] (**E**) that travels downward from its point of origin, at the drillpipe/BHA interface; the peak at 0.7930 *secs* is the delay that corresponds to a pulse (**F**), that is reflected off the stuck region. These delays translate to propagation distances of 3740 m and 4044 m respectively. In addition, echoes clustered around 0.83 *secs* are also seen, which is the delay corresponding to the reflection of the transmitted waveform (**M**) at the bottom free boundary.[20] The rest of the peaks in figure 5-30 a) are caused by ringing effects.

If the jarring operation is producing results, then one would expect the distributed stiffness in the stuck region to decrease. This is simulated in figure 5-30 b), where the distributed stiffness is now $K = 1.1 \times 10^8\ N/m\ /m$. The first two echoes (with delay times 0.7334 *secs* & 0.7930 *secs*) correspond to **E** and **F**

[18]It must be borne in mind that all delays have the direct arrival contribution subtracted out.
[19]The boldface letters serve as an identification to keep track of the various pulses and waveforms
[20]Propagation through the stuck region occurs above the cut–off frequency (452 Hz)

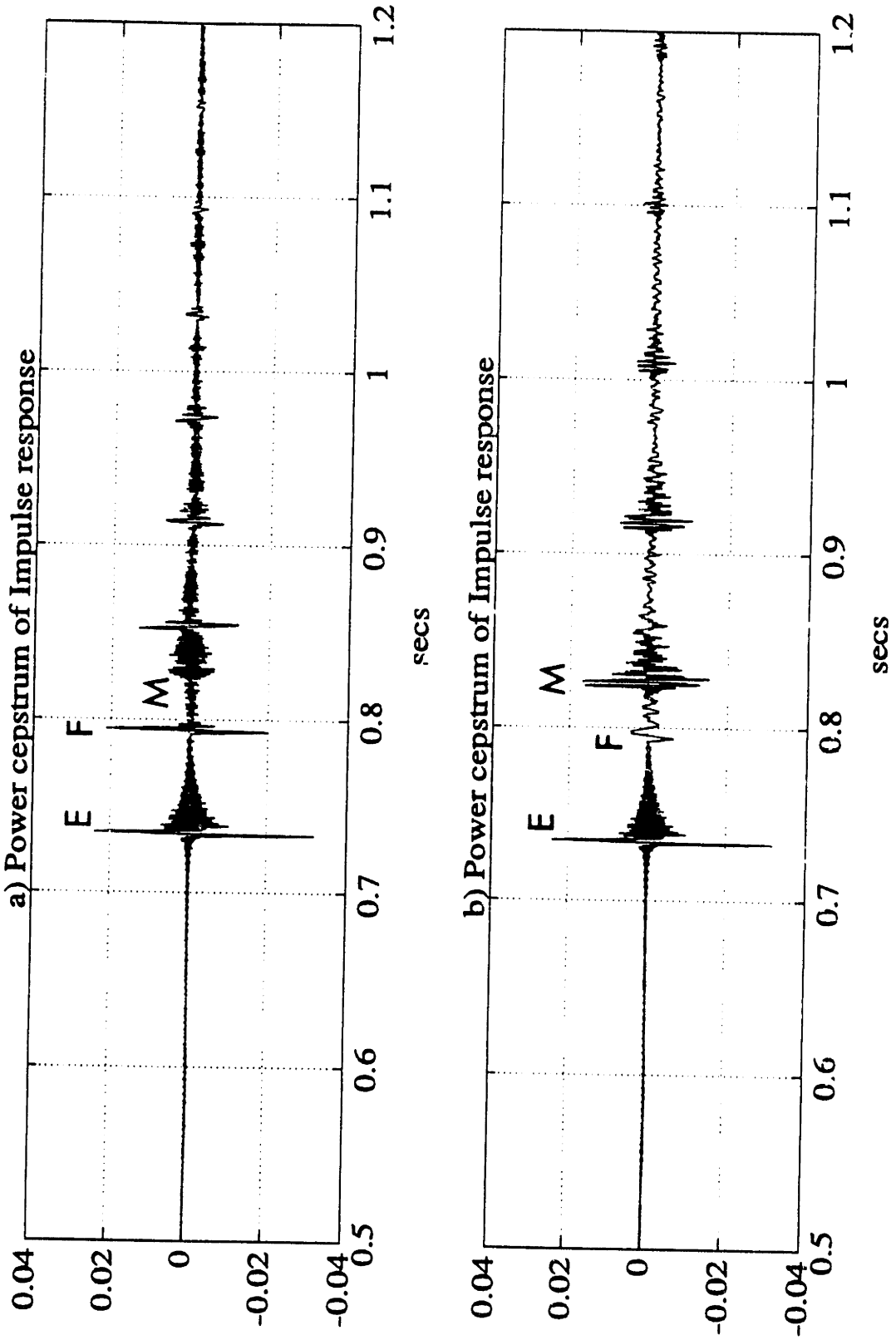

Figure 5-30: *Power cepstrum of response* at the surface (2 m below the MSD subsystem) due to a *unit force impulse* at a surface location (5 m below the MSD subsystem), for different levels of distributed stiffness

a) $K = 1.0 \times 10^9\ N/m\ /m$

b) $K = 1.0 \times 10^8\ N/m\ /m$

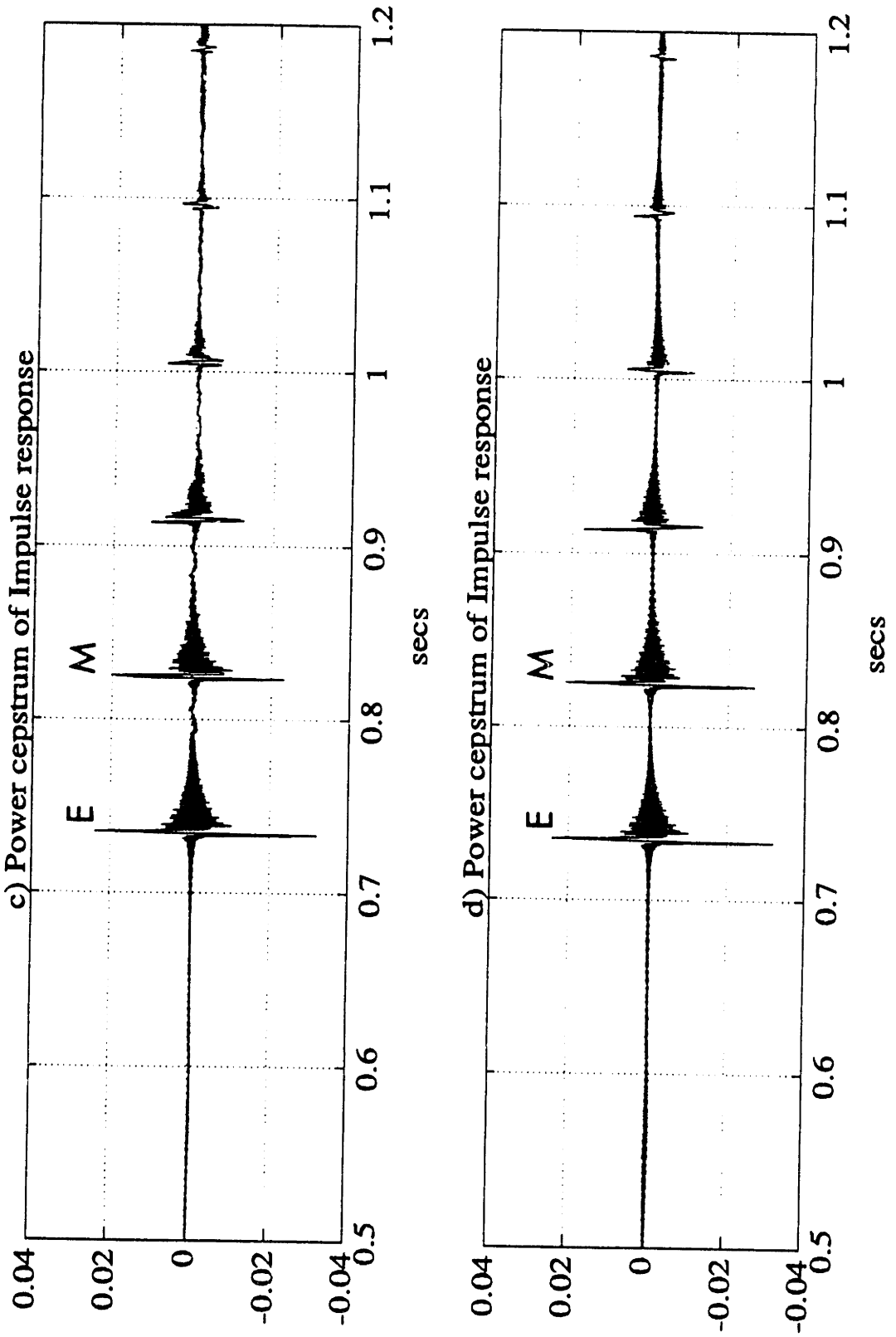

Figure 5-31: *Power cepstrum of response* at the surface (2 m below the MSD subsystem) due to a *unit force impulse* at a surface location (5 m below the MSD subsystem), for different levels of distributed stiffness

c) $K = 1.0 \times 10^7\ N/m\ /m$

d) $K = 0.0\ N/m\ /m$

respectively. The subsequent echo with a delay time of 0.8236 *secs* corresponds to **M**. It can be observed that the echo associated with reflection from the stuck region (**F**) is not as sharp as was in case a) due to a drop in the reflection coefficient for frequencies above the cut–off frequency. On the other hand, the delay time corresponding to the reflection of the transmitted waveform from the bottom boundary exhibits a strong and a narrow peak since a wider band of frequencies propagate through the stuck region as a result of a decrease in cut–off frequency (143 Hz).

In case c), the distributed stiffness is a factor of 10 lower than that in case b). In this case, the echo corresponding to the reflection from the stuck region is very small which implies that most of the energy propagates through the stuck region. A strong echo occurs at a delay time 0.8236 *secs* which corresponds to **M**.

The power cepstrum of the impulse response of a free drillstring is shown in figure 5-31 d). The peaks at 0.7334 *secs* and 0.8236 *secs* represent **E** + **M** respectively. The peaks are extremely sharp due to the dispersive effects being negligible.

Distributed Damping Model (DDM) :

Figures 5-32 a) & b) and 5-33 c) & d) show the power cepstrum of the impulse response for various levels of distributed damping in the stuck region.

Case a) represents the firmly stuck case with the stuck region modeled as a distributed damping of value $1.1 \times 10^6\ N - s/m\ /m$. It can be seen that strong echoes occur at times 0.7336 *secs* and 0.7918 *secs*. These represent time delays associated with reflections from the drillpipe/BHA interface and the stuck region respectively. The delays correspond to propagation distances of 3741 m and 4038 m, which is consistent with the drillpipe geometry. In this case, by virtue of very high damping, the stuck region behaves essentially as a rigid boundary; there is thus no transmission through the stuck region and

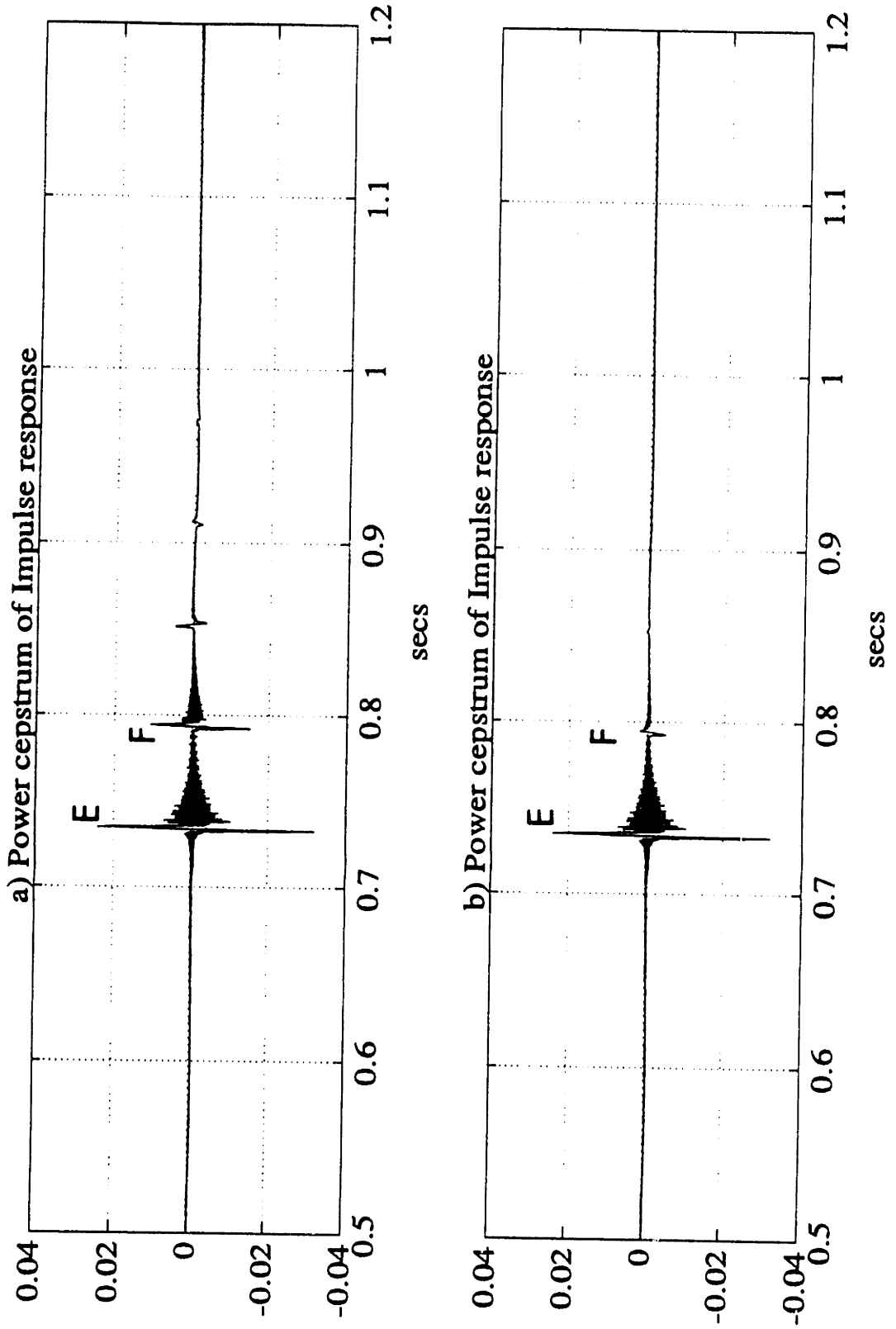

Figure 5-32: *Power cepstrum of response* at the surface (2 m below the MSD subsystem) due to a *unit force impulse* at a surface location (5 m below the MSD subsystem), for different levels of distributed damping

a) $R = 1.1 \times 10^6 N - s/m\ /m$

b) $R = 1.1 \times 10^5 N - s/m\ /m$

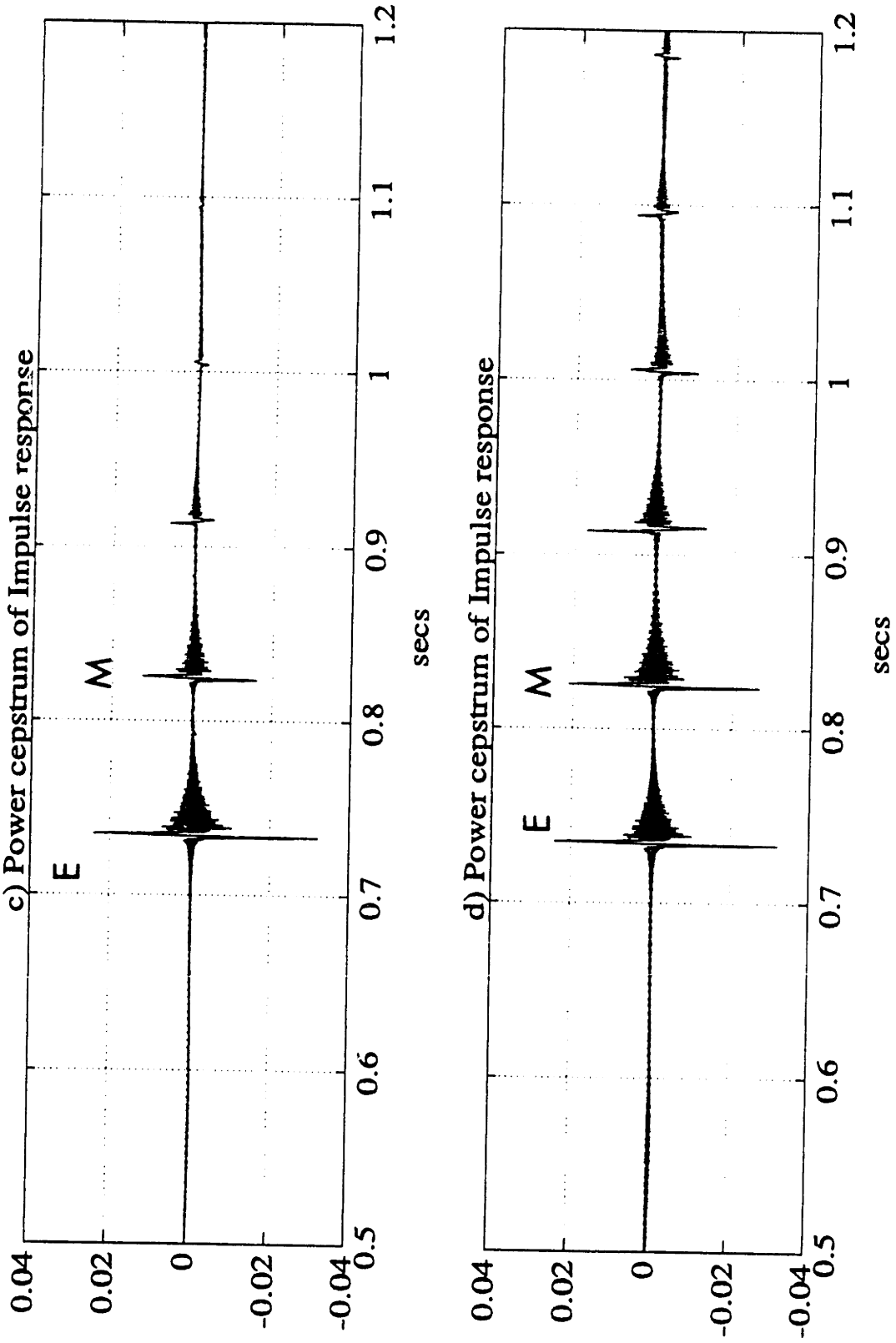

Figure 5-33: *Power cepstrum of response* at the surface (2 m below the MSD subsystem) due to a *unit force impulse* at a surface location (5 m below the MSD subsystem), for different levels of distributed damping

c) $R = 1.1 \times 10^4 N - s/m\ /m$

d) $R = 1.1 \times 10^2 N - s/m\ /m$

consequently, no echo corresponding to reflection from the free boundary at the bit, is seen.

Figure 5-32 b) shows a case where the distributed damping in the stuck region is reduced by a factor of 10 in comparison to case a). A strong echo from the drillpipe/BHA interface (corresponding to a delay time of 0.7336 *secs*) followed by a weak echo (corresponding to a delay time of 0.7927 *secs*) from the stuck region are seen. At the same time, no echoes associated with reflection of the transmitted waveform through the stuck region are seen. This goes to show that most of the input energy is being dissipated in the stuck region which signifies that the jarring operation is proving to be effective.

Case c) represents a case where the damping in the stuck region is even lower as a result of partial freeing of the BHA. From figure 5-33 c), it can be seen that there are no echoes associated with reflections from the stuck region. Echoes however occur at times 0.7336 *secs* and 0.8235 *secs* which correspond to reflections from the drillpipe/BHA interface and the free boundary at the bit. This indicates that some of the input energy is dissipated and some of it transmitted through the stuck region.

Finally, figure 5-33 d) shows the cepstrum of the impulse response of a free drillstring. This differs from case c) in that the echoes corresponding to reflections from the free boundary are much stronger. The peaks at delay times 0.7336 *secs* and 0.8236 *secs* correspond to reflections from the drillpipe/BHA interface and the bottom boundary respectively.

Thus, we have seen how the cepstrum of the impulse response measurements at the surface can be effectively employed to answer the questions that were raised at the outset of chapter 4 namely,

- Is the location of the stuck region determinable from surface measurements?
- Can anything be inferred about the nature of the stuck region by inspection

of surface responses ?... Does the stuck region behave as a conservative medium or is it absorptive in nature ?

- Is the jarring proving to be effective ?... Are we making progress towards freeing the drill string ?

Chapter 6

Conclusions

In this thesis, a mathematical model developed by H.Y. Lee for drillstring axial vibration was used to understand drillstring dynamics during jarring. This model was modified to include the effects of distributed stiffness, which caused an additional term to appear in the dispersion relation. The effect of this term was to introduce cut–off frequencies below which, only an evanescent wave field existed in the stuck region. The transfer matrix for the drillstring, modeled as a piecewise continuous complex pipe system, was built up with a knowledge of the transfer matrices for a mass-spring–damper system and a uniform bar. The transfer function was then obtained between the force measured at a surface location and a unit harmonic force at the input location. The impulse response was obtained by taking the inverse fourier transform of the transfer function and smoothed using a Blackman window.

The jarring action was modeled as a unit area impulse (in the time domain) delivered to the BHA at the jar location. It must be pointed out that a realistic jarring signal is not a true impulse, and the response in such a case is obtained either by a convolution of the impulse response with the true jarring signal or by forming the product of the transfer function and the fourier transform of the input signal. The surface force response due to a unit harmonic force excitation at the jar location was studied as a function of frequency, for progressively decreas-

ing values of 1) distributed stiffness and 2) distributed damping in the stuck region. This simulates a progress from a badly stuck case to a free drillstring. In case 1), the sticking mechanism is modeled as a conservative restraint on the BHA whereas in case 2), the stuck region is modeled as a dissipative medium. It was seen that the transfer functions exhibit distinct changes (in the positions of the poles and zeros), as one proceeds from a stuck to a free case. One could thus identify the location of the stuck region and evaluate the progress made during jarring by monitoring the positions of the poles and zeros. The poles and zeros in the distributed stiffness model are much sharper than those in the distributed damping model. The impulse responses are obtained from the transfer functions. It was noticed that it is not possible to distinguish between various signal arrivals from plots of the impulse responses, due to the nature of the reflected and transmitted waveforms at the stuck region. To overcome this problem, a different technique, known as *cepstral analysis* was employed. The peaks in the power cepstrum, in spite of having the same periodicity as in the impulse response, die away much more quickly and the arrivals from the different interfaces can easily be distinguished. In addition, the cepstral peaks produce distinctive signatures in the two different models of the stuck region as one approaches the free drillstring case from a stuck pipe condition.

However, since jars are normally tripped only under stuck conditions, it may not be feasible to obtain the baseline impulse response measurement and this served as the motivation behind analyzing a case, where a force impulse is delivered to the drillpipe at the surface and the resulting force response is also measured at a surface location for different values of distributed stiffness and distributed damping in the stuck region. The positions of the zeros of the transfer functions in this case, are dependent solely on the system parameters above the measurement location. The transfer function plots by themselves are therefore, not very useful in inferring anything about jarring effectiveness. The cepstra plots of the impulse responses are used to evaluate the efficacy of jarring in this case.

It has thus been demonstrated that it is possible to identify the stuck location and infer the nature of downhole sticking from surface force measurements. The power cepstrum plots of the impulse responses (due to a force impulse at the surface) can then be used to evaluate the progress of the jarring operation, by comparing them with the power cepstrum of the impulse response of a free drillstring.

Thus, one needs to have access to real data in order to validate our models. A first step in this direction would be to perform experiments designed at obtaining the response of a free drillstring to a force impulse at the surface, when it is off-bottom. Once the baseline impulse response measurement is in place, the effectiveness of jarring can be judged by comparing the cepstra of the impulse response (for an input force impulse at the surface) after every few jarring cycles.

Bibliography

[1] T.V. Aarrestad and A. Kyllingstad. Loads on drillpipe during jarring operations. *SPE/European Petroleum Conference*, November 1992.

[2] W.E. Askew. Computerized drilling jar placement. *SPE/IADC drilling conference*, February 1986.

[3] Léon Brillouin. *Wave Propagation and Group Velocity.* Academic Press, 1960.

[4] D.W. Dareing and B.J. Livesay. Longitudinal and angular drill string vibrations with damping. *ASME Journal of Engineering for Industry*, November 1968.

[5] Karl F. Graff. *Wave Motion in Elastic Solids.* Dover Publications, Inc., 1991.

[6] M.S. Kalsi et al. Transient dynamic analysis of the drillstring under jarring operations by the fem. *JPT*, November 1979.

[7] F.A. Leckie and E.C. Pestel. *Matrix Methods in Elastomechanics.* McGraw-Hill Book Company, Inc, 1963.

[8] Hyun Y. Lee. *Drill String Axial Vibration and Wave Propagation in Boreholes.* PhD thesis, MIT, 1991.

[9] Angelo Ligrone, J. Kim Vandiver, Paolo Ferrara, and Rama Rao V.N. Drillstring axial vibrations and shock absorber positioning criteria. *Offshore Mediterranean Conference*, March 1993.

[10] Richard H. Lyon. *Machinery Noise and Diagnostics.* Butterworths, Boston, 1987.

[11] James W. Nicholson et al. Case studies of the bending vibration and whirling motion of drill collars. *SPE/Drilling Engineering*, December 1990.

[12] Rama Rao V.N. Acoustic transmission through fluid-filled pipes in boreholes. Master's thesis, MIT, 1991.

[13] R.W. Schafer and A.V. Oppenheim. *Discrete-Time Signal Processing.* Prentice Hall, Englewood Cliffs, NJ, 1989.

[14] M.R. Skeem et al. Drill string dynamics during jar operation. *JPT*, November 1979.

[15] J. Kim Vandiver et al. The effect of surface and downhole boundary conditions on the vibration of drillstrings. *SPE/Annual Technical Conference*, September 1990.

[16] J. Kim Vandiver et al. Shock sub performance : Measured and predicted response. Technical report, Massachusetts Institute of Technology, 1991.

[17] J.K. Wang et al. A practical approach to jarring analysis. *SPE/IADC Drilling Conference*, March 1985.